SUPPORTED HYBRID METALLOCENE CATALYST, METHOD FOR PREPARING THE SAME, AND METHOD FOR PREPARING POLYOLEFIN USING THE SAME

BACKGROUND OF THE INVENTION

(a) Field of the Invention

The present invention relates to a supported metallocene catalyst used for preparing polyolefin whose physical properties and molecular weight distribution can be easily controlled, a method for preparing the same, and a method for preparing polyolefin using the same, more particularly to a supported metallocene catalyst wherein at least two kinds of metallocene compounds are supported on a metal oxide such as silica, a method for preparing the same, and a method for preparing polyolefin using the same.

(b) Description of the Related Art

The metallocene catalyst system comprises a main catalyst whose main component is a transition metal compound, mainly a Group IV metal, and an organometallic compound cocatalyst whose main component is aluminum. Such a catalyst offers a polymer having a narrow molecular weight distribution depending on the single site characteristics. The molecular weight and molecular weight distribution of polyolefin are important factors that determine the fluidity and mechanical properties that affect the physical properties and processability of a

polymer. To manufacture a variety of polyolefin products, it is important to improve melt processability through molecular weight distribution control (C.A. Sperat, W.A. Franta, H.W. Starkweather Jr., *J. Am. Chem. Soc.*, 75, 1953, 6127). Especially for polyethylene, toughness, strength, environmental stress cracking resistance (ESCR), and so forth are very important. Therefore, a method of preparing a polyolefin having a bimodal or broad molecular weight distribution to enhance mechanical properties and processability has been proposed.

The polyolefin having a bimodal and broad molecular weight distribution is a polymer that has two average molecular weights, one of which is higher and the other lower. Conventionally, there have been many attempts to prepare a polymer having such a molecular weight distribution. They can be categorized into the following three groups.

First, a method of preparing two polyolefins having different molecular weights by post reaction or mixing has been proposed (US Patent No. 4,461,873). However, such physical mixing requires additional production cost. Also, because the gel content is high due the compatibility of the two polymers, it cannot be applied to manufacturing containers and films.

Second, a method of preparing a polyethylene having a broad molecular weight distribution or a bimodal molecular weight distribution by differing injected

amounts of hydrogen gas and comonomers using more than two multistep reactors has been proposed (C.A. Sperat, W.A. Franta, H.W. Starkweather Jr., *J. Am. Chem. Soc.*, 75, 1953 6127, N. Kuroda, Y. Miyazaki, K. Matsumura, K. Jubo, M. Miyashi and T. Horie, 1979 Ger. 28,856,548). Although this method can solve the gel problem, the process is complex and the operation cost is high.

The third method, a method of mixing two different catalysts in a single reactor or applying more than two catalysts to a single support, is more useful than the above two methods. Most patents and literatures mention a metallocene compound and a Ziegler-Natta titanium compound supported on a single support (US Patent No. 6,444,605 B1, US Patent No. 6,399,531 B1, US Patent No. 6,417,129 B2, US Patent No. 6,399,723 B1, US Patent No. 5,614,456, Korea Patent Publication No. 1988-045993, Korea Patent Publication No. 1998-045994, Korea Patent Publication No. 1999-022334, Korea Patent Publication No. 2000-0042620).

A polyolefin prepared by this method has limited physical properties due to the specific polymerization characteristics of the Ziegler-Natta catalyst and the metallocene catalyst. For instance, when preparing a polyolefin using a metallocene catalyst, the stereoregularity, copolymerization characteristics, molecular weight, crystallinity, and so forth of the obtained polymer can be controlled by changing the ligand structure of the catalyst and the polymerization condition.

Accordingly, a polyolefin having ideal molecular weight distribution, stereo regularity, copolymerization characteristics, and so forth can be prepared by using several metallocene catalysts having specific characteristics. For the preparation of a polyolefin having a bimodal or broad molecular weight distribution using a metallocene catalyst, a method of using two different metallocene catalyst systems having different growth rate and termination rate constant has been proposed (J. A. Ewen, *Stud. Surf. Sci. & Catal.* vol. 1986 25, US Patent No. 6,384,161 B1). The Kaminsky group of Germany has reported that the molecular weight distribution (Mw/Mn) of ethylene polymerization has broadened from about 1.9 to 2.3 to about 4.1 to 10.0 when they used a hybrid metallocene catalyst system such as Cp_2ZrCl_2-Cp_2HfCl_2-MAO (A. Ahlers, W. Kaminsky, *Makromol. Chem., Rapid Commun.*, 9, 1988 457).

However, above-mentioned literatures and patents only disclose the polymerization using two catalysts. They just mention selection of organometallic compounds and homogeneous catalyst systems for controlling the molecular weight distribution and polymer properties, and they do not offer supported catalysts applicable to gas-phase and slurry processes.

The industrial polyolefin production processes can be classified into the high-pressure process, the solution process, the slurry process, the gas phase

process, and so forth. With the development of the metallocene catalyst, there have been many attempts to produce polyolefin using these processes and just replacing the catalyst. Until recently, the metallocene catalyst is mostly used for the solution process, the gas phase process and the slurry process. The gas phase and the slurry processes require apparent density control of the polymer to improve the production unit per unit volume of the reactor. In addition, the fouling problem, or sticking of the polymer on the reactor wall, should be solved. The most common method for increasing the apparent density and solving the fouling problem is to fix the homogeneous metallocene catalyst on a solid support such as silica, alumina or a metal oxide.

Among them, silica is the most frequently used as a support. When a silica support is dried at high temperature, the hydroxyl group on the surface is removed as water and a siloxane group is obtained, as in the following Scheme 1. If the drying temperature is 200 to 500 °C, only the easily removable hydroxyl group (-OH) is reversibly removed as water and the less reactive siloxane group is obtained. However, if the drying temperature is above 600 °C, even the hardly removable hydroxyl group is forcibly removed as water and the siloxane group with a large ring strain and high reactivity is obtained (I-S. Chuang and G. E. Maciel, *Journal of American Chemical Society* 118, 1996, 401). The highly reactive siloxane group

obtained by drying at the temperature over 600 ℃ reacts with an alkoxy silane group, as in Scheme 1 (J. Blmel, *Journal of American Chemical Society* 117, 1995, 2112; L. H. Dubois, *Journal of American Chemical Society* 115, 1993, 1190).

Scheme 1

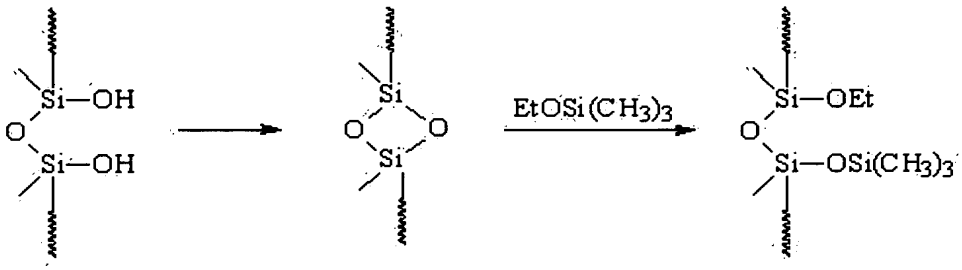

Here, the figure on the left is the ordinary silica, the figure on the center is the silica having a highly reactive siloxane group, which has been dried at a temperature over 600 ℃, and the figure on the right is the silica attached with an alkoxy silane group.

SUMMARY OF THE INVENTION

It is an object of the present invention to provide a supported hybrid metallocene catalyst, with which the final physical properties and the molecular weight distribution of polyolefin can be easily controlled, and a method for preparing the same.

It is another object of the present invention to provide a method for preparing polyolefin by applying a supported hybrid metallocene catalyst, which was obtained

by sequentially adding two different metallocene compounds, to a single polymerization reactor, in order to improve the processability and the physical properties of polyolefin and to significantly reduce the polyolefin production cost by cutting down the production processes.

To attain the objects, the present invention provides a supported hybrid metallocene catalyst, in which at least two different metallocene compounds are supported on a single support, wherein:

at least one metallocene compound is supported on the support by a chemical bond of its ligand to the support surface; and

the other metallocene compound is supported on the support by a chemical bond of its ligand to a cocatalyst chemically bonded to the support surface.

The present invention also provides the following two methods for preparing the supported hybrid metallocene catalyst:

The first method comprises:

a) a step of contacting a supported metallocene catalyst in which at least one metallocene compound is supported with a cocatalyst to prepare an activated supported metallocene catalyst; and

b) a step of supporting at least one metallocene compound different from the metallocene compound of the step a) on the activated supported metallocene

catalyst.

The second method comprises:

a) a step of contacting at least one metallocene compound with a cocatalyst to prepare an activated metallocene compound; and

b) a step of supporting the activated supported metallocene compound on a supported metallocene catalyst in which at least one metallocene compound different from the metallocene compound of the step a) is supported.

The present invention also provides a supported hybrid metallocene catalyst for preparing polyolefin having a bimodal or broad molecular weight distribution, which is obtained by supporting a) a catalyst component on b) a support, wherein

a) the catalyst component comprises:

i) a first metallocene compound having an acetal, ketal, tertiary alkoxyalkyl, benzyloxyalkyl, substituted benzyloxyalkyl, monothioacetal or monothioketal group;

ii) a second metallocene compound having a bridge linkage containing a Lewis base in cyclopentadiene, a cyclopentadiene derivative or a bridge group; and

iii) an organometallic compound containing a group XIII metal; and

b) the support has siloxane groups on the surface, on which the catalyst

component is supported.

The present invention also provides the following two methods for preparing a supported hybrid metallocene catalyst for preparing polyolefin having a bimodal or broad molecular weight distribution:

The first method comprises:

a) a step of preparing a first supported catalyst by supporting a first metallocene compound having an acetal, ketal, tertiary alkoxyalkyl, benzyloxyalkyl, substituted benzyloxyalkyl, monothioacetal or monothioketal functional group on a support having siloxane groups on the surface;

b) a step of preparing an activated first supported catalyst by contacting the first supported catalyst with an organometallic compound cocatalyst containing a group XIII metal; and

c) a step of supporting a second metallocene compound having a bridge linkage containing at least one Lewis base in cyclopentadiene, a cyclopentadiene derivative or a bridge group on the activated first supported catalyst to prepare a supported hybrid metallocene catalyst wherein the first metallocene compound and the second metallocene compound are supported.

The second method comprises:

a) a step of supporting a first metallocene compound having an acetal, ketal,

tertiary alkoxyalkyl, benzyloxyalkyl, substituted benzyloxyalkyl, monothioacetal or monothioketal functional group on a support having siloxane groups on the surface to prepare a first supported catalyst;

b) a step of contacting a second metallocene compound having a bridge linkage containing at least one Lewis base in cyclopentadiene, a cyclopentadiene derivative or a bridge group with an organometallic compound cocatalyst containing a group XIII metal to prepare an activated second metallocene compound; and

c) a step of supporting the activated second metallocene compound on the first supported catalyst to prepare a supported hybrid metallocene catalyst wherein the first metallocene compound and the second metallocene compound are supported.

The present invention also provides a method of olefin polymerization which comprises a step of polymerizing an olefinic monomer in the presence of a supported hybrid metallocene catalyst wherein at least two different metallocene compounds, which comprise a first metallocene compound whose ligand is supported to the support surface by chemical bonding, a second metallocene compound whose ligand is supported to a cocatalyst, which is chemically bonded to the support surface, by chemical bonding, a cocatalyst and a support, are supported on a single support.

The present invention also provides a method for preparing polyolefin having a bimodal or broad molecular weight distribution, which comprises a step of polymerizing an olefinic monomer in the presence of a supported hybrid metallocene catalyst wherein a catalyst component comprising:

i) a first metallocene compound having an acetal, ketal, tertiary alkoxyalkyl, benzyloxyalkyl, substituted benzyloxyalkyl, monothioacetal or monothioketal functional group;

ii) a second metallocene compound having a bridge linkage containing at least one Lewis base in cyclopentadiene, a cyclopentadiene derivative or a bridge group; and

iii) an organometallic compound cocatalyst containing a group XIII metal

is supported on a support having siloxane groups on the surface.

BRIEF DESCRIPTION OF THE DRAWINGS

Fig. 1 is a graph that shows the gel permeation chromatography (GPC) analysis for an olefin polymer prepared by using the supported hybrid metallocene catalyst of Example 7.

Fig. 2 is a graph that shows the gel permeation chromatography (GPC) analysis for an olefin polymer prepared by using the supported metallocene catalyst of Comparative Example 2.

DETAILED DESCRITPION OF THE PREFERRED EMBODIMENTS

Hereinafter, the present invention is described in more detail.

The present invention provides a supported hybrid metallocene catalyst which enables production of polyolefin having ideal properties and molecular weight distribution and controls the polymer structure better than the conventional supported hybrid catalyst of Ziegler-Natta and metallocene compound.

The present invention provides a supported hybrid catalyst consisting of at least two kinds of metallocene catalysts having different polyolefin polymerization characteristics, and thus enables preparation of polyolefins having a variety of properties and molecular weight distributions (broad and bimodal molecular weight distribution). The present invention also provides a supported hybrid catalyst which can easily control physical properties of prepared olefin polymers, a method for preparing the same, and a method of olefin polymerization using the same.

More specifically, the present invention provides offers a supported catalyst capable of easily controlling molecular weight distribution in a single reactor by supporting a metallocene compound inducing a low molecular weight polyolefin and a metallocene compound inducing a high molecular weight polyolefin on a single support together with a cocatalyst. Preferably, the low molecular weight polyolefin has a molecular weight ranging from 1,000 to 100,000, and the high molecular

weight polyolefin has a molecular weight higher than that of the low molecular weight polyolefin, ranging from 10,000 to 1,000,000.

First, a metallocene compound having a functional group such as an alkoxy group is supported on a support having highly reactive siloxane groups which have been generated during drying at high temperature as exemplified in Scheme 1, as shown in the following Scheme 2 (Korea Patent Publication No. 10-1998-0025282). Then, it is reacted with an alkylaluminum compound such as methylaluminoxane to prepare an activated supported catalyst to obtain a hybrid catalyst. The result is: a support with a trace of hydroxyl groups on the surface can be used, so that various side reactions due to the hydroxyl groups can be prevented, and therefore the supporting efficiency can be maximized. A metallocene catalyst having a different polymerization characteristic and a bridge linkage is supported to the activated supported catalyst.

More specifically, a first metallocene compound having a functional group such as an alkoxy group and capable of inducing low molecular weight is supported on a silica support having highly reactive siloxane groups on the surface, as seen in the following Scheme 2 or Scheme 3. Then, a cocatalyst such as an alkylaluminum compound and, subsequently, a second metallocene compound having a bridge linkage capable of inducing high molecular weight are reacted to prepare a new type

of supported hybrid catalyst. This supported hybrid catalyst is used to prepare polyolefin having a bimodal or broad molecular weight distribution.

Scheme 2

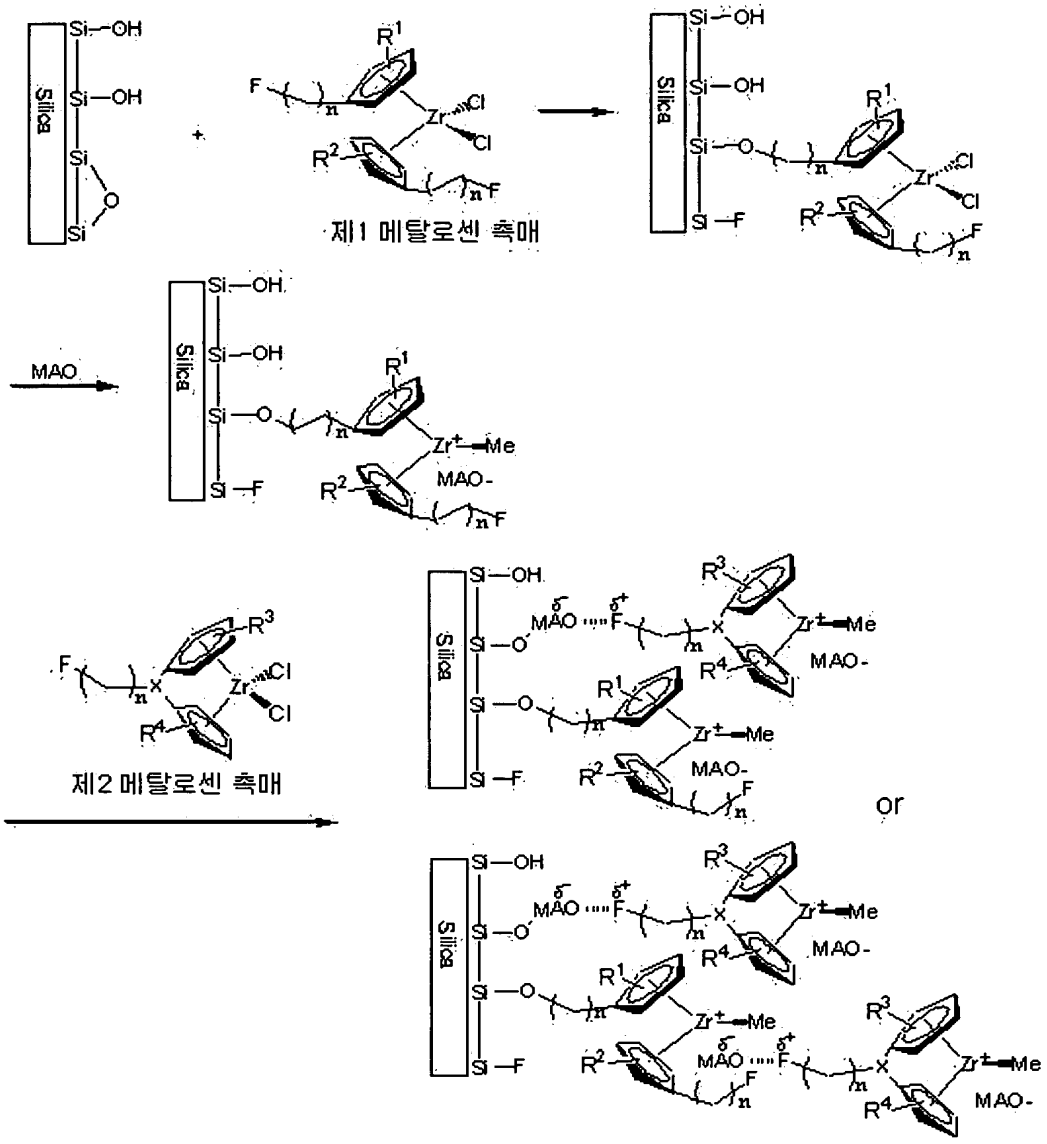

Scheme 3

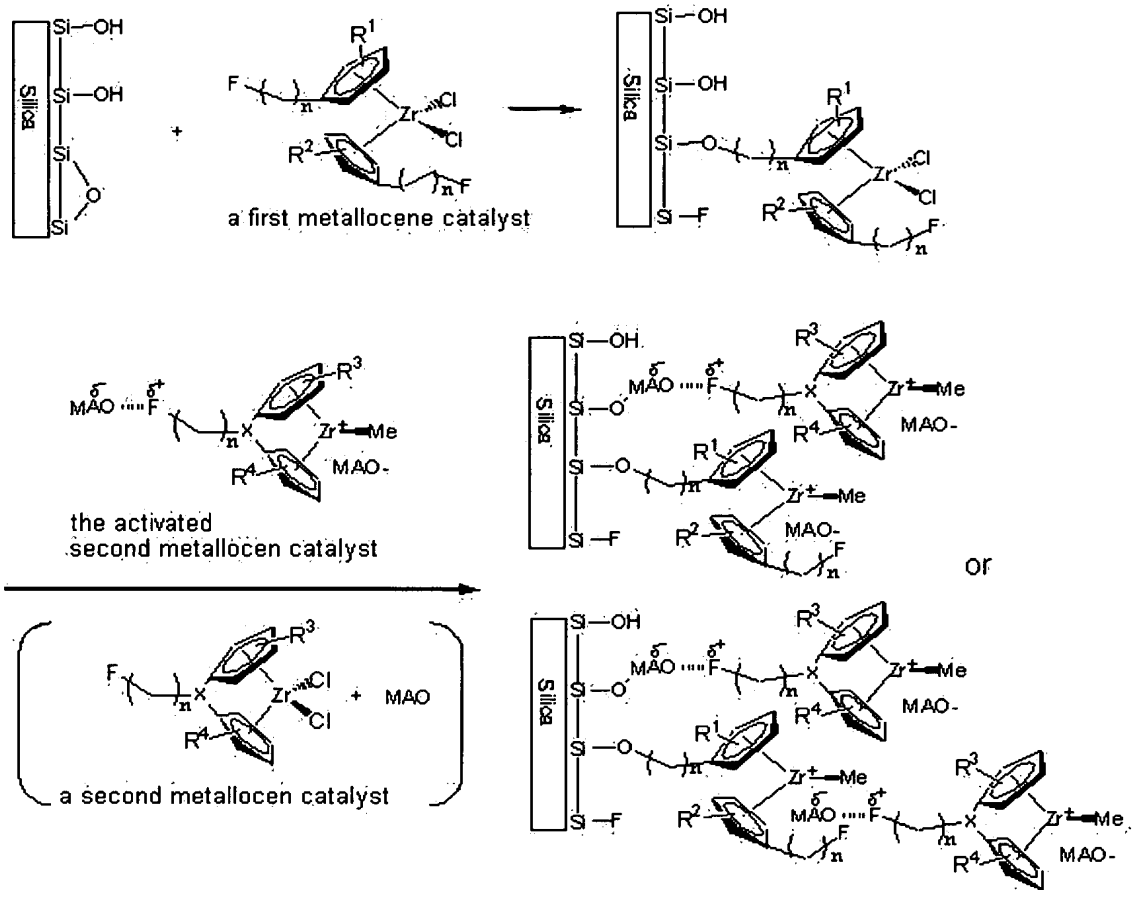

In Scheme 2 and Scheme 3, F is a functional group and X is a bridge group connecting two cyclopentadienyl groups.

Therefore, the supported hybrid metallocene catalyst of the present invention is a hybrid catalyst wherein a ligand of the first metallocene compound is supported on the support surface by chemical bonding and a ligand of the second metallocene compound is supported on a cocatalyst chemically bonded to the support surface by chemical bonding.

In general, the first metallocene catalyst having a functional group such as an alkoxy group induces low molecular weight polyolefin, and is represented by the following Chemical Formula 1:

Chemical Formula 1

$$(C_5R^1)_p(C_5R^2)MQ_{3-p}$$

Here,

M is a group IV transition metal;

each of (C_5R^1) and (C_5R^2) is cyclopentadienyl ~~which is a metalloid of a group XIV metal substituted by identical or different hydrogen radical, C_1 to C_{40} alkyl, cycloalkyl, aryl, alkenyl, alkylaryl, arylalkyl, arylalkenyl radical or hydrocarbyl~~; cyclopentadienyl wherein two neighboring carbon atoms of C_5 are connected by a hydrocarbyl radical to form one or more C_4 to C_{16} rings; or a substituted cyclopentadienyl ligand;

each of R^1 and R^2 is identical or different and a substituent selected from hydrogen radical, C_1 to C_{40} alkyl, cycloalkyl, aryl, alkenyl, alkylaryl, arylalkyl, or arylalkenyl radical; and at least one hydrogen radical comprised in the substituent of R^1 and R^2 is further substituted by a radical represented by the following Chemical Formula a, the following Chemical Formula b, or the following Chemical Formula c;

Q is a halogen radical; a C_1 to C_{20} alkyl radical, alkenyl radical, aryl radical,

alkylaryl radical, arylalkyl radical; or a C_1 to C_{20} alkylidene radical; and

P is 0 or 1; and

at least one hydrogen radical in R^1 and R^2 is substituted by a radical represented by the following Chemical Formula a, a radical represented by the following Chemical Formula b, or a radical represented by the following Chemical Formula c:

Chemical Formula a

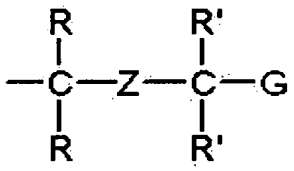

Here,

Z is an oxygen atom or a sulfur atom;

each of R and R' is identical or different hydrogen radical; C_1 to C_{40} alkyl, cycloalkyl, aryl, alkenyl, alkylaryl, arylalkyl; or arylalkenyl radical; and the two R's may be connected to form a ring;

G is a C_1 to C_{40} alkoxy, aryloxy, alkylthio, arylthio, phenyl or substituted phenyl, and may be connected to R' to form a ring;

if Z is a sulfur atom, G should be alkoxy or aryloxy; and

if G is alkylthio, arylthio, phenyl or substituted phenyl, Z should be an oxygen atom; and

Chemical Formula b

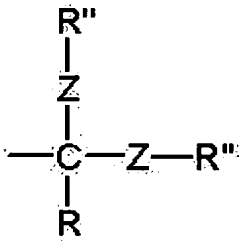

Here,

Z is an oxygen atom or a sulfur atom, and at least one of the two Zs is an oxygen atom;

each of R and R" is identical or different hydrogen radical; C_1 to C_{40} alkyl, cycloalkyl, aryl, alkenyl, alkylaryl, arylalkyl or arylalkenyl radical;

R and R" may be connected to form a ring; and

unless both R"s are hydrogen radicals, they may be connected to form a ring; and

Chemical Formula c

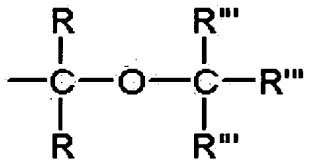

Here,

each of R and R"' is identical or different hydrogen radical; C_1 to C_{40} alkyl, cycloalkyl, aryl, alkenyl, alkylaryl, arylalkyl or arylalkenyl radical;

two neighboring R'''s may be connected to form a ring; and

if at least one of Rs is a hydrogen radical, all R'''s are not hydrogen radicals, and if at least one of R'''s is a hydrogen radical, all Rs are not hydrogen radical.

A typical example of the first metallocene compound represented by Chemical Formula 1 is $[A\text{-}O\text{-}(CH_2)_a\text{-}C_5H_4]_2ZrCl_2$ or $[A\text{-}O\text{-}(CH_2)_a\text{-}C_9H_6]ZrCl_3$. More preferably, a is an integer of 4 to 8; and A is selected from a group consisting of methoxymethyl, *t*-butoxymethyl, tetrahydropyranyl, tetrahydrofuranyl, 1-ethoxyethyl, 1-methyl-1-methoxyethyl or *t*-butyl (Lee, B. Y., Oh, J. S., *Organomet. Chem.*, 552, 1998, 313).

Typical but non-restrictive examples of the first metallocene compound of the present invention are as follows:

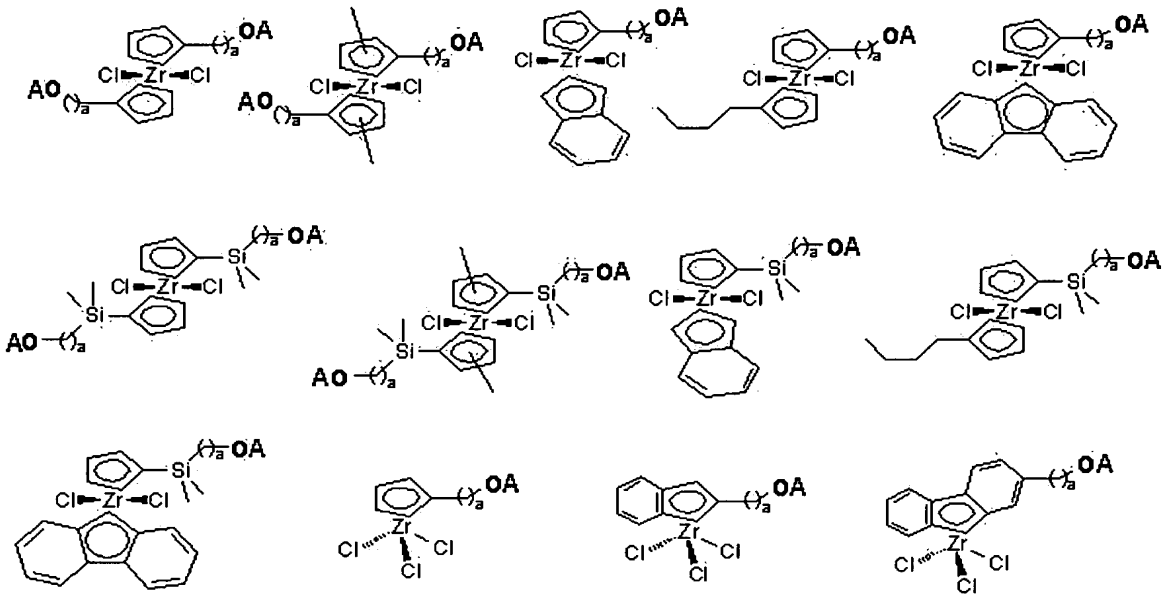

Here, definitions of A and a are the same as mentioned above.

The support used in the present invention is dried at high temperature, and thus has highly reactive siloxane groups on the surface. To be specific, silica, silica-alumina, silica-magnesia, and so forth, which have been dried at high temperature, can be used. The support may comprise oxides such as Na_2O, K_2CO_3, $BaSO_4$ and $Mg(NO_3)_2$, carbonates, sulfates or nitrates.

The most prominent characteristic of the present invention is the highly reactive siloxane groups on the support surface obtained by removing water and OH group by flowing vacuum-dried or dried air, nitrogen or inert gas at high temperature. The drying temperature is 300 to 1000 ℃, preferably 300 to 800 ℃, and more preferably 600 to 800 ℃.

It is better to have less support alcohol groups (-OH) on the support surface, however it is practically impossible to remove them all. Preferably the alcohol group (-OH) content is 0.1 to 10 mmol/g, more preferably 0.1 to 1 mmol/g, and most preferably 0.1 to 0.5 mmol/g. The alcohol group (-OH) content can be controlled by the support manufacture condition or drying condition (temperature, time and drying methods such as vacuum drying or spray drying). In order to prevent side reaction due to the trace OH group remaining after drying, it is possible to use a support whose alcohol groups (-OH) are removed chemically while preserving the highly

reactive siloxane groups (Korea Patent Publication No. 2001-003325).

The first metallocene compound is reacted with the support to prepare a first supported catalyst. The first metallocene compound is contacted with the support having highly reactive siloxane groups on the surface. From the reaction of the first metallocene compound and the support, one of the carbon-oxygen bonds present in a radical represented by Chemical Formula a, Chemical Formula b or Chemical Formula c is broken, and a new chemical bonding is formed to give the first supported catalyst.

The contact reaction of the first metallocene compound and the support can be carried out with or without a solvent. For the solvent, aliphatic hydrocarbon solvents such as hexane and pentane, aromatic hydrocarbon solvents such as toluene and benzene, chlorine substituted hydrocarbon solvents such as dichloromethane, ether solvents such as diethyl ether and THF, and other organic solvents such as acetone and ethyl acetate can be used. Preferably, hexane, heptane, toluene or dichloromethane is used.

The reaction temperature can range from -30 ℃ to 150 ℃, preferably from room temperature to 100 ℃, and more preferably from 70 to 90 ℃. The reacted supported catalyst can be used after removing the reaction solvent by filtration or distillation under reduced pressure. If necessary, it can be Soxhlet filtrated with an

aromatic hydrocarbon such as toluene.

The first supported catalyst of the present invention can be used for olefin polymerization without any treatment. The supported hybrid metallocene catalyst of the present invention is obtained by supporting a second metallocene compound, which is an organometallic compound capable of inducing high molecular weight polyolefin, on the first supported catalyst

The second metallocene compound can be supported on the first supported catalyst by two methods.

The first method is to prepare an activated first supported catalyst by activating the first supported catalyst with a cocatalyst as in Scheme 2, and then support the second metallocene compound on the first supported catalyst by contact reaction in a solvent.

The second method is to prepare an activated second metallocene compound by activating the second metallocene compound with a cocatalyst as in Scheme 3, and then support the second metallocene compound on the first supported catalyst by contact reaction in a solvent.

When activating the first supported catalyst or the second metallocene compound, an organometallic compound containing a group XIII metal is used as a cocatalyst. It is a cocatalyst commonly used for olefin polymerization using a

metallocene catalyst. Preferably, a compound represented by the following Chemical Formula 4, Chemical Formula 5 or Chemical Formula 6 is used as a cocatalyst, alone or in combination.

Chemical Formula 4

$-[Al(R^6)-O]_n-$

Here,

R^6 is a C_1 to C_{20} hydrocarbyl radical substituted by identical or different halogen radical, C_1 to C_{20} hydrocarbyl radical or halogen; and

a is an integer larger than 2.

This compound may have a linear, circular or network structure.

Chemical Formula 5

~~$N(R^7)_3$~~ $M'(R^7)_3$

Here,

~~N~~ M' is aluminum or boron; and

R^7 is a C_1 to C_{20} hydrocarbyl radical substituted by identical or different halogen radical, C_1 to C_{20} hydrocarbyl radical or halogen.

Chemical Formula 6

~~$[L-H]^+[NE_4]^-$ or $[L]^+[NE_4]^-$~~ $[L\text{-}H]^+[M'E_4]^-$ or $[L]^+[M'E_4]^-$

Here,

L is a neutral or cationic Lewis acid;

H is a hydrogen atom;

~~N~~M' is a group XIII element, such as aluminum and boron; and

E is a C_6 to C_{40} aryl radical substituted by one or more C_1 to C_{20} hydrocarbyl radicals containing a halogen radical, C_1 to C_{20} hydrocarbyl, alkoxy, phenoxy radical, nitrogen, phosphorus, sulfur or oxygen atom, and the four Es may be identical or different.

For the compound represented by Chemical Formula 4, there are methylaluminoxane (MAO), ethylaluminoxane, isobutylaluminoxane, butylaluminoxane, and so forth.

For the alkyl metal compound represented by Chemical Formula 5, there are trimethylaluminum, triethylaluminum, triisobutylaluminum, tripropylaluminum, tributylaluminum, dimethylchloroaluminum, dimethylisobutylaluminum, dimethylethylaluminum, diethylchloroaluminum, triisopropylaluminum, tri-s-butylaluminum, tricyclopentylaluminum, tripentylaluminum, triisopentylaluminum, trihexylaluminum, ethyldimethylaluminum, methyldiethylaluminum, triphenylaluminum, tri-*p*-tolylaluminum, dimethylaluminummethoxide, dimethylaluminumethoxide, trimethylboron, triethylboron, triisobutylboron, tripropylboron, tributylboron, and so

forth.

For the compound represented by Chemical Formula 6, there are triethylammoniumtetraphenylboron, tributylammoniumtetraphenylboron, trimethylammoniumtetraphenylboron, tripropylammoniumtetraphenylboron, trimethylammoniumtetra(*p*-tolyl)boron, tripropylammoniumtetra(*p*-tolyl)boron, triethylammoniumtetra(*o*,*p*-dimethylphenyl)boron, trimethylammoniumtetra(*o*,*p*-dimethylphenyl)boron, tributylammoniumtetra(*p*-trifluoromethylphenyl)boron, trimethylammoniumtetra(*p*-trifluoromethylphenyl)boron, tributylammonium tetrapentafluorophenylboron, N,N-diethylaniliniumtetraphenylboron, N,N-diethylaniliniumtetraphenylboron, N,N-diethylanilinium tetrapentafluorophenylboron, diethylammoniumtetrapentafluorophenylboron, triphenylphosphoniumtetraphenylboron, trimethylphosphoniumtetraphenylboron, triethylammoniumtetraphenylaluminum, tributylammoniumtetraphenylaluminum, trimethylammoniumtetraphenylaluminum, tripropylammoniumtetraphenylaluminum, trimethylammoniumtetra(*p*-tolyl)aluminum, tripropylammoniumtetra(*p*-tolyl)aluminum, triethylammoniumtetra(*o*,*p*-dimethylphenyl)aluminum, tributylammoniumtetra(*p*-trifluoromethylphenyl)aluminum, trimethylammoniumtetra(*p*-trifluoromethylphenyl) aluminum, tributylammoniumtetrapentafluorophenylaluminum, N,N-diethylaniliniumtetraphenylaluminum, N,N-diethylaniliniumtetraphenylaluminum, N,N-

diethylaniliniumtetrapentafluorophenylaluminum, diethylammonium tetrapentafluorophenylaluminum, triphenylphosphoniumtetraphenylaluminum, trimethylphosphoniumtetraphenylaluminum,triethylammoniumtetraphenylboron, tri butylammoniumtetraphenylboron, trimethylammoniumtetraphenylboron, tripropylammoniumtetraphenylboron, trimethylammoniumtetra(*p*-tolyl)boron, tripropylammoniumtetra(*p*-tolyl)boron, triethylammoniumtetra(*o*,*p*-dimethylphenyl) boron, trimethylammoniumtetra(*o*,*p*-dimethylphenyl)boron, tributylammoniumtetra(*p*-trifluoromethylphenyl)boron, trimethylammoniumtetra(*p*- trifluoromethylphenyl)boron, tributylammoniumtetrapentafluorophenylboron, N,N-diethylaniliniumtetraphenylboron, N,N-diethylaniliniumtetraphenylboron, N,N-diethylaniliniumtetrapentafluorophenylboron, diethylammonium tetrapentafluorophenylboron, triphenylphosphoniumtetraphenylboron, triphenylcarboniumtetraphenylboron, triphenylcarboniumtetraphenylaluminum, triphenylcarboniumtetra(*p*-trifluoromethylphenyl)boron, triphenylcarbonium tetrapentafluorophenylboron, and so forth.

As seen in Scheme 2 and Scheme 3, for the second metallocene compound to be supported effectively, the second metallocene compound should have a functional group (Lewis base) containing one or more group XV or group XVI hetero atoms such as oxygen, sulfur, nitrogen and phosphorus, in cyclopentadiene, the

cyclopentadiene derivative or the bridge group. And, it should be a compound capable of inducing higher molecular weight than the first metallocene compound.

The second metallocene compound having a bridge linkage containing at least one Lewis base in cyclopentadiene, the cyclopentadiene derivative or the bridge group is a compound represented by the following Chemical Formula 2 or Chemical Formula 3. It induces high molecular weight polyolefin during olefin polymerization.

Chemical Formula 2

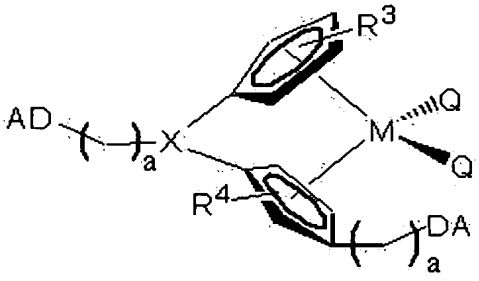

Chemical Formula 3

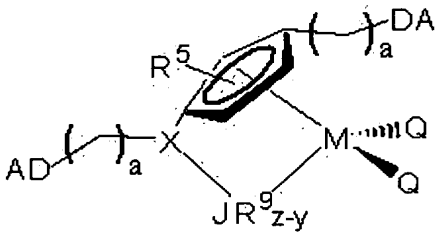

Here,

M is a group IV transition metal;

each of (C_5R^3), (C_5R^4) and (C_5R^5) is a cyclopentadienyl ~~which is a metalloid of a group XIV metal substituted by identical or different hydrogen radical, C_1 to C_{40} alkyl, cycloalkyl, aryl, alkenyl, alkylaryl, arylalkyl, arylalkenyl radical or hydrocarbyl~~; a cyclopentadienyl wherein two neighboring carbon atoms of C_5 are connected by a hydrocarbyl radical to form one or more C_4 to C_{16} ring; or a substituted

cyclopentadienyl ligand;

each of R^3, R^4, and R^5 is identical or different and a substituent selected from hydrogen radical, C_1 to C_{40} alkyl, cycloalkyl, aryl, alkenyl, alkylaryl, arylalkyl, or arylalkenyl radical; and at least one hydrogen radical comprised in the substituent of R^3, R^4, and R^5 is further substituted by a radical represented by the following Chemical Formula a, the following Chemical Formula b, the following Chemical Formula c, or the following Chemical Formula d;

each Q is identical or different halogen radical; C_1 to C_{20} alkyl radical, alkenyl radical, aryl radical, alkylaryl radical, arylalkyl radical; or C_1 to C_{20} alkylidene radical;

~~X is a bridge that binds two cyclopentadienyl ligands or cyclopentadienyl ligands comprising a C_1 to C_4 alkylene radical, dialkyl silicon or germanium, or alkyl phosphine or amine with JR^9_{z-y} by a covalent bond;~~

X is a bridge for binding two cyclopentadienyl ligands or a cyclopentadienyl ligand and JR^9_{z-y} by a covalent bond, which is a radical having the formula of C_mH_{2m-1}, monoalkyl silicon, monoalkyl germanium, phosphine, or amine, wherein m is an integer of 1 to 4;

R^9 is a hydrogen radical, a C_1 to C_{20} alkyl radical, an alkenyl radical, an aryl radical, an alkylaryl radical or an arylalkyl radical;

J is a group XV element or a group XVI element;

D is an oxygen or ~~nitrogen atom~~ amine;

A is a hydrogen radical, a C_1 to C_{20} alkyl radical, an alkenyl radical, an aryl radical, an alkylaryl radical, an arylalkyl radical, an alkylsilyl radical, an arylsilyl radical, methoxymethyl, *t*-butoxymethyl, tetrahydropyranyl, tetrahydrofuranyl, 1-ethoxyethyl, 1-methyl-1- methoxyethyl or *t*-butyl; and

a is an integer of 4 to 8~~; and~~

~~at least one hydrogen radical of R^3, R^4 and R^5 of (C_5R^3), (C_5R^4) and (C_5R^5) is substituted by a radical represented by Chemical Formula a, a radical represented by Chemical Formula b, a radical represented by Chemical Formula c, or a radical represented by the following Chemical Formula d~~:

Chemical Formula d

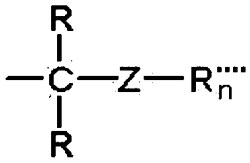

Here,

Z is an oxygen, sulfur, nitrogen, phosphorus or arsenic atom;

each of R is identical or different hydrogen radical, C_1 to C_{40} alkyl, cycloalkyl, aryl, alkenyl, alkylaryl, arylalkyl or arylalkenyl radical;

R"" is a hydrogen radical or C_1 to C_{40} alkyl, aryl, alkenyl, alkylaryl, alkylsilyl, arylsilyl, phenyl or substituted phenyl; and

n is 1 or 2, where if Z is oxygen or sulfur n is 1, and if Z is nitrogen, phosphorus or arsenic n is 2.

A typical example of the second metallocene compound of the present invention is $[(A\text{-}D\text{-}(CH_2)_a)(CH_3)X(C_5H_4)(9\text{-}C_{13}H_9)]ZrCl_2$ or $[(A\text{-}D\text{-}(CH_2)_a)](CH_3)X(C_5Me_4)(NCMe_3)]TiCl_2$. Preferably, a is an integer of 4 to 8, X is ~~methylene, ethylene~~ CH, C_2H_3, or silicon, D is an oxygen or ~~nitrogen atom~~ amine, and A is selected from a group consisting of hydrogen, C_1 to C_{20} alkyl, alkenyl, aryl, alkylaryl, arylalkyl, alkylsilyl, arylsilyl, methoxymethyl, *t*-butoxymethyl, tetrahydropyranyl, tetrahydrofuranyl, 1-ethoxyethyl, 1-methyl-1-methoxyethyl or *t*-butyl.

Typical but non-restrictive molecular structures of the second metallocene compound of the present invention are as follows:

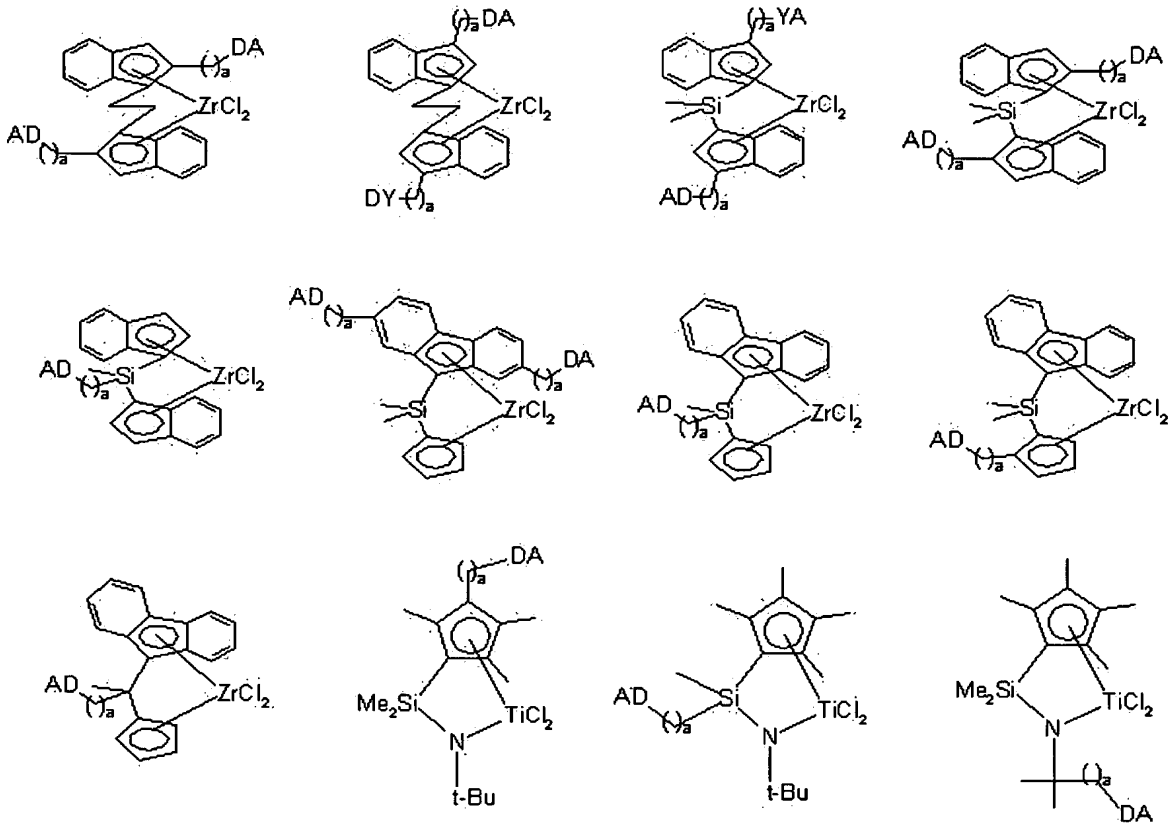

Here, definitions of D, A and a are the same as those in Chemical Formula 2 and Chemical Formula 3.

The group IV metal content of the finally obtained supported hybrid metallocene catalyst of the present invention is 0.1 to 20 wt%, preferably 0.1 to 10 wt%, and more preferably 1 to 3 wt%.

The molar ratio of [group XIII metal]/[group IV metal] of the supported hybrid metallocene catalyst is 1 to 10,000, preferably 1 to 1,000, and more preferably 10 to 100.

The molar ratio of the second metallocene compound to the first metallocene compound is recommended to be 0.01 to 100 for better control of the molecular weight distribution of the target polyolefin (Mw/Mn = 3 to 50).

The supported hybrid metallocene catalyst of the present invention can be used for olefin polymerization without any treatment. Also, it can be prepared into a pre-polymerized catalyst by contacting the hybrid catalyst with an olefinic monomer such as ethylene, propylene, 1-butene, 1-hexene and 1-octene.

For the polymerization process using the supported hybrid metallocene catalyst of the present invention, a solution process, a slurry process, a gas phase process or a combination of slurry and gas phase processes can be applied. A slurry process or a gas phase is preferable, and a slurry process or a gas phase using a single reactor is more preferable.

The supported hybrid metallocene catalyst of the present invention can be used in an olefin polymerization process after diluted into a slurry using an appropriate C_5 to C_{12} aliphatic hydrocarbon solvent, such as pentane, hexane, heptane, nonane, decane and isomers thereof, an aromatic hydrocarbon solvent such as toluene and benzene, or a hydrocarbon solvent substituted by a chlorine atom, such as dichloromethane and chlorobenzene. Preferably, the solvent is treated with a trace of aluminum to remove catalytic poisons like water, air, and so

forth.

Olefinic monomers such as ethylene, propylene, α-olefin and cyclic olefin can be polymerized using the supported hybrid metallocene catalyst of the present invention. Also, dienic olefinic monomers or trienic olefinic monomers having two or more double bonds can be polymerized. Examples of such monomers are ethylene, propylene, 1-butene, 1-pentene, 4-methyl-1-pentene, 1-hexene, 1-heptene, 1-decene, 1-undecene, 1-dodecene, 1-tetradecene, 1-hexadecene, 1-icosene, norbornene, norbornadiene, ethylidenenorbornene, vinylnorbornene, dicyclopentadiene, 1,4-butadiene, 1,5-pentadiene, 1,6-hexadiene, styrene, α-methylstyrene, divinylbenzene and 3-chloromethylstyrene. These monomers can also be polymerized in combination.

The temperature for polymerizing these monomers using the supported hybrid metallocene catalyst of the present invention is 25 to 500 °C, preferably 25 to 200 °C, and more preferably 50 to 100 °C. And, the polymerization pressure is 1 to 100 Kgf/cm^2, preferably 1 to 50 Kgf/cm^2, and more preferably 5 to 15 Kgf/cm^2.

With the supported hybrid metallocene catalyst of the present invention, which is obtained by supporting two or more different metallocenic transition compound catalysts capable of polymerizing polyolefins with different molecular weights on a metal oxide support such as silica, the physical properties and

molecular weight distribution of polyolefin can be easily controlled. A polyolefin prepared using the supported hybrid metallocene catalyst has a variety of physical properties and molecular weight distribution, and can be molded into various products, including rotation molded products, injection molded products, films, containers, pipes and fibers.

Hereinafter, the present invention is described in more detail through Examples and Comparative Examples. However, the following Examples are only for the understanding of the present invention, and the present invention is not limited by the following Examples.

EXAMPLES

Organic reagents and solvents for catalyst preparation and polymerization were purchased from Aldrich and purified by the standard methods. Ethylene (high purity) was purchased from Applied Gas Technology and filtered to remove moisture and oxygen before polymerization. Catalyst preparation, supporting and polymerization were carried out isolated from air and moisture to ensure reproducibility.

A 300 MHz NMR (Bruker) spectrum was obtained to identify the catalyst structure.

The apparent density was determined with Apparent Density Tester 1132

(APT Institute fr Prftechnik) according to DIN 53466 and ISO R 60.

The molecular weight and molecular weight distribution were determined from the GPC (gel permeation chromatography) analysis using Waters' 150CV+. The analysis temperature was 140 °C. Trichlorobenzene was used as a solvent, and the number-average molecular weight (M_n) and weight-average molecular weight (M_w) were determined after standardizing with polystyrene. The molecular weight distribution (polydispersity index, PDI) was calculated by dividing the weight-average molecular weight by the number-average molecular weight.

The polymer's melt index (MI) was determined by ASTM D-1238 (Condition: E, F, 190 °C). I_2 is the value determined at Condition E, and I_{21} is the value determined at Condition F. I_5 is an MI determined at a load of 5 Kg with other conditions the same. The polymer's density was determined by ASTM D-1505-68.

Preparation Example 1: Preparation of the first metallocene catalyst – Synthesis of $[Me_3SiO\text{-}(CH_2)_6\text{-}C_5H_4]_2ZrCl_2$

50 mL of pyridine was added to a flask containing 9.74 g of 1,6-hexanediol and 15.7 g of *p*-toluenesulfonyl chloride. The flask was put in a refrigerator and let alone for a day. 500 mL of 2 N HCl was added to the flask and extraction was carried out using 100 mL of diethyl ether. A small amount of moisture dissolved in ether was removed with anhydrous $MgSO_4$. After filtration, the ether was removed

by distillation under reduced pressure. From a column chromatography using silica gel and a diethyl ether solvent, 9.00 g of a compound with only one hydroxyl group tosylated was obtained (yield: 40 %).

100 mL of anhydrous THF was added to 8.12 g of the compound. Then, 45 mL of 2 N sodium cyclopentadiene (NaCp) was added in an ice bath. Three hours later, 200 mL of water was added and extraction was carried out using 100 mL of hexane. From a column chromatography using silica gel and hexane and diethyl ether (v/v = 1:1), 4.07 g of a 6-(hydroxy)hexylcyclopentadiene compound was obtained (yield: 82 %).

17.9 mmol of this compound was dissolved in 25 mL of THF. Then, 2.7 mL of chlorotrimethylsilane and 3.00 mL of triethylamine were added sequentially. All volatile materials were removed at vacuum and filtration was carried out using hexane. After removing the hexane by distillation under reduced pressure, distillation under reduced pressure (78 °C/0.2 torr) was carried out to obtain 3.37 g of a cyclopentadiene compound having a trimethylsilyl protected hydroxyl group, which is one of the first metallocene catalyst (yield: 79 %). Its structure was analyzed by ^{1}H NMR.

^{1}H NMR (300 MHz, $CDCl_3$): 6.5 - 5.9 (m, 3 H), 3.55 (t, 2 H), 2.92 (s, 1 H), 2.85 (s, 1 H), 2.33 (quintet, 2 H), 1.6 - 1.2 (m, 8 H), 0.09 (s, 9 H).

11.4 mmol of this compound was dissolved in 20 mL of THF. Then, 1.22 g of solid lithium diisopropylamide was added at -78 °C without contact with air. After slowly heating to room temperature, stirring was carried out for two hours. All volatile materials were removed with a vacuum pump, and then 20 mL of THF was added. After adding 2.15 g of $ZrCl_4(THF)_2$, stirring was carried out for 40 hours at 60 °C. All volatile materials were removed with a vacuum pump, and extraction was carried out using a mixture solvent of toluene and hexane. Then, 2.0 mL of chlorotrimethylsilane was added. After letting alone at room temperature for one hour, the compound was put in a refrigerator to obtain a white solid (yield: 70 %).

^1H NMR (300 MHz, $CDCl_3$): 6.34 (s, 2 H), 6.25 (s, 2 H), 3.62 (t, 2 H), 2.68 (t, 2 H), 1.6 - 1.2 (m, 8 H), 0.17 (s, 9 H).

Preparation Example 2: Preparation of the first metallocene catalyst – Synthesis of $[t\text{-Bu-O-}(CH_2)_6\text{-}C_5H_4]_2ZrCl_2$

t-Butyl-O-$(CH_2)_6$-Cl was prepared using 6-chlorohexanol according to the method reported in literature (*Tetrahedron Lett.* 2951 (1988)). NaCp was reacted with the compound as in Preparation Example 1 to obtain *t*-butyl-O-$(CH_2)_6$-C_5H_5 (yield: 60 %, b.p. 80 °C / 0.1 mmHg). Zirconium was attached by the same method to obtain another compound, which is also one of the target catalysts (yield: 92 %).

^1H NMR (300 MHz, $CDCl_3$): 6.28 (t, J = 2.6 Hz, 2 H), 6.19 (t, J = 2.6 Hz, 2 H),

3.31 (t, 6.6 Hz, 2 H), 2.62 (t, J = 8 Hz), 1.7 - 1.3 (m, 8 H), 1.17 (s, 9 H); ^{13}C NMR ($CDCl_3$): 135.09, 116.66, 112.28, 72.42, 61.52, 30.66, 30.61, 30.14, 29.18, 27.58, 26.00.

Preparation Example 3: Preparation of the second metallocene catalyst – Synthesis of *t*-Bu-O-$(CH_2)_6$)$(CH_3)Si(C_5H_4)(9\text{-}C_{13}H_9)ZrCl_2$

A *t*-Bu-O-$(CH_2)_6Cl$ compound and Mg(0) were reacted in a diethyl ether (Et_2O) solvent to obtain 0.14 mol of a *t*-Bu-O-$(CH_2)_6MgCl$ solution, which is a Grignard reagent. Then, a $MeSiCl_3$ compound (24.7 mL, 0.21 mol) was added at -100 °C. Strring was carried out for over 3 hours at room temperature. Then, the solution was filtered and dried at vacuum to obtain a *t*-Bu-O-$(CH_2)_6SiMeCl_2$ compound (yield: 84 %).

A fluorenyllithium (4.82 g, 0.028 mol)/hexane (150 mL) solution was slowly added for 2 hours to a *t*-Bu-O-$(CH_2)_6SiMeCl_2$ (7.7 g, 0.028 mol) solution dissolved in hexane (50 mL) at -78 °C. A white precipitate (LiCl) was filtered out, and extraction was carried out using hexane. All volatile materials were removed by vacuum drying to obtain a pale yellow oily (*t*-Bu-O-$(CH_2)_6)SiMe(9\text{-}C_{13}H_{10})$ compound (yield: 99 %).

A THF solvent (50 mL) was added, and a reaction with a C_5H_5Li (2.0 g, 0.028 mol)/THF (50 mL) solution was carried out at room temperature for over 3

hours. All volatile materials were removed by vacuum drying and extraction was carried out using hexane to obtain an orange oily (*t*-Bu-O-$(CH_2)_6$)$(CH_3)Si(C_5H_5)$(9-$C_{13}H_{10}$) compound, which is the target ligand (yield: 95 %). The structure of the ligand was identified by ^1H NMR.

^1H NMR (400MHz, $CDCl_3$): 1.17, 1.15 (*t*-BuO, 9H, s), -0.15, -0.36 (MeSi, 3H, s), 0.35, 0.27 (CH_2, 2H, m), 0.60, 0.70 (CH_2, 2H, m), 1.40, 1.26 (CH_2, 4H, m), 1.16, 1.12 (CH_2, 2H, m), 3.26 (*t*-BuOCH_2, 2H, t, 3JH-H = 7Hz), 2.68 (methylene CpH, 2H, brs), 6.60, 6.52, 6.10 (CpH, 3H, brs), 4.10, 4.00 (FluH, 1H, s), 7.86 (FluH, 2H, m), 7.78 (FluH, 1H, m), 7.53 (FluH, 1H, m), 7.43-7.22 (FluH, 4H, m)

Two equivalents of *n*-BuLi was added to a (*t*-Bu-O-$(CH_2)_6$)$(CH_3)Si(C_5H_5)$ (9-$C_{13}H_{10}$) (12 g, 0.028 mol)/THF (100 mol) solution at -78 ℃. Heating to room temperature, a reaction was carried out for over 4 hours to obtain an orange solid (*t*-Bu-O-$(CH_2)_6$)$(CH_3)Si(C_5H_5Li)$(9-$C_{13}H_{10}Li$) compound (yield: 81 %).

A dilithium salt (2.0 g, 4.5 mmol)/ether (30 mL) solution was slowly added to a $ZrCl_4$ (1.05 g, 4.50 mmol)/ether (30 mL) suspension at -78 ℃. A reaction was carried out for 3 hours at room temperature. All volatile materials were removed by vacuum drying, and the resultant oily liquid was filtered by adding a dichloromethane solvent. The filtered solution was vacuum dried, and hexane was added to induce precipitation. The resultant precipitate was washed several times with hexane to

obtain a red solid racemic-(*t*-Bu-O-$(CH_2)_6$)$(CH_3)Si(C_5H_4)(9\text{-}C_{13}H_9)ZrCl_2$ compound (yield: 54 %).

^{1}H NMR (400MHz, $CDCl_3$): 1.19 (*t*-BuO, 9H, s), 1.13 (MeSi, 3H, s), 1.79 (CH_2, 4H, m), 1.60 (CH_2, 4H, m), 1.48 (CH_2, 2H, m), 3.35 (*t*-BuOCH_2, 2H, t, 3JH-H = 7Hz), 6.61 (CpH, 2H, t, 3JH-H = 3Hz), 5.76 (CpH, 2H, d, 3JH-H = 3Hz), 8.13 (FluH, 1H, m), 7.83 (FluH, 1H, m), 7.78 (FluH, 1H, m), 7.65 (FluH, 1H, m), 7.54 (FluH, 1H, m), 7.30 (FluH, 2H, m), 7.06 (FluH, 1H, m)

^{13}C NMR (400MHz, $CDCl_3$): 27.5 (Me3CO, q, 1JC-H = 124Hz), -3.3 (MeSi, q, 1JC-H = 121Hz), 64.6, 66.7, 72.4, 103.3, 127.6, 128.4, 129.0 (7C, s), 61.4 (Me_3COCH_2, t, 1JC-H = 135Hz), 14.5 (ipso-$SiCH_2$, t, 1JC-H = 122Hz), 33.1, 30.4, 25.9, 22.7 (4C, t, 1JC-H = 119Hz), 110.7, 111.4, 125.0, 125.1, 128.8, 128.1, 126.5, 125.9, 125.3, 125.1, 125.0, 123.8 (FluC and CpC, 12C, d, 1JC-H = 171Hz, 3JC-H = 10Hz)

Preparation Example 4: Preparation of the second metallocene catalyst – Synthesis of $(CH_3)_2Si$(*t*-Bu-O-$(CH_2)_6$-$(C_5H_4)(9\text{-}C_{13}H_9)ZrCl_2$

A $Me_2SiCl(9\text{-}C_{13}H_{10})$ compound was obtained from a reaction of fluorenyllithium and Me_2SiCl_2 in hexane. After adding a *t*-Bu-O-$(CH_2)_6$-C_5H_5Li (0.016 mol; obtained from a reaction of *t*-Bu-O-$(CH_2)_6$-C_5H_5 and *n*-BuLi in THF) solution to a $Me_2SiCl(9\text{-}C_{13}H_{10})$ solution dissolved in a THF solvent (50 mL) at room

temperature, the reaction temperature was slowly increased to room temperature. The mixture was reacted for over 3 hours at room temperature, and all volatile materials were removed by vacuum drying. Hexane was added to the resultant oily liquid. The hexane solution was filtered and vacuum dried to obtain a pale yellow oily ($(CH_3)_2Si$(*t*-Bu-O- $(CH_2)_6$-(C_5H_5)(9-$C_{13}H_{10}$)) ligand (yield: 99 %). The structure of the ligand was identified by ^1H NMR.

^1H NMR (400MHz, C_6D_6): 1.09 (*t*-BuO, 9H, s), -0.13, -0.32, -0.61 (Me_2Si, 6H, s), 1.25 (CH_2, 2H, m), 1.24 (CH_2, 2H, m), 1.41 (CH_2, 4H, m), 2.25 (Cp-CH_2, 2H, m), 3.23 (*t*-$BuOCH_2$, 2H, d of t, 3JH-H = 7Hz), 6.35, 6.05, 5.70 (CpH, 5H, m, m, brs), 3.05 (methylene CpH, 2H, brs), 4.20, 4.00, 3.85 (FluH, 1H, s), 7.80 (FluH, 2H, m), 7.45 (FluH, 2H, m), 7.29-7.20 (FluH, 4H, m).

From a reaction of a dilithium salt and a $ZrCl_4$ compound, an orange solid racemic-$(CH_3)_2Si$(*t*-Bu-O-$(CH_2)_6$-(C_5H_4)(9-$C_{13}H_9$)$ZrCl_2$ compound, as in Preparation Example 3 (yield: 25 %).

^1H NMR (400MHz, $CDCl_3$): 1.16 (*t*-BuO, 9H, s), 1.11 (Me_2Si, 3H, s), 1.13 (Me_2Si, 3H, s), 1.43 (CH_2, 4H, m), 1.25 (CH_2, 4H, m), 2.45 (Cp-CH_2, 2H, m), 3.26 (*t*-$BuOCH_2$, 2H, t, 3JH-H = 7Hz), 5.41 (CpH, 1H, t, 3JH-H = 3Hz), 5.70 (CpH, 1H, t, 3JH-H = 3Hz), 6.28 (CpH, 1H, t, 3JH-H = 3Hz), 8.13 (FluH, 2H, m), 7.67-7.49 (FluH, 4H, m), 7.29 (FluH, 2H, m).

^{13}C NMR (400MHz, $CDCl_3$): 27.5 (Me_3CO, q, 1JC-H = 125Hz), -3.3 (Me_2Si, q, 1JC-H = 121Hz), 27.6, 66.3, 72.4, 102.6, 113.8, 128.8, 129.1, 141.9 (9C, s), 61.5 (Me_3COCH_2, t, 1JC-H = 141Hz), 30.5, 30.2, 30.0, 29.2, 25.9 (5C, t, 1JC-H = 124Hz), 111.6, 112.0, 119.7, 123.8, 123.9, 125.0, 126.3, 126.5, 128.0, 128.1, 128.7 (FluC and CpC, 11C d, 1JC-H = 161Hz, 3JC-H = 10Hz)

Preparation Example 5: Preparation of the second metallocene catalyst – Synthesis of (*t*-Bu-O-$(CH_2)_6$)$(CH_3)C(C_5H_4)$(9-$C_{13}H_9$)$ZrCl_2$

Pyrrolidine (12.5 mL, 0.15 mol) was added to a mixture of 8-butoxy-2-octanone (13.5 g, 0.067 mol) and cyclopentadiene monomer (9.0 g, 0.14 mol) in an anhydrous methanol solvent (200 mL) at room temperature. A reaction was carried out for 12 hours. An acetic acid (12 g, 0.2 mol)/water(200 mL) solution was added to the reaction solution. After stirring for an hour, the organic layer was extracted with an ether solvent (300 mL). The resultant liquid was distilled under reduced pressure (100 ℃, 500 mtorr) to obtain a pale yellow oily 6-methyl-6-*t*-butoxyhexylfulvene(6- methyl-6-*t*-buthoxyhexylfulvene) compound (yield: 40 %).

A fluorenyllithium (4.48 g, 0.026 mol)/THF (100 mL) solution was slowly added to a 6-methyl-6-*t*-butoxyhexylfulvene (6.5 g, 0.026 mol) solution dissolved in a THF solvent (50 mL) at -78 ℃. Stirring was carried out for 12 hours at room temperature. A saturated NH_4Cl/water solution and an ether solvent were added to

the reaction solution to extract the organic layer. From a chromatography, a yellow oily (*t*-Bu-O-$(CH_2)_6$)$(CH_3)C(C_5H_5)$(9-$C_{13}H_{10}$) ligand was obtained (yield: 97 %).

^{1}H NMR (400MHz, $CDCl_3$): 1.19 (*t*-BuO, 9H, s), 0.58, 0.89 (MeC, 3H, s), 1.90 (CH_2, 2H, m), 1.49 (CH_2, 2H, m), 1.30 (CH_2, 4H, m), 1.27 (CH_2, 2H, m), 3.31 (*t*-BuOCH_2, 2H, t, 3JH-H = 7Hz), 6.88, 6.62, 5.87 (CpH, 3H, brs), 3.07 (methylene CpH, 2H, brs), 4.15 (FluH, 1H, s), 7.72 (FluH, 1H, m), 7.67 (FluH, 1H, m), 7.55 (FluH, 1H, m), 7.36 (FluH, 1H, m), 7.28 (FluH, 1H, m), 7.24 (FluH, 1H, m), 7.04 (FluH, 1H, m), 6.76 (FluH, 1H, m)

Two equivalents of *n*-BuLi (1.6 M in hexane) was added to a (*t*-Bu-O-$(CH_2)_6$)$(CH_3)C(C_5H_5)$(9-$C_{13}H_{10}$) (3.2 g, 0.008 mol)/THF (50 mL) solution at -78 ℃. Stirring was carried out for 5 hours at room temperature to obtain a red solid (*t*-Bu-O-$(CH_2)_6$)$(CH_3)C(C_5H_4Li)$(9-$C_{13}H_9Li$) compound (yield: 88 %).

A dilithium salt (2.5 g, 4.4 mmol)/hexane (50 mL) solution was slowly added to a $ZrCl_4$ (1.02 g, 4.5 mmol)/hexane (50 mL) suspension at -78 ℃, and stirring was carried out for 12 hours at room temperature. All volatile materials were removed by vacuum drying. After extracting with a toluene (100 mL) solvent and washing several times with hexane, a red solid racemic-(*t*-Bu-O-$(CH_2)_6$)$(CH_3)C(C_5H_4)$ (9-$C_{13}H_9$)$ZrCl_2$ compound was obtained (yield: 31 %).

^{1}H NMR (400MHz, $CDCl_3$): 1.18 (*t*-BuO, 9H, s), 2.39 (MeC, 3H,s), 1.82 (CH_2,

2H, m), 1.59 (CH_2, 4H, m), 1.46 (CH_2, 2H, m), 1.22 (CH_2, 2H, m), 3.34 (*t*-$BuOCH_2$, 2H, t, 3JH-H = 7Hz), 6.33 (CpH, 2H, t, 3JH-H = 2Hz), 5.80-5.75 (CpH, 2H, m), 7.27 (FluH, 2H, m), 7.56 (FluH, 2H, m), 7.63 (FluH, 1H, d, 3JH-H = 9Hz), 7.82 (FluH, 1H, d, 3JH-H = 9Hz), 8.14 (FluH, 2H, m).

^{13}C NMR (400MHz, $CDCl_3$): 27.5 (Me_3CO, q, 1JC-H = 124Hz), -3.3 (MeSi, q, 1JC-H = 121Hz), 64.6, 66.7, 72.4, 103.3, 127.6, 128.4, 129.0 (7C, s), 61.4 (Me_3COCH_2, t, 1JC-H = 135Hz), 14.5 (ipso-SiCH2, t, 1JC-H = 122Hz), 33.1, 30.4, 25.9, 22.7 (4C, t, 1JC-H = 119Hz), 110.7, 111.4, 125.0, 125.1, 128.8, 128.1, 126.5, 125.9, 125.3, 125.1, 125.0, 123.8 (FluC and CpC, 12C, d, 1JC-H = 171Hz, 3JH-H = 10Hz)

Preparation Example 6: Preparation of the second metallocene catalyst – Synthesis of $(CH_3)_2C$(*t*-Bu-O-$(CH_2)_6$-(C_5H_4)(9-$C_{13}H_9$)$ZrCl_2$

A 6,6-dimethyl-3-(6-*t*-butoxyhexyl)fulvene compound was obtained using *t*-butoxyhexylcyclopentadiene and anhydrous acetone, as in Preparation Example 5 (yield: 59 %). A fluorenyllithium compound was used to obtain a yellow oily $(CH_3)_2C$(*t*-Bu-O-$(CH_2)_6$-(C_5H_5)(9-$C_{13}H_{10}$) ligand (yield: 70 %).

^1H NMR (400MHz, $CDCl_3$): 1.19, 1.20 (*t*-BuO, 9H, s), 1.06, 1.05, 1.02 (Me_2C, 6H, s), 1.27 (CH_2, 2H, m), 1.41 (CH_2, 2H, m), 1.58 (CH_2, 4H, m), 2.50, 2.46, 2.36 (Cp-CH_2, 2H, t, 3JH-H = 7Hz), 3.36 (*t*-$BuOCH_2$, 2H, d of t, 3JH-H = 7Hz), 6.53, 6.10,

6.00, 5.97, 5.69 (CpH, 5H, brs), 3.07 (methylene-CpH, 2H, brs), 4.14, 4.11, 4.10 (FluH, 1H, s), 7.70 (FluH, 2H, m), 7.33 (FluH, 2H, m), 7.23-7.10 (FluH, 4H, m).

From a reaction of a dilithium salt and a $ZrCl_4$ compound as in Preparation Example 5, an orange solid racemic-$(CH_3)_2C$(*t*-Bu-O-$(CH_2)_6$-(C_5H_4)(9-$C_{13}H_9$)$ZrCl_2$ compound was obtained (yield: 63 %).

^{1}H NMR (400MHz, $CDCl_3$): 1.16 (*t*-BuO, 9H, s), 2.35 (Me_2C, 3H, s), 2.40 (Me_2C, 3H, s) 1.46 (CH_2, 4H, m), 1.27 (CH_2, 4H, m), 1.20 (CH_2, 2H, m), 2.52 (Cp-CH_2, 2H, m), 3.27 (*t*-BuOCH_2, 2H, t, 3JH-H = 7Hz), 5.43 (CpH, 1H, t, 3JH-H = 3Hz), 5.67 (CpH, 1H, t, 3JH-H = 3Hz), 6.01 (CpH, 1H, t, 3JH-H = 3Hz), 8.15 (FluH, 2H, m), 7.80 (FluH, 2H, m), 7.54 (FluH, 2H, m), 7.26 (FluH, 2H, m)

^{13}C NMR (400MHz, $CDCl_3$): 27.5 (Me_3CO, q, 1JC-H = 124Hz), 15.3 (Me_2C, q, 1JC-H = 124Hz), 40.4 (Me_3C, s), 25.9 (Me_2C, s), 68.1, 72.4, 78.8, 113.8, 122.6, 136.4, 142.0 (7C, s), 61.5 (Me_3COCH_2, t, 1JC-H = 140Hz), 65.8 ($CpCH_2$, t, 1JC-H = 138Hz), 30.5, 29.7, 29.2, 27.6 (4C, t, 1JC-H = 124Hz), 103.0, 103.1, 117.2, 128.9, 128.2, 125.3, 124.9, 124.8, 123.4, 123.2, 123.1 (FluC and CpC, 11C d, 1JC-H = 171Hz, 3JC-H = 10Hz)

Preparation Example 7: Preparation of the second metallocene catalyst – Synthesis of [$(CH_3)_2Si(^tPr_2$-N-E *t*-(C_5H_4))(9-$C_{13}H_9$)]$ZrCl_2$

A [$(CH_3)_2Si(^tPr_2$-N(Et)(C_5H_4))(9-$C_{13}H_9$)]$ZrCl_2$ compound having an amine

group in cyclopentadiene was prepared by the method presented in literature (*Angew. Chem.* Int Ed., 39, 2000, 789).

Examples 1 to 11: Preparation of supported hybrid catalyst

Drying of support

Silica (XPO 2412, Grace Davison) was dehydrated for 15 hours at 800 ℃ in vacuum.

Preparation of the first supported catalyst

1.0 g of the silica was put in a glass reactor. After adding 10 mL of hexane, 10 mL of each hexane solution dissolving 50, 100 and 200 mg of the first metallocene compound prepared in Preparation Examples 1 and 2 was added. Then, a reaction was carried out for 4 hours at 90 ℃ while stirring the reactor. After the reaction was completed, the hexane was removed by layer separation. After washing three times with 20 mL of a hexane solution, the hexane was removed by suction to obtain a solid powder.

Preparation of the second supported catalyst – activation of the first supported catalyst

A methylaluminoxane (MAO) solution containing 12 mmol of aluminum in a toluene solution was added to the first supported catalyst. A reaction was carried out at 40 ℃ while stirring. The unreacted aluminum compound was removed by

washing a sufficient amount of toluene. Then, the remaining toluene was removed by suction at 50 ℃. The resultant solid can be used as a catalyst for olefin polymerization without further treatment.

Preparation of supported hybrid catalyst

A toluene solution, dissolving 50, 100 and 200 mg of each second metallocene compound prepared in Preparation Examples 3 to 7 respectively, was added to the second supported catalyst in a glass reactor. A reaction was carried out at 40 ℃ while stirring the reactor. After washing with a sufficient amount of toluene, drying was carried out to obtain a solid powder.

The resultant supported hybrid catalyst can be used as a catalyst without further treatment. Or, 30 psig of ethylene may be added for 2 minutes and a pre-polymerization can be carried out for an hour room temperature. To prove that the supported catalyst has a superior properties, such pre-polymerization was not carried out. The powder was vacuum dried to obtain a solid catalyst.

Comparative Examples 1 to 3

A first supported catalyst, on which only the first metallocene catalyst of Preparation Example 1 and Preparation Example 2 was supported (see Table 1), was prepared by the method for preparing the first supported catalyst of Examples 1 to 11 (see Fig. 2).

Comparative Example 4

A first supported catalyst, on which only the second metallocene compound of Preparation Example 3 was supported (see Table 1), was prepared by the method for preparing the first supported catalyst of Examples 1 to 11.

Example 12: Semibatch ethylene polymerization

50 mg of each supported catalyst prepared in Examples 1 to 11 and Comparative Examples 1 to 4 was weighed in a dry box and put in a 50 mL glass bottle. The bottle was sealed with a rubber diaphragm and taken out of the dry box, and a catalyst was ready for injection. The polymerization was performed in a 2 L metal alloy reactor for high pressure, equipped with a mechanical stirrer and capable of temperature control.

1 L of hexane dissolving 1.0 mmol of triethylaluminum and the prepared supported catalyst were added to the reactor without contact with air. The polymerization was carried out for an hour at 80 °C, continuously applying a gaseous ethylene monomer at a pressure of 9 Kgf/cm^2. The polymerization was terminated by stopping the stirring and exhausting the ethylene.

The resultant polymer was filtered through a polymerization solvent and dried in an 80 °C vacuum oven for 4 hours.

The ethylene polymerization activity, melt index of the polymer, apparent

density, molecular weight and molecular weight distribution for each prepared catalyst are shown in Table 2 below.

In ethylene polymerization using the supported catalysts of the present invention, there was no fouling, or sticking of polymer particles to the reactor wall or one another. Also, the apparent density was superior (0.34 to 0.45 g/cc). In addition, the weight-average molecular weight (M_w) could be controlled in the range of 180,000 to 600,000, and the molecular weight distribution could be controlled in a wide range of 2.5 to 11. The obtained polymer had a good shape (see Fig. 1).

Comparative Example 5

A first supported catalyst was prepared using bis(octylcyclopentadienyl) zirconium dichloride disclosed in US Patent No. 5,324,800, which has no functional group that can react with silica, by the method of Examples 1 to 11. The polymerization was carried out after a pre-polymerization.

50 mg of the supported catalyst was taken, and the polymerization was performed as in Example 12. The yield was 120 g. During the pre-polymerization and the polymerization, there occurred a severe fouling. The resultant particles had poor shape, and the apparent density was only 0.04 g/mL.

Comparative Example 6

A [2-ethoxyethyl-O-$(CH_2)_6$-$C_5H_4]_2ZrCl_2$ compound comprising only primary

alkyls, so as to have a relatively high Lewis basicity and having as many as four oxygen atoms, so as to easily bind to an inorganic support by a Lewis acid-base reaction, but having a structure in which the carbon-oxygen bond is difficult to be broken, which is similar to the catalyst presented as an example in US Patent No. 5,814,574 and US Patent No. 5,767,209, was synthesized by the method presented in literature (*J. Organomet. Chem.*, 552, 1998 313). The supporting was carried out by the same method of Examples 1 to 11. The polymerization was carried out after a pre-polymerization.

50 mg of the supported catalyst was taken, and the polymerization was performed as in Example 12. The yield was only 50 g. During the pre-polymerization and the polymerization, there occurred a severe fouling. The particle shape could not be controlled, and the apparent density was only 0.08 g/mL.

Comparative Example 7

The following test was carried out to prove the strong interaction of the functional group of the second metallocene compound and a group XIII compound (aluminum and boron compound).

Silica (PO 2412, Grace Davison) was dehydrated at 800 °C for 15 hours in vacuum. 10 g of the silica was put in a glass reactor. After adding 50 mL of hexane, 30 mL of a hexane solution dissolving 2 g of $[t\text{-Bu-O-}(CH_2)_6\text{-}C_5H_4]_2ZrCl_2$,

which is the first metallocene catalyst synthesized in Preparation Example 2, was added to the reactor. A reaction was carried out at 90 ℃ for 4 hours while stirring the reactor. After washing with a sufficient amount of hexane, drying was carried out. A methylaluminoxane solution containing 12 mmol of Al/g-silica was added and a reaction was carried out for an hour at 40 ℃.

An $^{i}Pr(C_5H_4)(9\text{-}C_{13}H_9)ZrCl_2$ [isopropyl-(cyclopentadienyl) (fluorenyl)zirconium dichloride] compound with no functional group was supported on the second metallocene compound as in Examples 1 to 11 to obtain the target catalyst.

The obtained solid catalyst was slurry polymerized in a hexane solvent as in Example 12. The resultant polymer showed severe fouling and the polymerization activity was 180 g. Therefore, it can be seen that in case $^{i}Pr(C_5H_4)(9\text{-}C_{13}H_9)ZrCl_2$ having no functional group was introduced as the second metallocene catalyst, there were no supporting effect at all.

As can be seen from above result, the catalyst system of the present invention has a functional group that can interact with the cocatalyst, so that there arises no problem such as fouling during slurry polymerization using a solvent like hexane, because the active ingredient of the catalyst is not leached from the support but tightly attached to the supported catalyst and therefore the polymer is maintained well.

Table 1

Classification	The first metallocene catalyst	Cocatalyst	The second metallocene catalyst	Supporting amount of the first/second metallocenes (g/g in g SiO_2)
Comparative Example 1	Preparation Example 1	-	-	0.2/0.0
Comparative Example 2	Preparation Example 2	-	-	0.2/0.0
Example 1	Preparation Example 2	MAO	Preparation Example 3	0.1/0.05
Example 2	Preparation Example 2	MAO	Preparation Example 3	0.1/0.1
Example 3	Preparation Example 2	MAO	Preparation Example 3	0.1/0.2
Comparative Example 3	Preparation Example 2	-	-	0.05/0.0
Example 4	Preparation Example 2	MAO	Preparation Example 3	0.05/0.05
Example 5	Preparation Example 2	MAO	Preparation Example 3	0.05/0.1
Example 6	Preparation Example 2	MAO	Preparation Example 3	0.05/0.2
Comparative Example 4	-	-	Preparation Example 3	0.0/0.2
Example 7	Preparation Example 2	MAO	Preparation Example 3	0.2/0.1
Example 8	Preparation Example 2	MAO	Preparation Example 3	0.1/0.1
Example 9	Preparation Example 2	MAO	Preparation Example 4	0.1/0.1
Example 10	Preparation Example 2	MAO	Preparation Example 5	0.1/0.1
Example 11	Preparation Example 2	MAO	Preparation Example 6	0.1/0.1
Comparative Example 5	Bis(octylcyclopentadienyl) zirconium dichloride	-	-	0.2/0.0
Comparative Example 6	[2-ethoxyethyl-O-$(CH_2)_6$-C_5H_4]$_2ZrCl_2$	-	-	0.2/0.0
Comparative Example 7	Preparation Example 2	MAO	$^{i}Pr(C_5H_4)(9\text{-}C_{13}H_9)ZrCl_2$	0.2/0.1

Table 2

Classification	Activity (g)	Apparent density (g/cc)	I_2 (g/10min)	I_{21}/I_5	Mw ($x10^3$)	DPI
Comparative Example 1	154	0.34	1.30	7.1	182	2.5
Comparative Example 2	186	0.34	120	7.4	176	2.8
Example 1	143	0.40	0.07	9.3	698	8.9
Example 2	177	0.41	0.04	9.3	735	7.9
Example 3	207	0.42	0.05	9.5	754	9.5
Comparative Example 3	53	0.43	1.30	9.7	218	2.7
Example 4	135	0.42	0.06	6.6	769	7.8
Example 5	158	0.41	0.04	9.6	765	7.3
Example 6	147	0.42	0.03	9.5	722	8.8
Comparative Example 4	155	0.41	0.04	10.5	822	5.2
Example 7	205	0.41	0.10	10.7	637	8.6
Example 8	160	0.40	0.04	9.5	710	8.5
Example 9	165	0.39	0.04	9.7	657	8.4
Example 10	166	0.41	0.04	9.6	667	7.6
Example 11	145	0.41	0.10	7.1	349	6.5
Comparative Example 5	120	0.04	0.70	7.3	290	2.5
Comparative Example 6	50	0.08	0.56	7.2	377	2.7
Comparative Example 7	180	0.12	0.10	8.3	585	5.7

Examples13 and 14: Copolymerization of continuous ethylene/α-olefin

1 kg of the supported hybrid catalyst of Example 7 was synthesized. The synthesized catalyst was put in a sealed contained under nitrogen atmosphere,

emulsified in 50 L of purified hexane, and put inside a 100 L stirring tank reactor. The stirring tank reactor was run at 200 rpm. The polymerization was carried out in a 200 L continuous stirring tank reactor for high pressure which is equipped with a mechanical stirrer, capable of temperature control and continuously stirrable at 250 rpm. The polymer slurry leaving the reactor was passed through a centrifuge and a drier to obtain a solid powder. Ethylene was fed at a rate of 10 to 15 kg/hr at 80 °C. The catalyst injection amount was controlled so that the ethylene pressure remains at 8 to 9 kgf/cm^2. Each 10 mL of the catalyst was injected at time intervals. The polymerization time was controlled by the solvent amount so that the stay time in the reactor is 2 to 3 hours. 1-Butene was used as an α-olefin to identify the copolymerization characteristics. A small amount of hydrogen was added to control the molecular weight.

Two polyethylenes were prepared with different injection amount of the catalyst prepared in Example 7 (Examples 13 and 14). The activity, apparent density, density, molecular weight, molecular weight distribution and basic physical properties of each polyethylene are given in the following Table 3.

The catalyst of the present invention caused no process interruption due to fouling. The apparent density of the polymer was good, in the range of 0.3 to 0.5 g/mL.

Table 3

Classification		Example 13	Example 14
Catalyst		Catalyst of Example 7	Catalyst of Example 7
Polymerization process		Continuous hexane slurry polymerization	Continuous hexane slurry polymerization
Comonomer		1-Butene	1-Butene
Activity (kg PE/g catalyst hr)		6.5	6.1
Apparent density (g/cm^3)		0.38	0.40
Density (g/cm^3)		0.945	0.952
MI (2.16kg)		0.02	2.0
MI (21.6kg)		1.42	90.10
MI (21.6kg)/MI (2.16kg)		71	44
Molecular weight distribution		Bimodal	Bimodal
Mw/Mn		8.6	5.6
Tensile characteristics	Tensile strength (kg/cm^2)	280	175
	Tensile elongation (%)	890	650
ESCR, F50 (%)		>1,000	>500
Izod impact strength	Room temperature	NB	NB
	-20 ℃	25	14

The supported metallocene catalyst of the present invention has one site of the ligand of the first metallocene compound strongly attached to the silica surface by chemical bonding. And, since the second metallocene compound which is supported after activation strongly interacts with the activator, few catalyst leaches

out of the surface during the polymerization process. Hence, there occurs no fouling, or sticking of the polymers to the reactor wall or one another, during the slurry polymerization or gas phase polymerization process. Also, the resultant polymer has superior particle shape and apparent density, so that it can be applied to the conventional slurry or gas phase polymerization process. The polyolefin prepared using the supported catalyst of the present invention has a variety of physical properties and molecular weight distribution, so that it can be molded into various products, including rotation molded products, injection molded products, films, containers, pipes and fibers. Particularly, the molecular weight distribution can be controlled with low production cost using a single reactor, thanks to the high polymerization activity.

While the present invention has been described in detail with reference to the preferred embodiments, those skilled in the art will appreciate that various modifications and substitutions can be made thereto without departing from the spirit and scope of the present invention as set forth in the appended claims.

Appendix A

Scheme 2

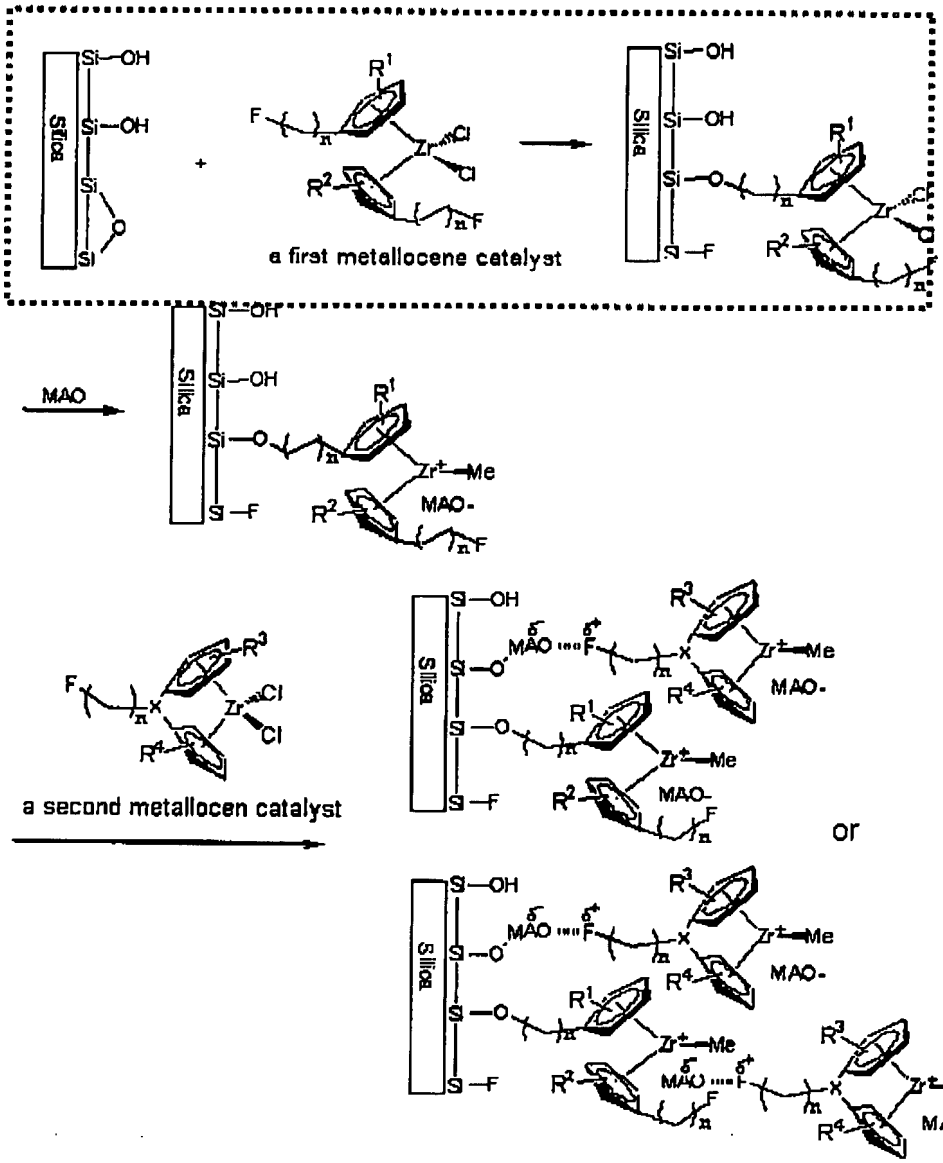

Appendix B

Scheme 3

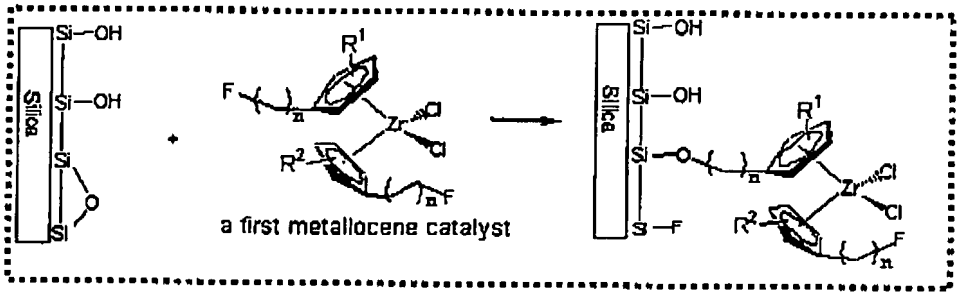

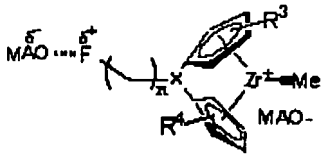

the activated
second metallocen catalyst

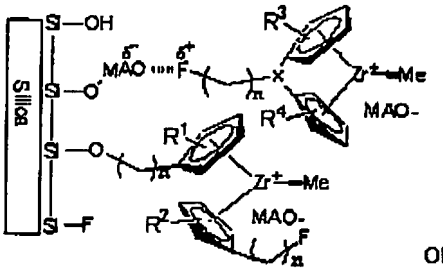

or

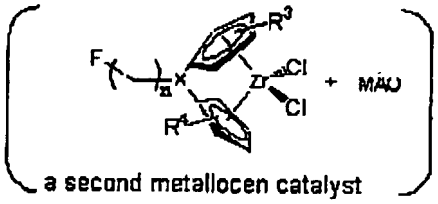

a second metallocen catalyst

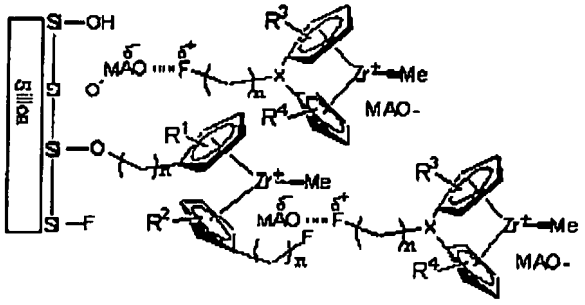

Organometallic Molecule–Inorganic Surface Coordination and Catalytic Chemistry. In Situ CPMAS NMR Delineation of Organoactinide Adsorbate Structure, Dynamics, and Reactivity

William C. Finch, Ralph D. Gillespie, David Hedden, and Tobin J. Marks*

Contribution from the Department of Chemistry, Northwestern University, Evanston, Illinois 60208-3113. *Received November 10, 1989*

Abstract: A 75.4-MHz ^{13}C CPMAS NMR spectroscopic study of the surface structures and reaction chemistry of a series of organoactinides adsorbed on various inorganic supports is reported. On Lewis acid surfaces such as dehydroxylated Al_2O_3, $MgCl_2$, and SiO_2–Al_2O_3, it is found that organothorium complexes of the type Cp'_2ThR_2 ($Cp' = \eta^5$-$(CH_3)_5C_5$; R = $^{13}CH_3$, $^{13}CH_2{}^{13}CH_3$), $Cp'ThR_3$ (R = $^{13}CH_2C_6H_5$), and Cp_3ThR ($Cp = \eta^5$-C_5H_5; R = $^{13}CH_3$), undergo heterolytic Th–C scission to transfer an alkyl anion to the surface forming Cp'_2ThR, $Cp'ThR_{3-n}$, or Cp_3Th adsorbate species with "cation-like" character. Probe studies with paramagnetic $Cp'_2U(^{13}CH_3)_2$ indicate that the majority of the transferred methyl groups of $Cp'_2U(^{13}CH_3)_2$/DA and $Cp'_2U(^{13}CH_3)_2/MgCl_2$ are located $\gtrsim$5 Å from the U(IV) ion. On less dehydroxylated or more basic supports such as SiO_2–MgO, SiO_2, and MgO, μ-oxo species of the type $Cp'_2Th(CH_3)O$– are formed, by Th–C protonolysis or by transfer of an alkyl group to the surface. For $Cp'_2U(^{13}CH_3)_2/SiO_2$, the majority of the resulting $^{13}CH_3$–Si(surface) functionalities are $\gtrsim$5 Å from the actinide center. In agreement with heterogeneous catalytic studies, the NMR data reveal that only a small percentage of $Cp'_2Th(^{13}CH_3)_2$/DA or $Cp'Th(^{13}CH_2C_6H_5)_3$/DA surface sites undergo reaction with ethylene or H_2 at 25 °C. In contrast, 50 ± 10% of $Cp'_2Th(^{13}CH_3)_2/MgCl_2$ sites undergo reaction with ethylene; >90 ± 10% of ethylene insertion/polymerization occurs at Th–CH_3 with k(propagation)/k(initiation) ≈ 12 in the initial stages. There is no evidence for methane evolution via C–H functionalization nor for significant rates of $Th(CH_2CH_2)_n{}^{13}CH_3$–$^{13}CH_3Mg$(surface) alkyl group permutation. At 25 °C, a large percentage of $Cp'_2Th(^{13}CH_3)_2/MgCl_2$ Th–CH_3 and Mg–CH_3 functionalities undergo hydrogenolysis, with Th–CH_3 being slightly more reactive. In competition experiments, Th–CH_3 is far more reactive than Mg–CH_3 in migratory CO insertion, and products are inferred to be, inter alia, η^2-acyl complexes. $Cp'_2Th(^{13}CH_3)_2/MgCl_2$ undergoes reaction with propylene to yield methane (derived from Th–CH_3), a Th(η^3-allyl) complex, and what appear to be propylene oligomers.

It is well-established that adsorption on high surface area metal oxides can profoundly enhance the reactivity/catalytic activity of metal hydrocarbyls.[1-3] While such phenomena are of considerable scientific and technological interest, our understanding of the surface coordination chemistry, much less the nature of the active catalytic sites, is at a very primitive level. Moreover, it is not clear that conventional photon/particle absorption, scattering, or diffraction surface science tools[4,5] will be particularly incisive in structurally characterizing such adsorbates on irregular surfaces at less than monolayer coverage.

Recent research in this laboratory has employed organoactinides[6] as model hydrocarbyl adsorbates.[7] Organoactinides have well-defined/controllable oxidation states, useful spectroscopic markers, a diversity of ligational possibilities, and a developing mechanistic/thermochemical foundation. Furthermore, adsorption of molecules such as Cp'_2AnR_2 ($Cp' = \eta^5$-$(CH_3)_5C_5$; An = Th, U; R = alkyl) on dehydroxylated γ-alumina[8] (DA; σ-OH ≈ 0.1 nm^{-2}) affords heterogeneous catalysts with very high activity for olefin hydrogenation and polymerization.[7] In contrast, adsorption upon partially dehydroxylated alumina[8] (PDA; σ-OH ≈ 4 nm^{-2}) or silica[8] (partially dehydroxylated or dehydroxylated; PDS or DS) yields adsorbates with marginal catalytic activity,[7b] while adsorption on $MgCl_2$ affords catalysts with intermediate activity.[7a] Interestingly, quantitative CO or protonolytic poisoning experiments indicate that ~4% of $Cp'_2An(CH_3)_2$/DA and ~35% of $Cp'_2An(CH_3)_2/MgCl_2$ sites are catalytically important in such transformations.[7a,9]

The above catalytic phenomenology suggests an intricate relationship between surface/adsorbate microstructure and activity and one that can only be partially addressed with chemical probes

(1) (a) Iwasawa, Y.; Gates, B. C. *Chemtech* **1989**, *3*, 173–181, and references therein. (b) *Surface Organometallic Chemistry: Molecular Approaches to Surface Catalysis*; Basset, J. M., et al., Eds.; Kluwer: Dordrecht, 1988. (c) Iwasawa, Y. *Adv. Catal.* **1987**, *35*, 187–264. (d) Hartley, F. R. *Supported Metal Complexes: A New Generation of Catalysts*; Reidel: Boston, 1985. (e) McDaniel, M. P. *Adv. Catal.* **1985**, *33*, 47–98. (f) Schwartz, J. *Acc. Chem. Res.* **1985**, *18*, 302–308. (g) Yermakov, Y. I.; Kuznetsov, B. N.; Zakharov, V. A. *Catalysis by Supported Complexes*; Elsevier: Amsterdam, 1981.

(2) (a) Xiaoding, X.; Boelhouwer, C.; Vonk, D.; Benecke, J. I.; Mol, J. C. *J. Mol. Catal.* **1986**, *36*, 47–66, and references therein. (b) Lamb, H. H.; Gates, B. C. *J. Am. Chem. Soc.* **1986**, *108*, 81–89, and references therein. (c) Basset, J. M.; Choplin, A. *J. Mol. Catal.* **1983**, *21*, 95–108, and references therein. (d) Yermakov, Y. I. *J. Mol. Catal.* **1983**, *21*, 35–55, and references therein.

(3) (a) Barbé, P. C.; Cecchin, G.; Noristi, L. *Adv. Polym. Sci.* **1986**, *81*, 1–81. (b) *Catalytic Polymerization of Olefins*; Keii, T., Soga, K., Eds.; Elsevier: Amsterdam, 1986. (c) Myers, D. L.; Lunsford, J. H. *J. Catal.* **1986**, *99*, 140–148, and references therein. (d) Choi, K.-H.; Ray, W. H. *J. Macromol. Sci., Rev. Macromol. Chem. Phys.* **1985**, *C25*, 1–56, 57–97. (e) Pino, P.; Rötzinger, B. *Macromol. Chem. Phys. Suppl.* **1984**, *7*, 41–61. (f) Karol, F. J. *Catal. Rev. Sci. Eng.* **1984**, *26*, 557–595. (g) Firment, L. E. *J. Catal.* **1983**, *82*, 196–212, and references therein.

(4) (a) Van Hove, M. A.; Wang, S.-W.; Ogletree, D. F.; Somarjai, G. A. *Adv. Quantum Chem.* **1989**, *20*, 1–184. (b) Somorjai, G. A. *Chemistry in Two Dimensions: Surfaces*; Cornell University Press: Ithaca, 1981; Chapters 2 and 5. (c) *Spectroscopy in Hetereogeneous Catalysis*; Delgass, W. N., Haller, G. L., Kellerman, R., Lunsford, J. H., Eds.; Academic Press: New York, 1979.

(5) Metal hydride functionalities can sometimes be detected by vibrational spectroscopy in such systems.[1e,3g]

(6) (a) Marks, T. J.; Streitwieser, A., Jr. In *The Chemistry of the Actinide Elements*, 2nd ed.; Katz, J. J., Seaborg, G. T., Morss, L. R., Eds.; Chapman and Hall: London, 1986; Chapter 22. (b) Marks, T. J. *Ibid.* Chapter 23.

(7) (a) Gillespie, R. D.; Burwell, R. L., Jr.; Marks, T. J. *Langmuir* In press. (b) He, M.-Y.; Xiong, G.; Toscano, P. J.; Burwell, R. L., Jr.; Marks, T. J. *J. Am. Chem. Soc.* **1985**, *107*, 641–652. (c) Burwell, R. L., Jr.; Marks, T. J. In *Catalysis of Organic Reactions*; Augustine, R. L., Ed.; Marcel Dekker, Inc.: New York, 1985; pp 207–224. (d) He, M.-Y.; Burwell, R. L., Jr.; Marks, T. J. *Organometallics* **1983**, *2*, 566–569. (e) Xiong, G.; Burwell, R. L., Jr.; Marks, T. J. Unpublished results.

(8) (a) Kijenski, J.; Baiker, A. *Catalysis Today* **1989**, *5(1)*, 1–120. (b) Knözinger, H. in ref 1b, Chapter 1. (c) Beránek, L.; Kraus, M. In *Comprehensive Chemical Kinetics*; Bamford, C. H., Tipper, C. F. H., Eds.; Elsevier: Amsterdam, 1978; pp 263–398. (d) Benesi, H. A.; Winquist, B. H. C. *Adv. Catal.* **1978**, *27*, 97–182. (e) Knözinger, H.; Ratnasamy, P. *Catal. Rev.-Sci. Eng.* **1978**, *17*, 31–70. (f) Lippens, B. C.; Steggerda, J. J. In *Physical and Chemical Aspects of Adsorbents and Catalysts*; Linsen, B. G., Ed.; Academic Press: London, 1970; Chapter 4. (g) Schwarz, J. A. *J. Vac. Sci. Technol.* **1975**, *12(1)*, 321–323. (h) Tanabe, K. *Solid Acids and Bases*; Kodansha: Tokyo, Academic Press: New York, 1970.

(9) That less than 100% of surface sites are catalytically significant is a common phenomenon in heterogeneous catalysis. See, for example: (a) Rooney, J. J. *J. Mol. Catal.* **1985**, *31*, 137–159, and references therein. (b) Boudart, M. *J. Mol. Catal.* **1985**, *30*, 27–37, and references therein.

0002-7863/90/1512-6221$02.50/0

(e.g., tracing the origin of methane evolved during adsorption).[7b] In this context, high-resolution solid-state NMR spectroscopy[10] offers considerable promise as a surface structural tool,[11] and in our earliest 15 MHz ^{13}C CPMAS studies of $Cp'_2Th(^{13}CH_3)_2$/DA, we detected an unprecedented transfer of a methyl group to an Al site on the surface (A).[12a] The Lewis acid character of the

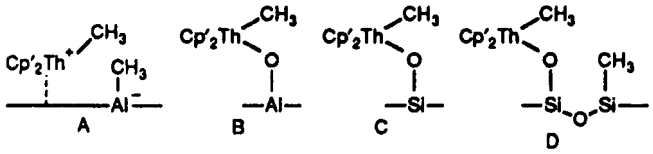

surface receptor sites, spectral similarities to cationic $Cp'_2Th(CH_3)^+BPh_4^-$/$Cp'_2Th(CH_3)(THF)_2^+BPh_4^-$ complexes,[13] and growing evidence that Cp'_2ThR^+-like species will be highly reactive[11e,14] suggested that A has electrophilic, "cation-like" character. In contrast, the negligible catalytic activity of $Cp'_2Th(CH_3)_2$ on PDA, PDS, and DS, along with spectral similarities to unreactive $Cp'_2Th(CH_3)OR$ compounds,[15] suggests different, "μ-oxo-like" adsorbate structures B, C, and D, respectively.[12] Nevertheless, these preliminary oxide support results leave many questions unanswered. From a descriptive, coordination chemistry standpoint, the generality of this picture in regard to support (other oxides, halides) and complex (other precursor structures) is unclear. Whether A might be a μ-alkyl,[16] E, whether Th–R and Al–R groups can interchange,[16] and what the reactivity of such surface functionalities is with respect to olefins, H_2, CO, etc., remain to be answered. Finally, the relevance of the above phenomenology to the observed catalytic properties and the structural models to the actual catalytic sites are unexplored.

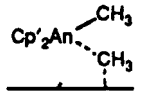

E

In the present contribution, we present a full discussion of our high field (75.4 MHz), high-resolution solid-state ^{13}C NMR investigations of supported organoactinide structural and surface chemistry.[17,18] This includes a full examination of a range of supports (Al_2O_3, $MgCl_2$, SiO_2–Al_2O_3, SiO_2–MgO, MgO) and metal complexes (Cp'_2AnR_2, $Cp'AnR_3$, Cp_3AnR), in situ chemical dosing/adsorbate reactivity studies, and the use of paramagnetic U(IV) adsorbates in a new approach to probing metrical aspects of the surface complexation. It is seen that this integrated chemical/spectroscopic approach affords a far more complete picture of this unusual but, in all likelihood, generalizable[1-3] surface organometallic chemistry. Moreover, important connections are demonstrated between the heterogeneous catalytic phenomenology and the spectroscopic structure/reactivity observations.

Experimental Section

Materials and Methods. All procedures were performed in Schlenk-type glassware interfaced to a high-vacuum (10^{-6}–10^{-5} Torr) line or in a nitrogen-filled Vacuum Atmospheres glovebox equipped with an efficient recirculating atmosphere purification system (typically 2–3 ppm O_2). Argon (Matheson, prepurified), hydrogen (Linde), and CO (Matheson CP) were purified further by passage through MnO/Vermiculite and Davison 4A molecular sieves. Other gases including propylene (Matheson), ethylene (Matheson), ethylene-*1,2*-$^{13}C_2$ (99% ^{13}C; Cambridge Isotopes), CO-^{13}C (99% ^{13}C; Cambridge Isotopes), and propylene-2-^{13}C (60% ^{13}C; MSD Isotopes) were purified by passage through MnO/SiO_2. The 3,3-dimethylbutene (Aldrich) was dried over Na/K, vacuum transferred into a storage tube equipped with a Teflon valve, and stored under an argon atmosphere. Pentane (Aldrich HPLC grade) was vacuum transferred from either Na/K or CaH_2 and stored in vacuo over Na/K in bulbs on the vacuum line.

The compounds $^{13}CH_3Li$·LiI,[12a] $Cp'_2Th(CH_3)_2$,[19] $Cp'_2Th(^{13}CH_3)_2$,[12a] $Cp_3Th(CH_3)$,[20] $[Cp'_2Th(\mu\text{-}H)H]_2$,[19] $Cp'Th(CH_2C_6H_5)_3$,[21] $Cp'_2Th(CH_2CH_3)_2$,[19] and $Cp'_2Th(CH_2CH_2CH_2CH_3)_2$[22] were prepared according to published procedures. $Cp'_2Th(^{13}CH_2{}^{13}CH_3)_2$ was prepared from $[Cp'_2Th(\mu\text{-}H)H]_2$ and 90% ethylene-*1,2*-$^{13}C_2$,[19] and $Cp_3Th(^{13}CH_3)$ was synthesized from Cp_3ThCl and $^{13}CH_3Li$·LiI.[20] By using the synthetic procedure for $Cp'Th(CH_2C_6H_5)_3$,[21] $Cp'Th(^{13}CH_2C_6H_5)_3$ was prepared from $C_6H_5{}^{13}CH_2Li$ and $Cp'ThCl_3(THF)_2$. The reagent, $C_6H_5{}^{13}CH_2Li$, was in turn prepared from $C_6H_5{}^{13}CH_3$ and *n*-butyllithium;[23] the ^{13}C labeled toluene was prepared from $C_6H_5{}^{13}COOH$ (Cambridge Isotope, 99% ^{13}C).[24] The complex $Cp'_2U(^{13}CH_3)_2$ was prepared from Cp'_2UCl_2 and $^{13}CH_3Li$·LiI by using the method for $Cp'_2U(CH_3)_2$.[19] The purity of these reagents was checked by ^1H NMR.

The supports DA and DS were prepared as previously described.[7,12] Magnesium chloride (surface area $\approx$ 100 $m^2\ g^{-1}$) was supplied by Dow Chemical Co. and was pretreated under high vacuum (10^{-5} Torr), 300°, 2 (this code indicates heating at 300 °C for 2 h). Alternatively, $MgCl_2$ was prepared by reaction of dibutylmagnesium (Lithium Corp. of America) with HCl (Matheson VLSI grade) in pentane by using greaseless high vacuum line techniques (surface area $\approx$ 100 $m^2\ g^{-1}$). It was again pretreated under high vacuum, 300°, 2. SiO_2–Al_2O_3 (Davison 970 grade, 13% Al_2O_3, 60–80 mesh material) was purified by the same procedure as for PHF Al_2O_3,[12] followed by treatment in flowing He, 950°, 0.5 (surface area $\approx$ 56 $m^2\ g^{-1}$). Partially dehydroxylated MgO (Calgon Maglite CG-1) was treated in flowing He, 680°, 0.5 (surface area $\approx$ 46 $m^2\ g^{-1}$), and SiO_2–MgO (Grace SM-30) was treated in flowing He, 800°, 0.5 (surface area $\approx$ 275 $m^2\ g^{-1}$). All supports were stored in vacuum-tight glass storage tubes under an inert nitrogen atmosphere.

Impregnation of Supports with Organoactinide Complexes. In a two-sided, fritted reaction vessel interfaced to the high vacuum line, a pentane

(10) (a) Gerstein, B. C.; Dybowski, C. R. *Transient Techniques in NMR of Solids*: Academic Press: Orlando, FL, 1985. (b) Fyfe, C. A. *Solid State NMR for Chemists*; CRC Press: Guelph, 1983. (c) Yannoni, C. S. *Acc. Chem. Res.* **1982**, *15*, 201–208. (d) Duncan, T. M.; Dybowski, C. *Surf. Sci. Rep.* **1981**, *1*, 157–250.

(11) For recent applications of ^{13}C CPMAS NMR to the characterization of organotransition-metal adsorbates and heterogeneous catalysts, see: (a) Weiss, K.; Lössel, G. *Angew. Chem., Int. Ed. Engl.* **1989**, *28*, 62–64. (b) Anderson, M. W.; Klinowski, J. *Nature* **1989**, *339*, 200–203. (c) Haw, J. F.; Richardson, B. R.; Oshiro, I. S.; Lazo, N. D.; Speed, J. A. *J. Am. Chem. Soc.* **1989**, *111*, 2052–2058. (d) Walter, T. H.; Thompson, A.; Keniry, M.; Shinoda, S.; Brown, T. L.; Gutowsky, H. S.; Oldfield, E. *J. Am. Chem. Soc.* **1988**, *110*, 1065–1068. (e) Dahmen, K. H.; Hedden, D.; Burwell, R. L., Jr.; Marks, T. J. *Langmuir* **1988**, *4*, 1212–1214. (f) Toscano, P. J.; Marks, T. J. *Organometallics* **1986**, *5*, 400–402.

(12) (a) Toscano, P. J.; Marks, T. J. *J. Am. Chem. Soc.* **1985**, *107*, 653–659. (b) Toscano, P. J.; Marks, T. J. *Langmuir* **1986**, *2*, 820–823.

(13) Synthesis, characterization, and chemistry of Cp'_2ThR^+ complexes: (a) Lin, Z.; LeMarechal, J. F.; Sabat, M.; Marks, T. J. *J. Am. Chem. Soc.* **1987**, *109*, 4127–4129. (b) Lin, Z.; LeMarechal, J. F.; Yang, X.-M.; Sabat, M.; Marks, T. J. Manuscript in preparation. (c) Marks, T. J. *Abstracts of Papers*; 197th National Meeting of the American Chemical Society, Dallas, TX; American Chemical Society: Washington, DC, April 9–14, 1989; INOR 8.

(14) (a) Hlatky, G. G.; Turner, H. W.; Eckman, R. R. *J. Am. Chem. Soc.* **1989**, *111*, 2728–2729. (b) Jordan, R. F.; LaPointe, R. E.; Bradley, P. K.; Baenziger, N. *Organometallics* **1989**, *8*, 2892–2903. (c) Gassman, P. G.; Callstrom, M. R. *J. Am. Chem. Soc.* **1987**, *109*, 7875–7876. (d) Jordon, R. F.; Echols, S. F. *Inorg. Chem.* **1987**, *26*, 383–386. (e) Jordan, R. F.; LaPointe, R. F.; Bagjur, C. S.; Echols, S. F.; Willett, R. *J. Am. Chem. Soc.* **1987**, *103*, 4111–4113. (f) Jordan, R. F.; Bagjur, C. S.; Dasher, W. E.; Rheingold, A. L. *Organometallics* **1987**, *6*, 1041–1051. (g) Jordan, R. F.; Bajgur, C. S.; Willett, R.; Scott, B. *J. Am. Chem. Soc.* **1986**, *108*, 7410–7411. (h) Jordan, R. F.; Dasher, W. E.; Echols, S. F. *J. Am. Chem. Soc.* **1986**, *108*, 1718–1719.

(15) (a) Lin, Z.; Marks, T. J. *J. Am. Chem. Soc.* In press. (b) Lin, Z.; Marks, T. J. *J. Am. Chem. Soc.* **1987**, *109*, 7979–7985.

(16) (a) Holton, J.; Lappert, M. F.; Pearce, R.; Yarrow, P. I. W. *Chem. Rev.* **1983**, *83*, 135–201, and references therein. (b) Evans, W. J.; Chamberlain, L. R.; Ulibarri, T. A.; Ziller, J. W. *J. Am. Chem. Soc.* **1988**, *110*, 6423–6432. (c) Busch, M. A.; Harlow, R.; Watson, P. L. *Inorg. Chem. Acta* **1987**, *140*, 15–20. (d) Holton, J.; Lappert, M. F.; Ballard, D. G. H.; Pearce, R.; Atwood, J. L.; Hunter, W. E. *J. Chem. Soc., Dalton Trans.* **1979**, 54–61. (e) Holton, J.; Lappert, M. F.; Ballard, D. G. H.; Pearce, R.; Atwood, J. L.; Hunter, W. E. *J. Chem. Soc., Dalton Trans.* **1979**, 45–53. (f) Huffman, J. C.; Streib, W. E. *J. Chem. Soc., Chem. Commun.* **1971**, *911*.

(17) For preliminary communication of some aspects of $Cp'_2Th(CH_3)_2$/$MgCl_2$ surface chemistry, see: Hedden, D.; Marks, T. J. *J. Am. Chem. Soc.* **1988**, *110*, 1647–1649.

(18) For a preliminary communication of related organozirconium surface chemistry, see ref 11e.

(19) Fagan, P. J.; Manriquez, J. M.; Maatta, E. A.; Seyam, A. M.; Marks, T. J. *J. Am. Chem. Soc.* **1981**, *103*, 6650–6667.

(20) Bruno, J. W.; Kalina, D. G.; Mintz, E. A.; Marks, T. J. *J. Am. Chem. Soc.* **1982**, *104*, 1860–1869.

(21) Mintz, E. A.; Moloy, K. G.; Marks, T. J.; Day, V. W. *J. Am. Chem. Soc.* **1982**, *104*, 4692–4695.

(22) (a) Bruno, J. W.; Marks, T. J.; Morss, L. R. *J. Am. Chem. Soc.* **1983**, *105*, 6824–6832. (b) Sonnenberger, D. A.; Morss, L. R.; Marks, T. J. *Organometallics* **1985**, *4*, 352–355.

(23) (a) Moloy, K. G. Ph.D. Thesis, Northwestern University, 1985. (b) *Chem. Abstr.* **1971**, *74*, 3723b.

(24) Benkeser, R. A. *J. Am. Chem. Soc.* **1970**, *92*, 3232–3233.

solution containing a measured quantity of the organoactinide complex of interest was filtered onto a carefully weighed quantity of support. The resulting slurry was then stirred for at least 2 h with exclusion of light. The slurry was next filtered, and the impregnated support was collected on the glass frit. This material was then washed with 5 × 5 mL portions of pentane distilled and condensed from the filtrate and was dried in vacuo. Maximum loadings of organoactinides on $MgCl_2$ were ~0.25 An/nm^2, while higher loadings (~0.5 An/nm^2) are achievable on DA and DS.

Reactions of Supported Organoactinides with Small Molecules. The following experiment is illustrative of the procedure used. In the recirculating glovebox, $Cp'_2Th(^{13}CH_3)_2$/DA (1.5 g, 160 μmol Th) was spread on the bottom of a 250-mL Erlenmeyer flask. The flask was equipped with a Teflon valve adapter through which it could be interfaced to the high vacuum line. The flask was sealed, removed from the glovebox, connected to the vacuum line, and evacuated. The vessel was then cooled to 77 K, and a measured quantity of ethylene was admitted. The flask was maintained at 77 K for 30 min and was then allowed to warm slowly to room temperature while continuously monitoring the pressure. At ca. −10 °C, uptake of ethylene began. After ensuring that the reaction was complete (4 h at room temperature), the flask was evacuated to remove any volatiles, resealed, and returned to the glovebox so that an NMR sample could be prepared. Reactions of CO, ^{13}CO, propylene, 60% propylene-2-^{13}C, and 3,3-dimethylbutene were conducted in the same way. For reactions with hydrogen, the procedure was modified such that after the initial evacuation of the flask containing the supported organoactinide, it was filled to ca. 1 atm with hydrogen and sealed off. After the desired reaction time, the excess hydrogen was removed in vacuo.

High-Resolution Solid-State ^{13}C NMR Spectroscopy. All ^{13}C solid-state NMR spectra were recorded on a Varian VXR300 spectrometer (75.4 MHz) equipped with either a Doty Scientific 7 mm or 5 mm high speed solids probe. High-power ^1H decoupling (~65 kHz decoupling field), cross-polarization (CP), and magic angle spinning (MAS) were employed for routine experiments. Air-sensitive samples were loaded into cylindrical sapphire rotors in the glovebox. The rotors were capped at both ends with either O-ring sealed Macor caps (7- and 5-mm rotors) or Kel-F caps (5-mm rotors only). Both types of caps provide an air-tight seal under nonspinning conditions. MAS was achieved by using boil-off nitrogen as the spinning gas to prevent sample exposure to air. Spinning rates of 3.5–4.2 kHz were routinely achieved with the 7-mm probe. With the 5-mm probe, spinning rates of up to 8.5 (Macor rotor caps) and 10.0 kHz (Kel-F caps) could be achieved. Control experiments using highly sensitive samples that undergo distinct color changes upon oxidation (NaC_5H_5; $Cp'_2U(CH_3)_2$/DA) or in which the rotor cap was briefly removed in air (to determine oxidation-induced spectral changes) indicated negligible sample deterioration in this spinning configuration over time periods as long as 72 h. For both probes, the magic angle was initially set by using neat KBr. The stability of the angle setting was routinely monitored by observing the aromatic carbon line shape of neat hexamethylbenzene. Spectra were referenced to tetramethylsilane (δ 0) by using the aromatic carbon resonance of hexamethylbenzene (δ 132.1) as a secondary reference by the substitution method. The ^{13}C 90° pulse width and the initial Hartmann–Hahn matching condition were determined by using the hexamethylbenzene standard sample.

For routine spectra of neat and supported organoactinides, the optimum cross-polarization contact time was found to be 4.0–4.5 ms (7-mm probe) and 2.5 ms (5-mm probe). The optimum recycle time was found to be 4–5 s. For neat organoactinide complexes, satisfactory spectra could be obtained by coaddition of 100–500 transients, while for supported organoactinides, the coaddition of 5000–15 000 transients was necessary. Before Fourier transformation, all FID's were weighted with a standard apodization function, $\exp(-t^2/a^2)$, where a = 0.04 s for neat organoactinides (~3 Hz line broadening) and a = 0.003 s for supported organoactinides (~120 Hz line broadening).

Because of the paramagnetism, atypical methods were necessarily employed to obtain $Cp'_2U(^{13}CH_3)_2$ ^{13}C NMR spectra. The solution $^{13}C\{^1H\}$ spectrum (C_6D_6) of $Cp'_2U(^{13}CH_3)_2$ was measured on the JEOL FX90 using a 50 kHz window. The U-$^{13}CH_3$ resonance was located at δ 1480, and variation of the transmitter offset confirmed that this peak was not a foldover. The Cp′–CH_3 resonance was located at δ −30, and the Cp′–C signal was not observed. In the solid-state ^{13}C CPMAS NMR spectrum of $Cp'_2U(^{13}CH_3)_2$ obtained by the standard procedure (vide supra), the Cp′–CH_3 resonance was very broad (2500 Hz) and appeared at δ −32. No other resonances were observable by using CP techniques, presumably due to the short ^{13}C T_1's. However, the U–$^{13}CH_3$ resonance could be observed by application of simple 90° ^{13}C observation pulses combined with dipolar ^1H decoupling and MAS. This resonance evidenced an extensive manifold of spinning sidebands, and the largest possible spectral window was employed (100 kHz). The spectrum was referenced by setting the upfield edge of the window to δ 200 by using the carbonyl resonance of liquid acetone (δ 205.4) as a secondary reference. With this external referencing, the U-$^{13}CH_3$ isotropic chemical shift was located at δ 1430 and confirmed by varying both the transmitter offset and the spinning speed. Unfortunately, the spectral window was not large enough to encompass the entire sideband pattern.

Results and Discussion

We begin with a structurally oriented discussion of the ^{13}C CPMAS NMR spectroscopy of $Cp'_2Th(^{13}CH_3)_2$ adsorbed on various dehydroxylated (i.e., having the lowest surface OH coverage readily achievable by thermal or chemical means) supports. We then probe the generality of selected aspects of the surface chemistry by using $Cp'Th(^{13}CH_2C_6H_5)_3$, $Cp_3Th(^{13}CH_3)$, and $Cp'_2Th(^{13}CH_2{}^{13}CH_3)_2$ as labeled adsorbates. Methyl group spatial relationships in surface complexes are next examined by using paramagnetic $Cp'_2U(^{13}CH_3)_2$ as an adsorbate. Finally, the surface chemistry of the $Cp'_2An(^{13}CH_3)_2$/support complexes is examined, in situ, with respect to ethylene polymerization and H_2, CO, and propylene reactivity.

NMR Spectroscopy of $Cp'_2Th(^{13}CH_3)_2$ Adsorbed on Various Supports. Dehydration of γ-alumina at 950–1000 °C produces a mixture of γ (cubic) and δ (orthorhombic) alumina (DA) having a coverage of ~0.1 Bronsted acid OH groups, 4 Lewis base oxide groups, and 5.5 Lewis acid Al^{3+} centers nm^{-2}.[7b,8] Figure 1A shows the 75.4-MHz ^{13}C CPMAS spectrum of $Cp'_2Th(^{13}CH_3)_2$ adsorbed on DA at a coverage of ca. 0.25 Th nm^{-2}. Assignments (Table I) follow straightforwardly from $^{13}C/^{12}C$ substitution, dipolar dephasing experiments,[25] and data for model compounds. The low field (δ 71.0) methyl signal is assigned to a "cation-like" Th^+–CH_3 functionality (cf., δ 71.8 in $Cp'_2Th(CH_3)^+B(C_6H_5)_4^-$)[13] and the upfield signal to an ^{27}Al–CH_3 functionality. This latter assignment and the quadrupole-induced broadening[26] are supported by model compounds,[12a] and the expected[26] line narrowing is observed at higher magnetic fields. Several experiments were also carried out to probe the motional characteristics of $Cp'_2Th(^{13}CH_3)_2$/DA. Cessation of dipolar decoupling and Bloch decay experiments[10,27] yielded featureless spectra, while variable CP time experiments[27] (0.8–10.0 ms) produced no significant changes in relative spectral intensities. Thus, any motional processes that appreciably average C–H dipolar interactions do not differ greatly in anisotropy. Spectra of $Cp'_2Th(^{13}CH_3)_2$/DA frequently exhibit a second, smaller Th–$^{13}CH_3$ signal at δ ≈ 60. This feature is the dominant Th–$^{13}CH_3$ resonance in $Cp'_2Th(^{13}CH_3)$/PDA and is assigned to a $Cp'_2Th(CH_3)O$– μ-oxo species (B) on the basis of $Cp'_2Th(CH_3)OR$ model compound data (δ 58.4 for R = $CH(t\text{-}C_4H_9)_2$).[12b] It likely arises from protonolysis[7b] by residual surface AlOH groups.

$MgCl_2$ crystallizes in the layered $CdCl_2$ structure with octahedrally coordinated Mg^{2+} cations between sheets of Cl^- anions.[28] High surface area $MgCl_2$ prepared via prolonged grinding or chemical routes has a more complex and poorly understood structural chemistry.[3,28] This material is the preferred support for "third generation" Ziegler–Natta catalysts[3] and exhibits a Lewis acid surface chemistry.[3] The spectrum of Cp'_2Th-

(25) (a) Alemany, L. B.; Grant, D. M.; Alger, T. D.; Pugmire, R. J. *J. Am. Chem. Soc.* **1983**, *105*, 6697–6704. (b) Opella, S. J.; Frey, M. H. *J. Am. Chem. Soc.* **1979**, *101*, 5854–5856.

(26) (a) Harris, R. K.; Nesbitt, G. J. *J. Magn. Reson.* **1988**, *78*, 245–256. (b) Jonsen, P. *J. Magn. Reson.* **1988**, *77*, 348–355. (c) Olivieri, A. C.; Frydman, L.; Grasselli, M.; Diaz, L. E. *J. Magn. Reson.* **1988**, *76*, 281–289. (d) Naito, A.; Ganapathy, S.; McDowell, C. A. *J. Magn. Reson.* **1982**, *48*, 367–381. (e) Hexanu, J. G.; Frey, M. H.; Opella, S. J. *J. Am. Chem. Soc.* **1981**, *103*, 224–226.

(27) (a) Bronnimann, C. E.; Maciel, G. E. *J. Am. Chem. Soc.* **1986**, *108*, 7154–7159. (b) Schilling, F. C.; Bovey, F. A.; Tonelli, A. E.; Tseng, S.; Woodward, A. E. *Macromolecules* **1984**, *17*, 728–733. (c) Maciel, G. E.; Haw, J. F.; Chuang, I.-S.; Hawkins, B. L.; Early, T. A.; McKay, D. R.; Petrakis, L. *J. Am. Chem. Soc.* **1983**, *105*, 5529–5535. (d) Pfeifer, H.; Meiler, W.; Deininger, D. *Annu. Rep. NMR Spectrosc.* **1983**, *15*, 291–356. (e) Duncan, T. M.; Dybowski, C. *Surf. Sci. Rep.* **1981**, *1*, 157–250.

(28) (a) Wells, A. F. *Structural Inorganic Chemistry*, 5th ed.; Oxford University Press: New York, 1984; p 350. (b) Marigo, A.; Martorana, A.; Zannetti, R. *Makromol. Chem., Rapid Commun.* **1987**, *8*, 65–68. (c) Bassi, I. W.; Polato, F.; Calcaterra, M.; Bart, J. C. J. *Z. Kristallogr.* **1982**, *159*, 297–302, and references therein.

Table I. Solid-State ^{13}C NMR Chemical Shift Data and Assignments[a]

complex	Cp′–C	An–C(α)[b]	Cp′–CH_3	others
$Cp'_2Th(^{13}CH_3)_2$	123.1	68.5	12.0	
$Cp'_2Th(^{13}CH_3)_2$/DA	124.2	71.0	10.2	−12.0 (Al–CH_3)
$Cp'_2Th(^{13}CH_3)_2/MgCl_2$	124.0	69.0	10.0	−8.0 (Mg–CH_3)
$Cp'_2Th(^{13}CH_3)_2$/DS	124.2	59.0	9.2	−5.4 (Si–CH_3)
$Cp'_2Th(^{13}CH_3)_2$/DSA		74.0	10.0	−6.0 (Al–CH_3 and/or Si–CH_3)
		60.0		
$Cp'_2Th(^{13}CH_3)_2/SiO_2$–MgO	124.1	59.1	8.7	−7.3 (Si–CH_3 + Mg–CH_3)
$Cp'_2Th(^{13}CH_3)_2$/MgO	121.3	62.1	9.8	
		55.5		
		52.3		
$Cp'_2Th(^{13}CH_3)$[$OSiMe_2(t$-Bu)][c]	122.7	59.2	12.6	21.7 (*t*-Bu–CH_3), 20.3 (*t*-Bu–C), 1.1, −0.2 (Si–CH_3)
	123.4			
$Cp'_2Th(^{13}CH_3)$[$OCH(t$-Bu)$_2$][c]	123.2	58.4	13.5	94.4 (O–CH), 38.5 (*t*-Bu–C), 30.6 (*t*-Bu–CH_3)
$Cp'_2Th(^{13}CH_3)Cl$[d]	126.3	67.6	12.5	
$Cp'_2Th(^{13}CH_3)_2$/PDA[d]	125.0	66.3	10.7	
$Cp'_2Th(^{13}CH_2{}^{13}CH_3)_2$	122.2	69.6	12.2	11.4 (Th–CH_2CH_3)
$Cp'_2Th(^{13}CH_2{}^{13}CH_3)_2/MgCl_2$	126.3	76.0	10.0	20.0 (br, Mg–CH_2CH_3, Mg–CH_2CH_3, Th–CH_2CH_3)
$Cp_3Th(^{13}CH_3)$		36.3		117.6 (Cp–C)
$Cp_3Th(^{13}CH_3)$/DA				119.2 (Cp–C)
				−15.4 (Al–CH_3)
$Cp'Th(^{13}CH_2C_6H_5)_3$	123.3	81.6	13.0	145–120 (C_6H_5)
		78.9		
		76.0		
$Cp'Th(^{13}CH_2C_6H_5)_3$/DA	126.8	95.0	10.1	20.2 (Al–$CH_2C_6H_5$)
		75.2		
		66.4		
$[Cp'_2Th(\mu\text{-}H)H]_2$	123.5		12.7	
$[Cp'_2Th(\mu\text{-}H)H]_2$/DA	125.6		10.7	
$[Cp'_2Th(\mu\text{-}H)H]_2/MgCl_2$	128.8		11.5	
$Cp'_2Th(CH_2CH_2CH_2CH_3)_2$	122.2	81.0	11.8	34.3, 32.1 (β and γ CH_2)
	122.7	93.8		15.3 (CH_3)
$Cp'Th(CH_2C_6H_5)(OC_6H_5)_2$	138.0	35.4		
		32.3		
$Cp'_2U(^{13}CH_3)_2$		1430	−25	
$Cp'_2U(^{13}CH_3)_2$/DA				−14.4 (Al–CH_3)
$Cp'_2U(^{13}CH_3)_2/MgCl_2$				−10.4 (Mg–CH_3)
$Cp'_2U(^{13}CH_3)_2$/DS				−7.4 (Si–CH_3)

[a] Versus external TMS. [b] σ-bonded carbon atom. [c] Reference 12b. [d] Reference 12a.

$(^{13}CH_3)_2/MgCl_2$ (Figure 1B; ca. 0.25Th nm^{-2}) is similar to that of $Cp'_2Th(^{13}CH_3)_2$/DA with a "cation-like" Th–CH_3 resonance and a Mg–CH_3 resonance at δ −8.0 (cf., δ −10.8 in solid CH_3MgBr).[29] Dipolar dephasing and $^{13}C/^{12}C$ substitution support this assignment (Table I). Interestingly, Bloch decay experiments yield a featureless ^{13}C spectrum except for a weak signal in the Mg–CH_3 region, suggesting limited isotropic mobility of these surface functionalities. The weak spectral feature at ca. δ 60 can be assigned on the basis of results with PDA (vide infra)[11a] and other supports (vide infra) to a $Cp'_2Th(CH_3)O$– species (B).[30a]

Figure 1C presents the CPMAS spectrum of $Cp'_2Th(^{13}CH_3)_2$ adsorbed on highly dehydroxylated (ca. 0.4 σ-OH nm^{-2})[30b] silica (DS; ca. 0.25Th nm^{-2}). Assignments are given in Table I. On the basis of model compounds, the resonance at δ −5.4 is ascribed to a surface Si–CH_3 functionality (cf., δ −1.0 for $^{13}CH_3Li$ adsorbed on DS).[12b] The Th–CH_3 resonance at δ 59.0 occurs at considerably higher field than is associated with "cation-like" species (vide supra), but in close proximity to δ Th–CH_3 for $Cp'_2Th(CH_3)OR'$ model complexes (δ 59.2, R′ = $Si(CH_3)_2(t\text{-}C_4H_9)$).[12b] These results are most compatible with a fully Th–O σ-bonded "μ-oxo-like" structure (e.g., D). Noteworthy in addition to the absence of a "cation-like" species is the complete lack of olefin hydrogenation activity by $Cp'_2Th(^{13}CH_3)_2$/DS.

Highly dehydroxylated SiO_2–Al_2O_3 (DSA) is a strong Lewis acid.[8] The CPMAS spectrum of $Cp'_2Th(^{13}CH_3)_2$/DSA (Figure 1D) bears similarities to those of both $Cp'_2Th(^{13}CH_3)_2$/DS and $Cp'_2Th(^{13}CH_3)_2$/DA. Peaks assignable (Table I) to Si–CH_3 (δ −6.0) and $Cp'_2Th(^{13}CH_3)O$– (δ 60.0) species are clearly discernable as is a Th–CH_3 resonance in the "cation-like" region (δ

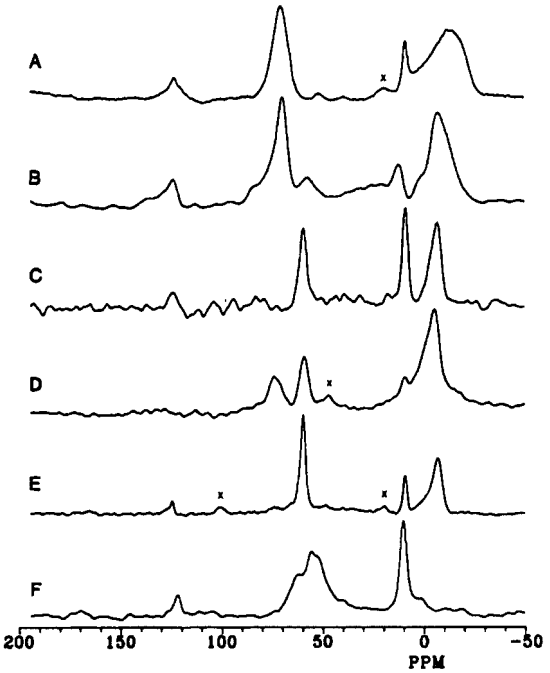

Figure 1. ^{13}C CPMAS NMR spectra (75.4 MHz, 4 s repetition, 4.5 ms contact time) of (A) $Cp'_2Th(^{13}CH_3)_2$/DA (13 200 scans), (B) $Cp'_2Th(^{13}CH_3)_2/MgCl_2$ (6050 scans), (C) $Cp'_2Th(^{13}CH_3)_2$/DS (10 125 scans), (D) $Cp'_2Th(^{13}CH_3)_2$/DSA (16 100 scans), (E) $Cp'_2Th(^{13}CH_3)_2/(SiO_2/MgO)$ (11 450 scans), and (F) $Cp'_2Th(^{13}CH_3)_2$/MgO (11 563 scans).

(29) (a) Toscano, P. J.; Marks, T. J. Unpublished results. (b) For relevant solution data, see: Leibfritz, D.; Wagner, B. O.; Roberts, J. D. *Justus Liebigs Ann. Chem.* **1972**, *763*, 173–183.

(30) (a) That initial adsorption of $Cp'_2Th(CH_3)_2$ on $MgCl_2$ releases 0.20–0.30 CH_4/Th supports the protonolytic origin of this species (Gillespie, R. D.; Marks, T. J. Unpublished results). (b) McDaniel, M. P.; Welch, M. B. *J. Catal.* **1983**, *82*, 98–109.

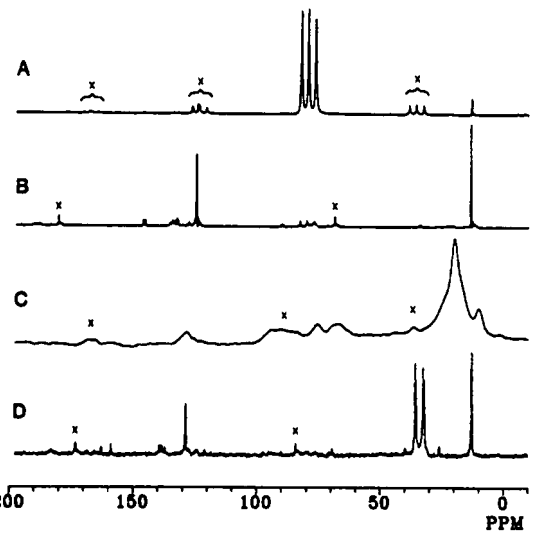

Figure 2. ^{13}C CPMAS NMR spectra (75.4 MHz, 4 s repetition time, 4.5 ms contact time) of (A) $Cp'Th(^{13}CH_2C_6H_5)_3$ as a neat solid (1220 scans), (B) $Cp'Th(CH_2C_6H_5)_3$ as a neat solid (620 scans), (C) $Cp'Th(^{13}CH_2C_6H_5)_3$/DA (3000 scans), and (D) $Cp'Th(CH_2C_6H_5)(OC_6H_5)_2$ as a neat solid (896 scans); X denotes a spinning sideband.

70.0). Although an accompanying Al–CH_3 functionality cannot be rigorously identified, the spectral line shape in the δ −20–20 region is consistent with the presence of an underlying, quadrupolar-broadened ^{27}Al–CH_3 signal superimposed upon the narrower Si–CH_3 resonance. The spectrum on DSA is thus compatible with both structures A and D. $Cp'_2Th(CH_3)_2$/DSA catalyzes the hydrogenation of propylene.[7a]

The surface of dehydroxylated SiO_2–MgO (DSM) functions as a weak Lewis acid,[8d,h] while that of MgO (NaCl crystal structure[31]) functions as a weak Lewis base.[8d,h] The CPMAS spectrum of $Cp'_2Th(^{13}CH_3)_2$/DSM (Figure 1E, Table I) exhibits a high field resonance at δ −7.3 assignable to Si–CH_3 and/or Mg–CH_3 groups (vide supra). The Th–CH_3 signal at δ 59.1 is consistent with a $Cp'_2Th(CH_3)O$– σ-bonded structure. The CPMAS spectrum of $Cp'_2Th(^{13}CH_3)_2$/partially dehydroxylated MgO (PDM, Figure 1F, Table I) provides no evidence of methyl transfer to surface Mg^{2+} centers. Rather, only relatively high field Th–CH_3 signals at δ 62.1, 55.5, and 52.3 are observed. These can be ascribed to $Cp'_2Th(CH_3)O$– species with the multiplicity of Th–CH_3 chemical shifts presumably reflecting the heterogeneity of surface microenvironments. The basic spectral pattern is reminiscent of that exhibited by $Cp'_2Th(^{13}CH_3)_2$/PDA.[12a] Attempts to further dehydroxylate MgO by heating in flowing He at 900 °C yields a low surface area material (<10 m^2/g^{-1}) which does not adsorb significant quantities of $Cp'_2Th(^{13}CH_3)_2$. In accord with the lack of detectable "cation-like" species for $Cp'_2Th(^{13}CH_3)_2$/DSM and $Cp'_2Th(^{13}CH_3)_2$/PDM, neither substance exhibits significant olefin hydrogenation activity.[7a]

Spectroscopy of Other Actinide Hydrocarbyls Adsorbed on Alumina and Magnesium Chloride. Figure 2A presents the ^{13}C CPMAS spectrum of solid $Cp'Th(^{13}CH_2C_6H_5)_3$. The resonances at δ 123.3 and δ 13.0 are ascribed to the Cp′–C and Cp′–CH_3 groups, respectively (Table I). The crystallographically nonequivalent[21] Th–$^{13}CH_2$ moieties give rise to the three intense signals at δ 81.8, 79.0, and 76.2; assignment is confirmed by the diminution of these features in $Cp'Th(CH_2C_6H_5)_3$ (Figure 2B). The aromatic benzyl carbon atoms give rise to several resonances in the δ 145–120 region. The CPMAS spectrum of $Cp'Th(^{13}CH_2C_6H_5)_3$/DA is shown in Figure 2C. In addition to Cp′–C and Cp′–CH_3 resonances at δ 126.8 and 10.1, respectively, an intense ^{27}Al–CH_2 signal is observed at δ 20.2 (δ 21.0 in Al$(CH_2C_6H_5)_3$)[32] and downfield shifted Th–CH_2 features at ~δ 95

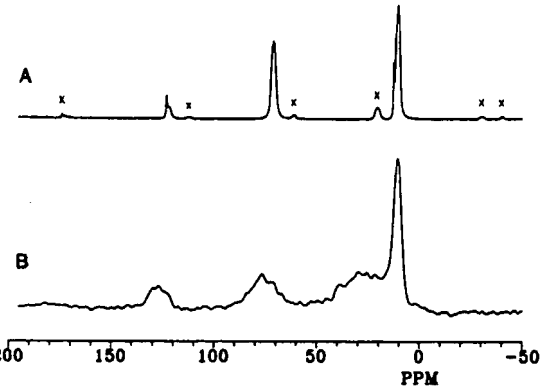

Figure 4. ^{13}C CPMAS NMR spectra (75.4 MHz, 4 s repetition time, 4.5 ms contact time) of (A) $Cp'_2Th(^{13}CH_2{}^{13}CH_3)_2$ as a neat solid (572 scans) and (B) $Cp'_2Th(^{13}CH_2{}^{13}CH_3)_2/MgCl_2$ (5620 scans).

(other Th–CH_2– resonances at δ 75.2 and 66.4). The ^{27}Al–CH_2 assignment is additionally supported by the observation of an identical feature when $Li^{13}CH_2C_6H_5$ is adsorbed on DA. These results for $Cp'Th(^{13}CH_2C_6H_5)_3$/DA are in accord with benzyl transfer to Al^{3+} surface sites and the formation again of "cation-like" species (e.g., F). Evidence against a σ-bonded μ-oxo species (e.g., G) is provided by the spectrum of the aryloxide

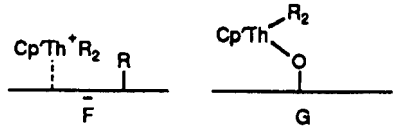

$Cp'Th(CH_2C_6H_5)(OC_6H_5)_2$[33] (Figure 2D). As in the case of $Cp'_2Th(CH_3)_2$ versus $Cp'_2Th(CH_3)OR$ (vide supra), alkoxide ligands induce an upfield displacement of hydrocarbyl α-carbon resonances. Thus, the Th–CH_2 signals now occur at δ 35.4 and 32.3. In accord with the "cationic" formulation for $Cp'Th(CH_2C_6H_5)_3$/DA, this material exhibits very high activity for olefin hydrogenation and polymerization (higher than $Cp'_2Th(CH_3)_2$/DA).[7b,34] However, as assayed by CO poisoning experiments, less than ~3% of the $Cp'Th(CH_2C_6H_5)_3$/DA sites are catalytically significant.[7b]

The CPMAS spectrum of solid $Cp_3Th(^{13}CH_3)$ (Figure 3A)[35a] consists of readily assigned[35b] resonances at δ 117.6 (Cp–C) and δ 36.3 (Th–$^{13}CH_3$). When $Cp_3Th(^{13}CH_3)$ is adsorbed upon DA, the spectrum (Figure 3B, Table I)[35a] shows essentially complete transfer of the methyl groups to surface Al^{3+} sites, as evidenced by an ^{27}Al–CH_3 resonance at δ −15.4. The Cp–C resonance is assigned at δ 119.2 with no residual Th–CH_3 signal detected (Table I). The formulation of surface Cp_3Th^+ cationic species (e.g., H) finds close analogy in known $(RC_5H_4)_3Th^+B(C_6H_5)_4^-$

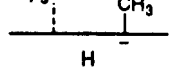

complexes.[13a] Consistent with the lack of a Th–C/H σ-bond and a high degree of coordinative saturation, Cp_3ThCH_3/DA is inactive for olefin hydrogenation except at very high temperatures.[7b]

Additional experiments were conducted on $MgCl_2$, beginning with $Cp'_2Th(^{13}CH_2{}^{13}CH_3)_2$, for reasons that will become evident in a following section. In the spectrum of neat $Cp'_2Th(^{13}CH_2{}^{13}CH_3)_2$ (Figure 4A), four resonances are observed and can be readily assigned (Table I): δ 122.2 (Cp′–C), 69.6 (Th–CH_2–), 12.2 (Cp′–CH_3), and 11.4 (Th–CH_2CH_3). $Cp'_2Th(CH_2CH_3)_2$ exhibits a similar spectrum with less intense resonances where expected. Although the Cp′ line widths are unaffected by ^{13}C enrichment, both ethyl resonances are noticeably

(31) As probed by LEED, the (100) surface of single crystal MgO differs imperceptibly from the bulk structure: Urano, T.; Kanaji, T.; Kaburagi, M. *Surf. Sci.* **1983**, *134*, 109–121.
(32) Zelta, L.; Gatti, G. *Org. Magn. Reson.* **1972**, *4*, 585–589.
(33) Sternal, R. S. Ph.D. Thesis, Northwestern University, 1988.
(34) Gillespie, R. D.; Burwell, R. L., Jr.; Marks, T. J. Unpublished results.
(35) (a) See section at end regarding Supplementary Material. (b) Fischer, R. D. In *Fundamental and Technological Aspects of Organo-f-Element Chemistry*; Marks, T. J., Fragalà, I. L., Eds.; Reidel: Dordrecht, 1985; Chapter 8, and references therein.

broader in $Cp'_2Th(^{13}CH_2{}^{13}CH_3)_2$ (~150 Hz broader with the same FID weighting). This broadening is doubtless a consequence of residual ^{13}C–^{13}C dipolar coupling[36a] that is not completely removed by the MAS employed as well as ^{13}C–^{13}C scalar coupling (anticipated to be ~35 Hz[36b]). The spectrum of $Cp'_2Th(^{13}CH_2{}^{13}CH_3)_2/MgCl_2$ (Figure 4B) is consistent with the "cation-like" model advanced for $Cp'_2Th(^{13}CH_3)_2/MgCl_2$ with Cp′–C at δ 126.3, a Th–CH_2– resonance centered at lower field (δ 76.0), a broad Mg–CH_2– resonance centered at ca. δ 20 (δ −2.9 in CH_3CH_2MgBr),[29b] and sharper coincident Th–CH_2CH_3, Mg–CH_2CH_3, and Cp′–CH_3 signals at δ 10.0 (δ 12.2 in CH_3CH_2MgBr). An alternative assignment would attribute the broad envelope at δ 40–0 to overlapping Mg–CH_2– and Mg–C–H_2CH_3 resonances, broadened by the heterogeneity of surface environments, residual ^{13}C–^{13}C dipolar coupling, and scalar coupling.

Attempts were also made to adsorb $Cp_3Th(^{13}CH_3)$ on $MgCl_2$ by using the standard procedures. However, thorough pentane washing removed all traces of the organometallic, and a CPMAS spectrum could not be detected.

A Paramagnetic Probe of Surface Alkyl–Actinide Spatial Relationships. The great bulk of Th(IV) and U(IV) organometallic chemistry is rather similar[6,19,37] as are the catalytic properties of $Cp'_2Th(CH_3)_2/DA$ and $Cp'_2U(CH_3)_2/DA$.[7b] However, U(IV) is paramagnetic ($5f^2$), and ligand resonances generally experience large paramagnetic shifts combined with relatively narrow (due to short electron spin–lattice relaxation times) line widths.[6,19,38,39] In general, the observed solution paramagnetic shifts are composed of "dipolar" (from magnetic anisotropy in the absence of cubic symmetry) and "contact" spin density delocalization (from a variety of mechanisms, including polarization of ligand orbitals by metal 6s and 6p orbitals as well as direct covalent spin density transfer from metal 5f orbitals) contributions.[38–40] Assuming a purely f orbital description for U(IV) (unquenched orbital angular momentum) and a point dipole approximation, the dipolar shift for ligand nucleus i in solution can be expressed in terms of structure-dependent geometric factors and the magnetic anisotropy of the complex (eq 1).[38,39] Here, N is Avogadro's number, the

$$\Delta H_i^{dip} = -\frac{1}{3N}[\chi_{zz} - \tfrac{1}{2}(\chi_{yy} + \chi_{xx})]\frac{3\cos^2\theta_i - 1}{r_i^3} - \frac{1}{2N}(\chi_{xx} - \chi_{yy})\frac{\sin\theta_i^2\cos 2\psi_i}{r_i^3} \quad (1)$$

χ's are magnetic susceptibility tensors, r_i is the metal-to-nuclear distance, and the angles θ and ψ fix the r_i vector within the molecular coordinate system. For axial symmetry, the expression simplifies considerably (eq 2).[38,39] In cases of axial symmetry

$$\Delta H_i^{dip} = -\frac{1}{3N}(\chi_\parallel - \chi_\perp)\frac{3\cos^2\theta_i - 1}{r_i^3} \quad (2)$$

(uranocenes, Cp_3UX), it has been possible to approximately decompose the observed paramagnetic shifts into dipolar and spin delocalization contributions.[39,40] No attempt has been made to perform such a decomposition for Cp'_2UR_2[15a,b,19] complexes; however, the signs and magnitudes of the observed paramagnetic shifts are roughly similar to those of the corresponding (same R) Cp_3UR complexes.[39b,c]

In randomly oriented powders or when immobilized on a surface, the ligand NMR spectra of organoactinide complexes will be modified by those anisotropic components of the dipolar[40,41] and spin delocalization[38,40] shifts which are normally averaged to zero by rapid tumbling in solution. To a first approximation, these should be similar in form to chemical shift anisotropies[42] and the anisotropic components of Knight shifts[43] and should in principal be removable (or reduced to a tractable sideband pattern)[10,43a,44] by sufficiently rapid MAS. The solution ^{13}C NMR

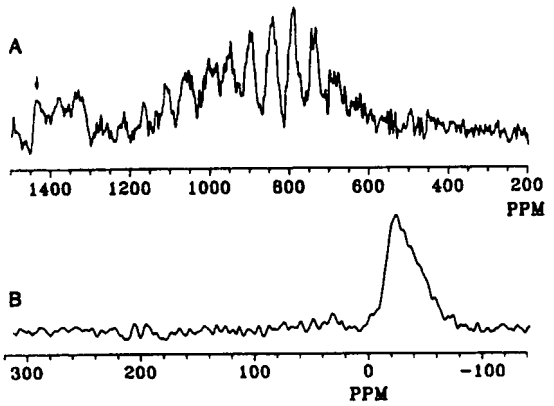

Figure 5. Solid-state ^{13}C NMR spectra (75.4 MHz) of neat $Cp'_2U(^{13}CH_3)_2$. (A) Downfield region acquired with MAS only (5 s repetition, 522 scans). The arrow indicates the centerband of the spectrum. (B) Upfield region acquired with CPMAS (5 s repetition, 4.5 ms contact time, 512 scans).

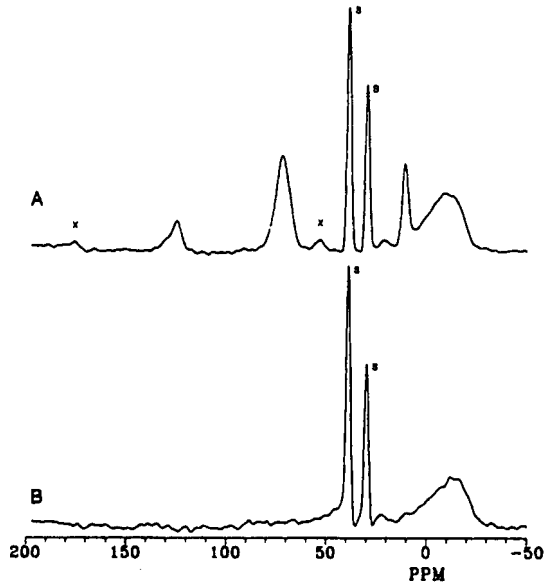

Figure 6. ^{13}C CPMAS NMR spectra (75.4 MHz, 4 s repetition time, 4.5 ms contact time) of (A) $Cp'_2Th(^{13}CH_3)_2/DA$ (1330 scans) and (B) $Cp'_2U(^{13}CH_3)/DA$ (8938 scans). Adamantane (resonances denoted by S) added as an internal intensity standard.

(36) (a) Menger, E. M.; Vega, S.; Griffin, R. G. *J. Am. Chem. Soc.* **1986**, *108*, 2215–2218, and references therein. (b) Harris, R. K. *Nuclear Magnetic Resonance Spectroscopy*; Longman Scientific: Harlow, 1986; Chapter 8–20.

(37) (a) Marks, T. J.; Ernst, R. D. In *Comprehensive Organometallic Chemistry*; Wilkinson, G. W., Stone, F. G. A., Abel, E. W., Eds.; Pergamon Press: Oxford, 1982; Chapter 21. (b) Marks, T. J.; Day, V. W. in ref 35, Chapter 4. (c) Roth, S. Ph.D. Thesis, University of Hawaii, 1988.

(38) (a) Gamp, E.; Shimomoto, R.; Edelstein, N.; McGarvey, B. R. *Inorg. Chem.* **1987**, *26*, 2177–2782, and references therein. (b) Bertini, I.; Luchinat, C. *NMR of Paramagnetic Molecules in Biological Systems*; Benjamin: Menlo Park, CA, 1986; Chapter 10. (c) McGarvey, B. R. In *Organometallics of the f-Elements*; Marks, T. J., Fischer, R. D., Eds.; Reidel Publishing Co.: Dordrecht, 1979; Chapter 10. (d) Fischer, R. D. *Ibid.* Chapter 11.

(39) (a) Luke, W. D.; Streitwieser, A., Jr. *ACS Symp. Series* **1980**, *131*, 93–140. (b) Marks, T. J.; Kolb, J. R. *J. Am. Chem. Soc.* **1975**, *97*, 27–35. (c) Marks, T. J.; Seyam, A. M.; Kolb, J. R. *J. Am. Chem. Soc.* **1973**, *95*, 5529–5539.

(40) (a) McGarvey, B. R.; Nagy, S. *Inorg. Chem.* **1987**, *26*, 4198–4203. (b) McGarvey, B. R. *Can. J. Chem.* **1984**, *62*, 1349–1355. (c) McGarvey, B. R. *J. Chem. Phys.* **1976**, *65*, 955–961. (d) McGarvey, B. R. *J. Chem. Phys.* **1976**, *65*, 962–968.

(41) Reuveni, A.; McGarvey, B. R. *J. Magn. Reson.* **1978**, *29*, 21–33.

(42) Nayeem, A.; Yesinowski, J. P. *J. Chem. Phys.* **1988**, *89*, 4600–4608, and references therein.

(43) (a) Toscano, P. J.; Marks, T. J. *J. Am. Chem. Soc.* **1986**, *108*, 437–444. (b) Reference 9b, Chapter 4. (c) Mehring, M. *Principles of High Resolution NMR in Solids*, 2nd ed.; Springer-Verlag: Berlin, 1983; Chapter 2. (d) Andrew, E. R.; Hinshaw, W. S.; Tiffen, R. S. *J. Magn. Reson.* **1974**, *15*, 191–195, and references therein.

(44) (a) Walter, T. J.; Oldfield, E. *J. Chem. Soc., Chem. Commun.* **1987**, 646–647. (b) Ganapathy, S.; Chacko, V. P.; Bryant, R. G.; Etter, M. C. *J. Am. Chem. Soc.* **1986**, *108*, 3159–3165. (c) Ganapathy, S.; Bryant, R. G. *J. Magn. Reson.* **1986**, *70*, 149–152. (d) Campbell, G. C.; Crosby, R. C.; Haw, J. T. *J. Magn. Reson.* **1986**, *69*, 191–195.

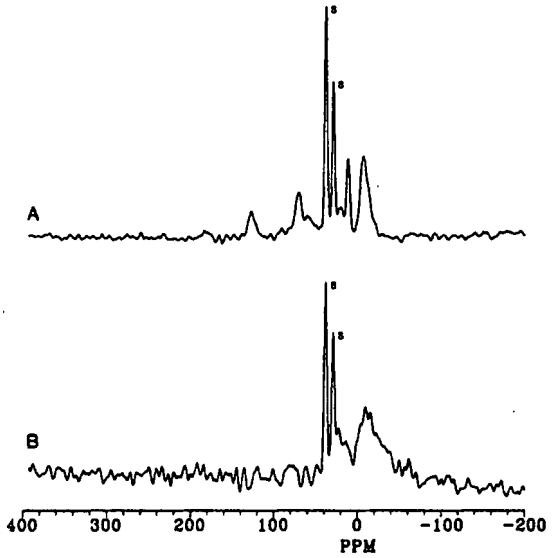

Figure 7. ^{13}C CPMAS NMR spectra (75.4 MHz, 4 s repetition time, 4.5 ms contact time) of (A) $Cp'_2Th(^{13}CH_3)_2/MgCl_2$ (2737 scans) and (B) $Cp'_2U(^{13}CH_3)_2/MgCl_2$ (5127 scans). Adamantane (resonances denoted by S) added as an internal intensity standard.

spectrum of $Cp'_2U(^{13}CH_3)_2$ exhibits a U–CH_3 resonance at δ 1480 ppm, considerably downfield from that of the diamagnetic thorium analogue (δ 68.5). Hence, the effects of the U(IV) center are extremely large for this directly σ-bonded alkyl group. The Cp′–CH_3 resonance occurs at δ −30.0, and the Cp′–C signal could not be located. For solid $Cp'_2U(^{13}CH_3)_2$, it was found that the U–CH_3 signal could be most effectively observed (presumably because of the very short T_1 and very large shift) without CP techniques. As a consequence of the large solid-state paramagnetic anisotropy, an extensive spinning sideband pattern is observed (Figure 5A). Variation of the spectral window and spinning rate allowed location of the U–CH_3 resonance at δ 1430 ± 20. Considering the slight differences in the FX90 and VXR300 probe temperatures and the experimental difficulties in acquiring the solid-state spectrum, this result is in good agreement with that in solution (δ 1480, vide supra). The Cp′–CH_3 signal could be observed by standard CPMAS as a broad peak at δ −25 (Figure 5B), only slightly displaced from the solution position (δ −30, vide supra). These results indicate that useful ^{13}C spectra of Cp'_2UR_2 complexes can be recorded in the solid state and that MAS sufficiently removes condensed phase anisotropy effects to reveal isotropic spectral features. The large shifts imparted to proximate nuclei suggest an efficacious means to probe metal–alkyl group distances on the surface.

Figure 6A and B shows CPMAS spectra of $Cp'_2Th(^{13}CH_3)_2$/DA and $Cp'_2U(^{13}CH_3)_2$/DA, respectivley, at identical loadings. Adamantane has been added as an internal standard for normalizing intensities. The spectrum of $Cp'_2U(^{13}CH_3)_2$/DA evidences no obvious Cp′U or U–CH_3 specral features either in Figure 6B or in scans over wider sweepwidths. Of course, such features are expected to be broad and rather weak under these conditions (cf., Figure 5). In contrast, the center of the Al–CH_3 signal in $Cp'_2U(^{13}CH_3)_2$/DA is only slighly displaced upfield ($\lesssim$5 ppm) from that in $Cp'_2Th(^{13}CH_3)_2$/DA, is only slightly broadened, and represents 90 ± 10% of the expected spectral intensity. If the Cp′–CH_3 resonance were present at the same field position as in neat $Cp'_2U(^{13}CH_3)_2$, it would be a broad envelope extending from $\sim\delta$ −50–0, having ca. 1/10 the intensity of the Al–CH_3 signal, i.e., it would likely be obscured by the Al–CH_3 resonance. These results indicate that little if any U(IV) unpaired spin density or magnetic anisotropy is transmitted to the majority of the Al–CH_3 moieties. In similar experiments Th, U pairs were also examined for the $Cp'_2An(^{13}CH_3)_2/MgCl_2$ (Figure 7) and $Cp'_2An(^{13}CH_3)_2/SiO_2$ (Figure 8) systems. In both cases, the surface methyl group signals experience little displacement ($\lesssim$5 ppm) and only minor broadening. In both cases, 90 ± 10% of the methyl signal intensity is accounted for. Again, little interaction is observed between the majority of surface methyl groups and the U(IV) center.

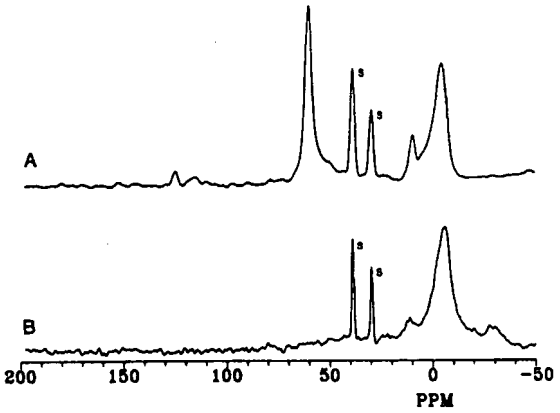

Figure 8. ^{13}C CPMAS NMR spectra (75.4 MHz, 4 s repetition time, 4.5 ms contact time) of (A) $Cp'_2Th(^{13}CH_3)_2$/DS (4668 scans) and (B) $Cp'_2U(^{13}CH_3)$/DS (10000 scans). Adamantane (resonances denoted by S) added as an internal intensity standard.

While exact quantitative analysis of U···CH_3(surface) interactions requires detailed, presently unavailable knowledge of surface $Cp'_2UCH_3^+$ magnetic anisotropy and spin delocalization, it is still possible to make physically reasonable, qualitative estimations of the range of possible U···CH_3(surface) distances. In doing so, it is pragmatically assumed that spin delocalization and dipolar shifts are roughly similar to those in the well-studied, axially symmetric Cp_3UR series.[35b,38b,39b,c,45] That observed solution shift patterns for alkyl groups are similar in Cp_3UR and $Cp'_2UR_2/Cp'_2U(Cl)R/Cp'_2U(OR')R$ complexes[15a,19,45] argues that the sums of the spin delocalization and dipolar terms are not terribly different. Where data exist for similar ligands, U(IV)-induced spin delocalization shifts do not differ greatly.[38a,39,46] In Cp_3UCH_3 at room temperature, $\Delta H^{dip} \approx +130$ ppm (upfield) and $\Delta H^{spin\ deloc} \approx +50$ ppm (upfield; in accord with a $5f^2$ polarization mechanism).[38,39] If a similar magnetic anisotropy is assumed for $Cp'_2U(CH_3)_2$, then geometric factors (eq 2) and metrical data lead to an estimate for $\Delta H^{dip}(U-^{13}CH_3)$ of ca. +300 ppm upfield. That a large, polarization-derived downfield shift dominates the observed spectral characteristics (vide infra) should not be surprising for a directly bound nucleus.[38,39] The simplest model for adsorbate structure would involve incremental displacement of the methyl group from the U(IV) center (I). Since

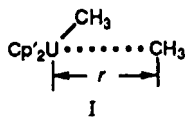

I

the spin delocalization shift is ultimately dependent on metal–ligand orbital overlap,[38,39] it is expected to attenuate far more rapidly with increasing r than the through-space dipolar term. Assuming the magnetic anisotropy and angular part of the geometric factor remain approximately constant with changing r in structure I, the question becomes how large r must become to reduce ΔH^{dip} to the magnitudes observed in the spectra of adsorbed $Cp'_2U(^{13}CH_3)_2$ (Figures 6–8). This dipolar-shift-only analysis is admittedly approximate but allows an assessment of how the surface CPMAS spectra can vary with r. Assuming that U–CH_3 = 2.43 Å in $Cp'_2U(CH_3)_2$,[37c] then the diminution ΔH^{dip} = 300 → 10 ppm corresponds to an ca. 7.6 Å increase in r. Even a more conservative 100 → 10 ppm decrease would correspond to an ca. 5.3 Å increase in r. This argument would be equally applicable to cases in which ΔH^{dip} was of opposite sign. For dynamic systems, ΔH^{dip} would be the weighted average of the spectral parameters

(45) Fagan, P. J.; Manriquez, J. M.; Marks, T. J. in ref 38c, Chapter 4.
(46) For example, in $U(H_3BC_2H_5)_4$ the spin delocalization shift of the bridging hydrogen atoms is ca. 150 ppm downfield,[38a] whereas in $Cp_3UH_3BC_2H_5$ it is ca. 60 ppm downfield.[39b]

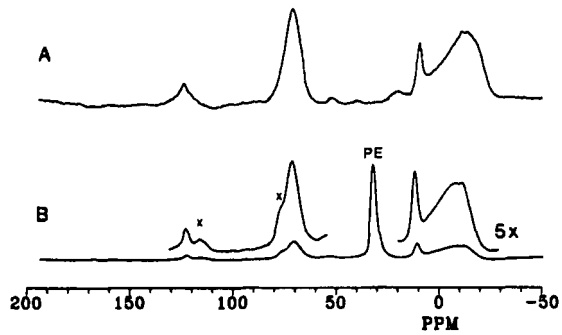

Figure 9. ^{13}C CPMAS NMR spectra (75.4 MHz, 5 s repetition time, 4.5 ms contact time) of (A) $Cp'_2Th(^{13}CH_3)_2$/DA (13 200 scans) and (B) $Cp'_2Th(^{13}CH_3)_2$/DA exposed to 30 equiv of ethylene (8835 scans). PE denotes a polyethylene $(-CH_2CH_2-)_x$ resonance, an X a spinning sideband.

in the instantaneous geometries occupied. Importantly, these results readily rule out μ-alkyl geometries such as structure E and argue that the location of the transferred methyl group on the surface must be some angstroms distant from the actinide center ($\geq$5 Å).

Adsorbate Reaction Chemistry. Ethylene. In addition to probing adsorbate structure, CPMAS NMR offers the fascinating opportunity to directly probe adsorbate reactivity. For example, the relative reactivity of An–alkyl versus surface–alkyl groups or of "cation-like" versus "μ-oxo" species can be *directly* examined via in situ competition experiments with a variety of reagents. It will be seen that the study of polymerization processes by using isotopically labeled reagents is particularly informative since the immobilized products encode "memory" effects. Experiments were first carried out in which $Cp'_2Th(^{13}CH_3)_2$/support systems were incrementally dosed with measured amounts of gaseous reagents and CPMAS spectra recorded. All possible efforts were made to rigorously exclude oxygen and water (see Experimental Section).

Ethylene polymerization was investigated by using high vacuum line experiments in which $Cp'_2Th(^{13}CH_3)_2$/support catalysts were exposed to measured quantities of ethylene. Exposures were carried out at 77 K to allow diffusion of ethylene into the pores of the catalyst prior to polymerization, thus minimizing mass transport effects. The catalyst was then slowly warmed to room temperature, during which time ethylene uptake could be detected manometrically. The $Cp'_2Th(^{13}CH_3)_2$/DA + ethylene system (Figure 9) reveals that incremental doses of olefin result in the growth of polyethylene resonances, with PE–CH_2– expected at δ 33 and PE–CH_3 expected at δ 10–15 (degenerate with the Cp′–CH_3 signal),[47] but induces no perceptible changes in the $Cp'_2Th(^{13}CH_3)_2$/DA spectrum. Since insertion of ethylene into a Th–$^{13}CH_3$ or Al–$^{13}CH_3$ bond would result in large $^{13}CH_3$ chemical shift displacements, and since no obvious diminution of relative signal intensities is evident, it is concluded that only a small percentage of the surface sites is responsible for the polymerization ($\lesssim$10%). Importantly these results agree well with the aforementioned carbonylation and protonolysis poisoning assays[7a,b] of the active site percentages, i.e., $\leq$4%. As a point of reference, note that at room temperature in toluene solution, neither $Cp'_2Th(CH_3)_2$ nor typical $Cp'_2Th(CH_3)X$ compounds (X = alkoxide, Cl, O_3SCF_3) undergo significant reaction with ethylene (1 atm) over the course of several hours. However, the cationic complex $Cp'_2Th(CH_3)^+B(C_6H_5)_4^-$ catalyzes ethylene polymerization with $N_t \approx 1$ min^{-1}.[12]

Ethylene dosing experiments were also conducted with $Cp'Th(^{13}CH_2C_6H_5)_3$/DA and $Cp_3Th(^{13}CH_3)$/DA. In the former case, the growth of polyethylene signals was detected, but no change in either Th–$^{13}CH_2$– or Al–$^{13}CH_2$– resonances could be observed. Again, polymerization is deduced to occur at only a small percentage of the surface sites, in agreement with catalytic poisoning assays.[7b] Exposure of $Cp_3Th(^{13}CH_3)$/DA samples to

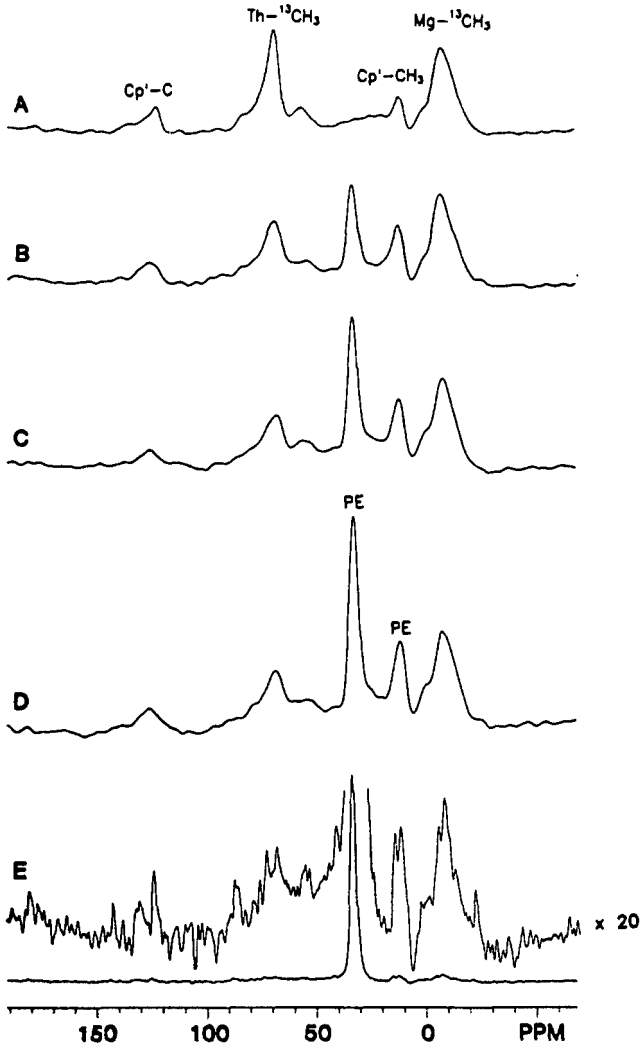

Figure 10. ^{13}C CPMAS NMR spectra (75.4 MHz, 4 s repetition time, 4.5 ms contact time) of (A) $Cp'_2Th(^{13}CH_3)_2/MgCl_2$ (6050 scans), (B) $Cp'_2Th(^{13}CH_3)_2/MgCl_2$ exposed to 5.0 equiv of ethylene (5700 scans), (C) $Cp'_2Th(^{13}CH_3)_2/MgCl_2$ exposed to 10.0 equiv of ethylene (5700 scans), (D) $Cp'_2Th(^{13}CH_3)_2/MgCl_2$ exposed to 16.0 equiv of ethylene (5900 scans), and (E) $Cp'_2Th(^{13}CH_3)_2/MgCl_2$ exposed to 350 equiv of ethylene (6000 scans). PE denotes the location of a polyethylene signal.

ethylene doses under identical conditions results neither in the development of polyethylene signals nor in alteration of the existing adsorbate spectrum. This result is also in accord with results of catalytic studies[7b] and with a polymerization mechanism requiring an initiating, surface Th–alkyl or Th–H functionality.

In principal, it should be possible to estimate the degree of ethylene polymerization from these CPMAS spectra via the relative intensities of the CH_2 and CH_3 signals. However, since longer chains will have considerable mobility, which in turn will degrade CP efficiency,[27,47] we are reluctant to quantitatively analyze such data without exhaustive calibration studies. Furthermore, as noted above, the Cp′–CH_3 and PE–CH_3 signals are nearly coincident.

One characteristic of $MgCl_2$-supported Ziegler–Natta catalysts vis-à-vis those supported on more conventional materials (e.g., Al_2O_3, SiO_2) is a far higher percentage of active sites.[3] This effect is also observed in catalytic studies of $MgCl_2$-supported organoactinides.[7a] The results of progressively dosing a $Cp'_2Th(^{13}CH_3)_2/MgCl_2$ catalyst with ethylene are shown in Figure 10. In contrast to $Cp'_2Th(^{13}CH_3)_2$/DA + ethylene, the development of polyethylene resonances is accompanied by an unambiguous initial decay of the Th–$^{13}CH_3$ signal relative to the Cp′–C resonance. The intensity of this signal continues to fall with ethylene dosing, finally levelling off at ~50% of the initial signal area relative to Cp′–C. During this same period, the polyethylene–CH_2 resonance continues to increase in relative intensity, while that

(47) Vander Hart, D. L.; Pérez, E. *Macromolecules* **1986**, *19*, 1902–1909, and references therein.

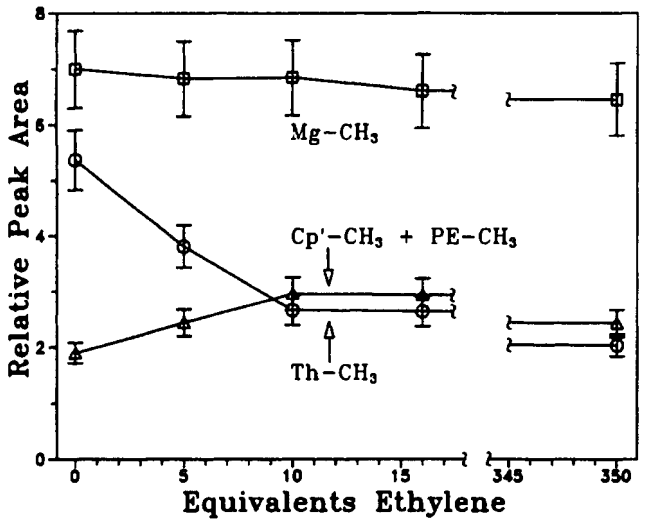

Figure 11. Relative CPMAS spectral peak areas of a $Cp'_2Th(^{13}CH_3)_2/MgCl_2$ sample exposed to the quantities of ethylene indicated.

of the $Mg-^{13}CH_3$ signal is essentially unchanged. Spectra of $Cp'_2Th(^{13}CH_3)_2/MgCl_2$ and $Cp'_2Th(^{13}CH_3)_2/MgCl_2$ + 5 equiv of ethylene recorded as a function of Cp contact time (1, 3.5, 4, and 9 ms) indicate that this quantitation is not adversely affected by changes in CP dynamics. Indeed, a strength of this assay is that it quantitates untransformed starting material of known CP and spin–lattice relaxation characteristics, rather than an emerging product of unknown characteristics.

Relative spectral peak areas for the $Cp'_2Th(^{13}CH_3)_2/MgCl_2$ + ethylene experiment are plotted in Figure 11 as a function of equivalents of added ethylene. It is concluded that 50 ± 10% of the $Th-CH_3$ sites undergo olefin insertion under the experimental conditions. This result is in favorable agreement with protonolytic poisoning experiments, which indicate 35 ± 10% of $Cp'_2Th(CH_3)_2/MgCl_2$ sites are active for propylene hydrogenation at −63 °C.[7a] In terms of selectivity, greater than 90 ± 10% of olefin insertion events take place at the surface $Th-CH_3$ functionality versus less than 10 ± 10% at the $Mg-CH_3$ bond. Furthermore, comparison of the $Th-CH_3$ peak intensity in Figure 11 versus the summed $Cp'-CH_3$ + $PE-CH_3$ peak intensities as a function of added ethylene provides an important self-consistency check. If $PE-^{13}CH_3$ formation only occurs at the expense of $Th-^{13}CH_3$ moieties, then the consumption of the latter species should be correlated with the formation of the former. The coincidence of the levelling-off portions of the $PE-^{13}CH_3$ and $Th-^{13}CH_3$ plots in Figure 11 substantiates this relationship. That the entirety of the $Th-^{13}CH_3$ intensity is not recovered in the $PE-^{13}CH_3$ resonance is evidence of (not surprisingly) rather different methyl group motional characteristic, hence CP efficiencies.[27,47] It is also possible to estimate $k_{propagation}/k_{initiation}$ for the polymerization via analysis of the diminution of the $Th-^{13}CH_3$ signals as a function of ethylene uptake. Assuming that 50% of the $Cp'_2ThCH_3^+$ surface sites undergo ethylene insertion at a uniform rate ($\theta_{ThCH_3}k_iP_{olefin}$), that subsequent ethylene insertions also occur at a uniform rate ($\theta_{Th(CH_2CH_2)_nCH_3}k_pP_{olefin}$), and that neither chain transfer (β-H elimination) nor chain termination is important, then eq 3 applies.[48] M is equivalents monomer consumed, I_0 is the initial equivalents of initiator ($Th-CH_3$) present, and f is the fraction of the initiator

$$\frac{M}{I_0 f} = -\frac{k_p}{k_i}\left[1 + \frac{\ln(1-f)}{f}\right] + 2 \qquad (3)$$

consumed. For the initial region of ethylene uptake in Figure 10 (0–5 equiv), this relationship yields $k_p/k_i \approx 12$ ($M \approx 5$; $f \approx 0.6$). This result can be compared to relative ethylene insertion rates in the analogous, homogeneous Cp'_2Sc-R system of $k(R = CH_2CH_2CH_3)/k(R = CH_3) = 7.5$ (4) at −80 °C.[51c]

An alternative or at least competing interpretation of the spectral changes observed in Figure 10 would be a vinylic C–H activation process,[16a,49-52] which would also result in ethylene-dependent decay of the $Th-^{13}CH_3$ signal (eq 4). To test such

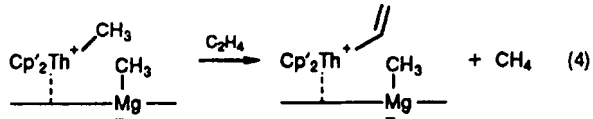

(4)

an alternative, gases evolved in the $Cp'_2Th(CH_3)_2/MgCl_2$ + ethylene reaction were collected by vacuum line techniques (77 K silica gel trap) and released as a pulse to a calibrated gas chromatography system.[7a,b] Any evolved methane was below the detection limits, hence ≲2% of the Th sites react in this manner.

The experiments of Figure 10 reveal other interesting aspects of $Cp'_2Th(^{13}CH_3)_2/MgCl_2$ surface chemistry. First, the $Th-^{13}CH_3$ feature at δ 60 assigned to a $Cp'_2Th(CH_3)O-$ species (B) does not significantly change in intensity with ethylene dosing. This lower reactivity is in accord with other observations on $Cp'_2Th(OR')CH_3$ chemistry in solution.[15a,b,19] Second, these spectra and those recorded several days later evidence no perceptible variations in the residual $Th-^{13}CH_3$ and $Mg-^{13}CH_3$ spectral intensities. Thus, transalkylative exchange of Th–R and Mg–R′ groups must be slow on the time scale of days.

In principle, it should also be possible to carry out an experiment complementary to Figure 10 in which $Cp'_2Th(CH_3)_2/MgCl_2$ is incrementally dosed with $^{13}CH_2{=}^{13}CH_2$. In this case, the relative reactivity (but not the fraction of reactive sites) of the $Th-CH_3$ and $Mg-CH_3$ moieties would be monitored by the growth of the corresponding $Th-^{13}CH_2-$ or $Mg-^{13}CH_2-$ signals. Efforts to conduct such experiments and to observe well-resolved $M-^{13}CH_2-$ signals as opposed to broad envelopes were frustrated by several factors. First, for significant degrees of ethylene polymerization, the very large $(^{13}CH_2{}^{13}CH_2)_n$ resonance creates severe dynamic range problems and spinning sidebands in the spectral region expected for the $Th-^{13}CH_2-$ signal (cf., Figure 4). Secondly, the $M-^{13}CH_2{}^{13}CH_2-$ resonances are expected to be broadened by $^{13}C-^{13}C$ scalar and unremoved dipolar coupling (vide supra).[36] Thirdly, diffraction structural, NMR spectroscopic, and theoretical results indicate that Cp'_2AnR_2 complexes occupy a very shallow potential energy surface for deformations of the Th–C(α)–C(β) valence angles.[6d,52b,53] Such distortions are frequently accompanied by C(α)H "agostic" interactions, (e.g., J). For NMR

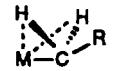

J

spectroscopy, solid-state $\delta^{13}C(\alpha)$ parameters can therefore occur over a surprisingly broad spectral range and C(α) nonequivalences are common in Cp'_2ThR_2 CPMAS spectra.[52b,54] A relevant example containing an n alkyl group is that of $Cp'_2Th(n\text{-}C_4H_9)_2$ (Figure 12,[35a] Table I). Assignment of the solution spectrum follows straightforwardly from $^{13}C\{^1H\}$ and coupled spectra: δ

(48) (a) Szwarc, M. *Adv. Polym. Sci.* **1983**, *49*, 1–177. (b) Nanda, V. S.; Jain, R. K. *J. Polym. Sci.* **1964**, *A2*, 4583–4590. (c) Litt, M. *J. Polym. Sci.* **1962**, *58*, 429–454. (d) This equation has been derived for a transferless and terminationless living polymerization in the "slow initiation" regime. Considering the substantial polydispersities observed in most heterogeneous ethylene polymerization processes,[3] the present working assumption that initiation and propagation are described by single rate constants is clearly an approximation.

(49) Rothwell, I. P. In *Activation and Functionalization of Alkanes*; Hill, C. A., Ed.; Wiley: New York, 1989; Chapter V, and references therein.

(50) Watson, P. J.; Parshall, G. W. *Acc. Chem. Res.* **1985**, *18*, 51–56.

(51) (a) Thompson, M. E.; Baster, S. M.; Bulls, A. R.; Burger, B. J.; Nolan, M. C.; Santarsiero, B. D.; Schaefer, W. P.; Bercaw, J. E. *J. Am. Chem. Soc.* **1987**, *109*, 203–219. (b) Bercaw, J. E.; Davies, D. L.; Wolczanski, P. T. *Organometallics* **1986**, *5*, 443–450. (c) Parkin, G.; Bunel, E.; Burger, B. J.; Trimmer, M. S.; Van Asselt, A.; Bercaw, J. E. *J. Mol. Catal.* **1987**, *41*, 21–39. Burger, B. J.; Thompson, M. E.; Cotter, W. D.; Bercaw, J. E. *J. Am. Chem. Soc.* **1990**, *112*, 1566–1577.

(52) (a) Fendrick, C. M.; Marks, T. J. *J. Am. Chem. Soc.* **1986**, *108*, 425–437. (b) Bruno, J. W.; Smith, G. M.; Marks, T. J.; Fair, C. K.; Schultz, A. J.; Williams, J. M. *J. Am. Chem. Soc.* **1984**, *108*, 40–56. (c) Smith, G. M.; Carpenter, J. C.; Marks, T. J. *J. Am. Chem. Soc.* **1986**, *108*, 6805–6807.

(53) (a) Tatsumi, K.; Nakamura, A. *J. Am. Chem. Soc.* **1987**, *109*, 3195–3206. (b) Tatsumi, K.; Nakamura, A. *Organometallics* **1987**, *6*, 427–428.

(54) Smith, G. M. Ph.D. Thesis, Northwestern University, 1987.

122.2 (Cp′–C), 89.2 (Th–CH_3), 31.4, 31.1 (C(β) and C(α)), 14.4 (C(δ)), and 11.2 (Cp′–CH_3). The major difference in the CPMAS spectrum (Figure 12B) is the large magnetic nonequivalence observed for the C(α) resonances, viz., δ 81.0 and 93.8. Similar effects are observe in $Cp'_2Th[CH_2C(CH_3)_3]_2$ ($\Delta\delta \approx 26$) and $Cp'_2Th[CH_2Si(CH_3)_3]_2$ ($\Delta\delta = 27$) and are associated with major solid-state structural distortions (e.g., J).[6d,52b] This behavior suggests that the Th–C(α) resonances of surface-bound Th-($^{13}CH_2{}^{13}CH_2)_nCH_3$ species are likely to occur over a broad spectral range, reflecting the modest energies required for Th–C(α)–C(β) deformation, differing n values, and the heterogeneity.

Supported organoactinide hydrides are also active olefin hydrogenation and polymerization catalysts.[7b] That the surface chemistry is similar to that of the supported hydrocarbyls is verified by CPMAS studies of $[Cp'_2Th(\mu\text{-}H)H]_2/MgCl_2$. The spectrum of the supported complex is essentially identical with that of $Cp'_2Th(^{13}CH_3)_2/MgCl_2$ except for the absence of Th–$^{13}CH_3$ and Mg–$^{13}CH_3$ signals (Table I). Dosing with ethylene gives rise to the characteristic signatures of polyethylene (Figure 13)[35a] minus, of course, the strong PE–$^{13}CH_3$ resonance previously observed at δ 12 (Figure 10). In work to be reported elsewhere,[55] we show that ^1H MAS NMR spectroscopy is an effective method to detect surface-bound organoactinide hydrides and to monitor their chemical transformations.

Additional Adsorbate Chemistry. Hydrogenolytic transformations of actinide–alkyl bonds are important in both olefin hydrogenation[4] and, for molecular weight control, in polymerization catalysis. Exposing $Cp'_2Th(^{13}CH_3)_2/DA$ samples to large molar excesses of H_2 at temperatures up to 100 °C for a period of several hours effects no perceptible changes in the CPMAS spectrum. This result agrees excellently with the low percentage of active olefin hydrogenation sites inferred from poisoning studies.[7a,b] We estimate that $<10 \pm 10\%$ of the Th–CH_3 or Al–CH_3 sites undergo hydrogenolysis under these conditions. In contrast, exposure of $Cp'_2Th(^{13}CH_3)_2/MgCl_2$ to excess H_2 at room temperature for 1 h (Figure 14) results in diminution of *both* the Th–$^{13}CH_3$ and Mg–$^{13}CH_3$ signals, with the former decaying slightly more rapidly. Interestingly, samples exhibiting a significant $Cp'_2Th(^{13}CH_3)O$– resonance at $\delta \approx 60$ respond differently in that hydrogenolytic diminution of the $\delta \approx 70$ $Cp'_2ThCH_3^+$ resonance is not accompanied by a significant decay of the μ-oxo Th–$^{13}CH_3$ signal. This additional example of lower surface $Cp'_2Th(CH_3)O$– reactivity is again in accord with the solution chemistry of these less electrophilic species.[13,21] That the chemistry of Figure 14B indeed generates reactive surface hydrides is confirmed by the observation that exposure of such samples to ethylene results in the formation of polyethylene (Figure 14C).

The potency of CO as a poison of $Cp'_2Th(CH_3)_2$/support catalytic activity promoted studies with this reagent. The reaction of $Cp'_2Th(CH_3)_2/MgCl_2$ with 1 equiv of ^{13}CO (CO/Th = 1) is quantitative by manometry; however, no new ^{13}CO-derived features are evident in the δ −50–489 region of the CPMAS spectrum. In contast, exposure of $Cp'_2Th(^{13}CH_3)_2/MgCl_2$ to 1 equiv of either CO or ^{13}CO results in a nearly identical spectrum with disappearance of the Th–$^{13}CH_3$ signal, no change in the Cp′–C, Cp′–CH_3, or Mg–$^{13}CH_3$ resonances, and two new features of approximately equal intensity at δ 31 and δ 17 (Figure 15).[35a] No other resonances are observed in the δ −50–489 spectral region. Although the interpretation of these changes is not unambiguous, note that typical organothorium dihaptoacyl (K) chemical shifts are ~δ 350 (–$^{13}C(O)CH_3$) and ~δ 30 (–$C(O)^{13}CH_3$).[6b,37,45,56,57]

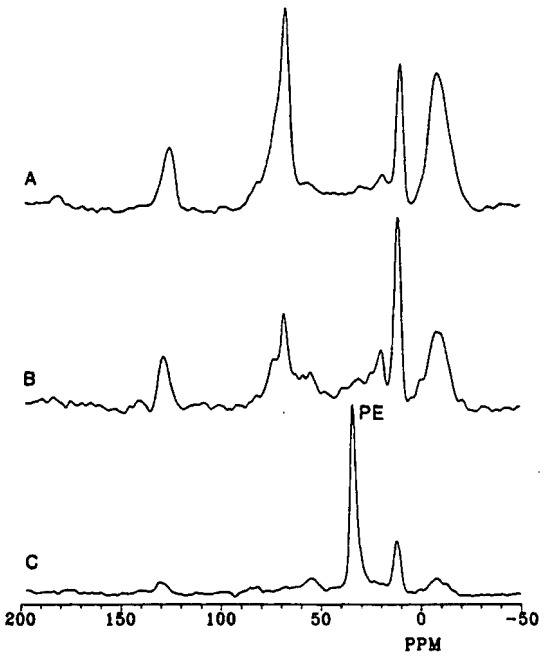

Figure 14. ^{13}C CPMAS NMR spectra (75.4 MHz, 4 s repetition time, 4.5 ms contact time) of (A) $Cp'_2Th(^{13}CH_3)_2/MgCl_2$ (8082 scans), (B) $Cp'_2Th(^{13}CH_3)_2/MgCl_2$ exposed to a large excess of H_2 (9492 scans), and (C) $Cp'_2Th(^{13}CH_3)_2/MgCl_2 + H_2$ followed by treatment with excess (20 equiv) ethylene (6220 scans).

The CSA of an acyl carbon is likely to be large, and combined with the heterogeneity of surface environments as well as possible coordination to acidic sites (e.g., L),[58] it is not surprising that this signal is not readily detected.

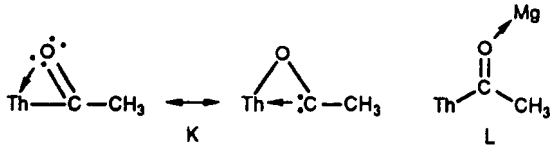

The reactivity of $Cp'_2Th(^{13}CH_3)_2/MgCl_2$ with respect to propylene was also investigated. CPMAS NMR (Figure 16A)[35a] of a sample exposed to 15 equiv of propylene (6 h at 25 °C) reveals almost complete disappearance of of Th–$^{13}CH_3$ and partial disappearance of Mg–$^{13}CH_3$. Gas-trapping/GC-based experiments reveal that under these conditions propylene exposure releases 1.1 ± 0.3 CH_4/Th. This observation suggests an allylic C–H activation process, previously observed for analogous (Cp'_2Ln-R, R = alkyl) organolanthanide complexes[59] (eq 5). Subsequent ex-

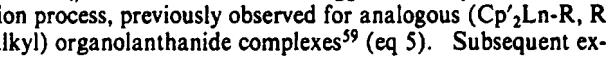

posure of this sample to H_2 (1 h at 25 °C) released 0.2 CH_4/Th, large quantities of propane and propylene, but no detectable C_4 products (isobutane, isobutylene, *n*-butane, etc.). Higher propylene oligomers would not be detected in this assay. Treatment with water also failed to evolve C_4 products. These results are in accord with the aforementioned NMR spectroscopic evidence (Figure 16A)[35a] for some residual surface methyl groups. Since the support was likely to have adsorbed propylene during the initial propylene dosing and since $Cp'_2Th(CH_3)_2/MgCl_2$ is a propylene hydrogenation catalyst,[7a] nothing about an η^3-allyl (eq 5) can be inferred from the C_3 products. However, the absence of isobutane argues

(55) (a) Finch, W. C.; Gillespie, R. D.; Marks, T. J. *Abstracts of Papers*, 197th National Meeting of the American Chemical Society, Dallas, TX; American Chemical Society: Washington, DC, April 9–14, 1989; INOR 33. (b) Finch, W. C.; Gillespie, R. D.; Marks, T. J. Manuscript in preparation.

(56) (a) Tatsumi, K.; Nakamura, A.; Hofmann, P.; Hoffmann, R.; Moloy, K. G.; Marks, T. J. *J. Am. Chem. Soc.* **1986**, *108*, 4467–4476, and references therein. (b) Moloy, K. G.; Fagan, P. J.; Manriquez, J. M.; Marks, T. J. *J. Am. Chem. Soc.* **1986**, *108*, 56–67, and references therein. (c) Sonnenberger, D. C.; Mintz, E. A.; Marks, T. J. *J. Am. Chem. Soc.* **1984**, *106*, 3484–3491. (d) Fagan, P. J.; Maatta, E. A.; Marks, T. J. *ACS Symp. Ser.* **1981**, *152*, 53–78. (e) Marks, T. J.; Manriquez, J. M.; Fagan, P. J.; Day, V. W.; Day, C. S.; Vollmer, S. H. *ACS Symp. Ser.* **1980**, *131*, 1–29.

(57) For example, in $Cp'_2Th[\eta^2\text{-}C(O)CH_3]^+B(C_6H_5)_4^-$, $\delta(CO) = 348.2$ and $\delta(CH_3) = 33$ (toluene-d_8 solution; Lin, Z.; Marks, T. J. Unpublished results).

(58) Waymouth, R. M.; Clauser, K. R.; Grubbs, R. H. *J. Am. Chem. Soc.* **1986**, *108*, 6385–6387.

(59) (a) Jeske, G.; Lauke, H.; Mauermann, H.; Sweptson, P. N.; Schumann, H.; Marks, T. J. *J. Am. Chem. Soc.* **1985**, *107*, 8091–8103. (b) Jeske, G.; Schock, L. E.; Swepston, P. J.; Schumann, H.; Marks, T. J. *J. Am. Chem. Soc.* **1985**, *107*, 8103–8110. (c) Jeske, G.; Lauke, H.; Mauermann, H.; Schumann, H.; Marks, T. J. *J. Am. Chem. Soc.* **1985**, *107*, 8111–8118.

against significant Th–CH_3 single step insertion chemistry (e.g., eq 6). However, the NMR feature at ~δ 25 is conceivably a

(6)

$^{13}CH_3$ end group of a propylene oligomer which would not have been detected in the trapping/GC assays (cf., δ 22.5 in solid isotactic and δ 21.0 in solid syndiotactic polypropylene[60,61]). $Cp'_2Ln(\eta^3$-allyl) and Cp'_2Ln(isobutyl) compounds are known to undergo propylene insertion (in competition with allylic C–H activation) to yield propylene oligomers.[50,59] Further support for the importance of allylic C–H functionalities here is provided by the observation that prolonged exposure of $Cp'_2Th(^{13}CH_3)_2/MgCl_2$ to 3,3'-dimethylbutene has no effect on the CPMAS spectrum (eq 7).

(7)

Additional information on the $Cp'_2Th(^{13}CH_3)_2/MgCl_2$ + propylene reaction is provided by studies with propylene 60% ^{13}C labeled in the C-2 position. The CPMAS spectrum (Figure 16B)[35a] reveals a multiplicity of resonances in the δ 20–70 and δ 120–150 regions. The most straightforward interpretation is in terms of repetitive propylene insertion by a surface η^3-allyl (M) to yield a mixture of oligomers (eq 8) of varying chain length (note

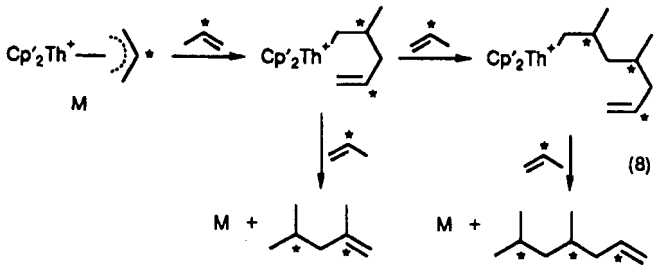

(8)

that an η^3-allyl can be regenerated via a competing process[59] analogous to eq 5), end group, and stereo- and possibly regioregularity. Thus, spectral features in the δ 140–155 region can be assigned to C2 resonances of an η^3-allyl (δ 147.3 and δ 153.3 in solid $Cp'Th(\eta^3\text{-}C_3H_5)_3$[33,62]) or to the C2 carbon of an olefinic end group (cf., eq 8; δ 140–145 in analogous olefins[63]). The resonance at ~δ 60 is assigned to an unreactive $Cp'_2Th(^{13}CH_3)O$– species, while the signals in the δ20–45 region must be due, predominantly, to labeled positons of propylene oligomers. Note that methine resonances in regioirregular polypropylenes fall in the range ~δ 28.3–38.5 in solution.[61] It is conceivable that lower molecular weights, different chain folding on the surface, olefin isomerization, and possible chemisorptive interactions with the surface[8] would increase the chemical shift dispersion further.

Conclusions

The results of this chemical/spectroscopic investigation considerably amplify what is known about organoactinide hydrocarbyl adsorbate structure and reactivity. Connections have been drawn between catalysis and spectroscopy which also convey implications for other adsorbed hydrocarbyl systems.[3]

Basically, three CPMAS spectroscopic patterns are observed for supported actinide hydrocarbyls. On strong Lewis acids (DA, $MgCl_2$, DSA), transfer of alkyl groups to acceptor sites on the surface is observed and is accompanied by residual low field Th–$^{13}C(\alpha)H_2R$ adsorbate resonances. The nature of the surface receptor site and NMR spectral similarities to species such as $Cp'_2Th(CH_3)^+BPh_4^-$ and $Cp'_2Th(CH_3)(THF)_2^+BPH_4^-$[13] suggest "cation-like" character. The present work shows this pattern is generalizable to other supports ($MgCl_2$, DSA), complexes ($Cp'ThR_3$, Cp_3ThR), and hydrocarbyl groups (ethyl, benzyl). From NMR experiments using paramagnetic U(IV) probes, it can be surmised that the great majority of $Cp'_2Th(CH_3)_2$-derived adsorbate molecules on both DA and $MgCl_2$ are not μ-alkyls (E) but rather the transferred surface alkyl moiety is ≳5 Å displaced from the actinide center. The second type of CPMAS pattern is observed on hydroxylated supports (PDA, PDS, MgO) where it is known[7] that extensive An–R protonolysis occurs. Here, the Th–$^{13}C(\alpha)H_2R$ resonance is at considerably higher field (in the region of $Cp'_2Th(CH_3)O$-type complexes), and no transferred surface alkyl group is evident. A "μ-oxo-like" structure (B, C) is suggested for these adsorbates. Traces of these structures are occasionally observed on Lewis acid supports and provide an interesting reactivity comparison. The third type of spectroscopic pattern is observed on dehydroxylated supports without strong Lewis acid character and having relatively weak surface metal–oxygen bonds (DS, portions of the DSA surface). Here both a "μ-oxo-like" Th–$^{13}C(\alpha)H_2R$ resonance *and* a transferred surface alkyl resonance are observed, suggesting a structure such as D. Paramagnetic probes indicate that the majority of the surface alkyl groups are ≳5 Å from the actinide center.

In regard to heterogeneous olefin hydrogenation and polymerization catalysis, the present NMR results add considerably to the structure-catalytic activity picture that is emerging. Importantly, significant catalytic activity is only observed in systems exhibiting "cation-like" spectral signatures[11e,13] (and metal alkyl or hydride bonds to effect the catalysis), while negligible activity is observed in systems exhibiting only "μ-oxo-like" ($Cp'_2Th(CH_3)O$–) spectral features.[12b,19] Moreover, "μ-oxo-like" species do not display significant reactivity in direct competition with "cation-like" species on the same surface. These reactivity trends accord well with solution chemical expectations.[6,13,14,15,19] Furthermore, the fractions of surface organoactinide complexes reactive in stoichiometric dosing experiments monitored by NMR are in good agreement with percentages of active sites assayed by catalytic CO and/or H_2O poisoning experiments.[7a,b] Thus, only ~4% of $Cp'_2Th(CH_3)_2/DA$ sites are important in propylene hydrogenation and ethylene polymerization as deduced by catalytic poisoning,[7a,b] while the present NMR studies evidence ethylene polymerization by a fraction of sites below the detection limit (Figure 9; ≲10% of the total) and response to hydrogenolysis at the same level. In contrast, 35 ± 10% of $Cp'_2Th(CH_3)_2/MgCl_2$ sites are found to be significant for propylene hydrogenation by catalytic poisoning,[7a] while the present NMR studies show 50 ± 10% of the observed sites active for ethylene insertion (Figures 10 and 11) and a comparable or larger percentage reactive with respect to hydrogenolysis (Figure 14).

The gross structural formulation for alkyl-transferred surface sites as "cation-like" (A) follows from chemical, structural, and spectroscopic analogies to solution chemistry.[13,14] Not surprisingly, the chemical properties of a particular "cation-like" adsorbate are expected to be highly dependent upon the characteristics of the local counterion—in this case, the local support microstructure. This surface is not expected to be topologically uniform[8] and it is likely, depending upon the bulk support structure and local heterogeneities, that different adsorbate sites will experience different counterion/surface interactions. The present results for spectroscopically "cation-like" $Cp'_2Th(CH_3)_2/DA$ and $Cp'_2Th(CH_3)_2/MgCl_2$ adsorbates underscore this point, and solution[12,13,64,65] results tell us that a completely noncoordinating anion

(60) (a) Bunn, A.; Cudby, M. E. A.; Harris, R. K.; Packer, K. J.; Say, B. J. *J. Chem. Soc., Chem. Commun.* **1981**, 15–16. (b) Bunn, A.; Cudby, M. E. A.; Harris, R. K.; Packer, K. J.; Say, B. J. *Polymer* **1982**, *23*, 694–698.
(61) Asakura, T.; Nishiyama, Y.; Doi, Y. *Macromolecules* **1987**, *20*, 616–620, and references therein.
(62) For additional η^3-allyl ^{13}C NMR data, see: Mann, B. E.; Taylor, B. F. *^{13}C NMR Data for Organometallic Compounds*; Academic Press: New York, 1981; pp 200–209.
(63) Silverstein, R. M.; Bassler, G. C.; Morrill, T. C. *Spectrometric Identification of Organic Compounds*, 4th ed.; Wiley: New York, 1981; Chapter 5.
(64) (a) Miller, P. K.; Abney, K. D.; Rappé, A. K.; Anderson, O. P.; Strauss, S. H. *Inorg. Chem.* **1988**, *27*, 2255–2261. (b) Colsman, M. R.; Noirot, M. D.; Miller, M. M.; Anderson, O. P.; Strauss, S. H. *J. Am. Chem. Soc.* **1988**, *110*, 6886–6888. (c) Moirot, M. D.; Anderson, O. P.; Strauss, S. H. *Inorg. Chem.* **1987**, *26*, 2216–2223, and references therein.
(65) (a) Liston, D. J.; Reed, C. A.; Eigenbrot, C. W.; Scheidt, W. R. *Inorg. Chem.* **1987**, *26*, 2739–2740. (b) Shelley, K.; Reed, C. A.; Lee, Y. J.; Scheidt, W. R. *J. Am. Chem. Soc.* **1986**, *108*, 3117–3118. (c) Shelley, K.; Finster, D. C.; Lee, Y. J.; Scheidt, W. R.; Reed, C. A. *J. Am. Chem. Soc.* **1985**, *107*, 5955–5959.

is difficult to achieve.

Further surface-solution chemistry connections are seen in $Cp'_2Th(CH_3)_2/MgCl_2$ CO dosing experiments, which evidence irreversible migratory insertion processes, most likely of the type previously observed in solution. $Cp'_2Th(CH_3)_2/MgCl_2$ propylene chemistry is dominated by initial allylic C-H activation/methane elimination. Subsequent chemistry involves olefin insertion and oligomerization as well as η^3-allyl formation. All of these have been previously noted in f-element solution chemistry.

Acknowledgment. We are grateful to the Division of Chemical Sciences, Office of Basic Energy Sciences, Office of Energy Research, U.S. Department of Energy, for support of this research under Grant DE-FG02-86ER13511. We thank Dr. Jean-Francois LeMarechal for generous gifts of several samples.

Supplementary Material Available: Figures 3, 12, 13, 15, and 16 showing NMR spectra (6 pages). Ordering information is given on any current masthead page.

Synthesis, Structure, and Reactivity of Metallacycle-Carbene and -Bis(carbene) Complexes. A New Intramolecular Carbene-Carbene Coupling Process

Joseph M. O'Connor,*[1a] Lin Pu,[1a,c] and Arnold L. Rheingold*[1b]

Contribution from the Departments of Chemistry, University of California at San Diego, La Jolla, California 92093, and University of Delaware, Newark, Delaware 19716.
Received November 27, 1989

Abstract: Halide ion abstraction from the neutral iridiacyclopentadiene complexes, Ir(CR=CRCR=CR)$(PPh_3)_2$Cl (**1**, R = CO_2CH_3), and Ir(CR=CRCR=CR)$(PPh_3)_2$(CO)(Cl) (**2**, R = CO_2CH_3), leads to high yields of the cationic complexes, Ir(CR=CRCR=CR)$(PPh_3)_2$(L)(L')$^+BF_4^-$ (**3**, L = CO, L' = H_2O; **4**, L = CO, L' = $NCCH_3$; **5**, L = L' = $NCCH_3$; and **6**, L = CO, L' = PMe_3). Reaction of complex **1** and 3-butyn-1-ol generates the first example of a metallacycle-carbene complex Ir(CR=CRCR=CR)$(PPh_3)_2$(Cl)[=C$(CH_2)_3$O] (**7**; 81%). Similarly, reaction of **3** or **4** and 3-butyn-1-ol leads to formation of the carbene complex Ir(CR=CRCR=CR)$(PPh_3)_2$(CO)[=C$(CH_2)_3$O]$^+BF_4^-$ (**8**; 96%). Reaction of **4** and 4-pentyn-2-ol gives a 95% yield of the substituted carbene complex Ir(CR=CRCR=CR)$(PPh_3)_2$(CO)[=C$(CH_2)_2$CHCH$_3$O]$^+BF_4^-$ (**9**). The acetonitrile analogues, Ir(CR=CRCR=CR)$(PPh_3)_2(NCCH_3)$[=C$(CH_2)_3$O]$^+BF_4^-$ (**10**) and Ir(CR=CRCR=CR)$(PPh_3)_2(NCCH_3)$[=C$(CH_2)_2$CHCH$_3$O]$^+BF_4^-$ (**11**), are also prepared in excellent yield. The bis(carbene) complex Ir(CR=CRCR=CR)$(PPh_3)_2$[=C$(CH_2)_3$O]$_2^+BF_4^-$ (**12**) is available in one step from **5** (87%). The mixed bis(carbene) complex Ir(CR=CRCR=CR)$(PPh_3)_2$[=C$(CH_2)_2$CHCH$_3$O][=C$(CH_2)_3$O]$^+BF_4^-$ (**13**) is prepared from **7** by sequential reaction with $AgBF_4$ and 4-pentyn-2-ol. Complex **8** crystallizes in space group *Cc*, with a = 12.723 (2) Å, b = 21.195 (4) Å, c = 18.432 (3) Å, β = 90.37 (1)°, V = 4970 (1) Å^3, Z = 4, $R(F)$ = 3.11%, and $R_w(F)$ = 3.76%. Complex **12** crystallizes in space group $P\bar{1}$, with a = 12.951 (2) Å, b = 13.371 (2) Å, c = 18.071 (4) Å, α = 78.42 (2)°, β = 79.27 (2)°, γ = 78.14 (1)°, V = 2966 (1) Å^3, Z = 2, $R(F)$ = 4.35%, $R_w(F)$ = 4.87%. Reaction of compounds **8** and **9** with pyridine gives the pyridinium-substituted acyl complexes Ir(CR=CRCR=CR)$(PPh_3)_2$(CO)[C(=O)$CH_2CH_2CH_2NC_5H_5$]$^+BF_4^-$ (**14**) and Ir(CR=CRCR=CR)$(PPh_3)_2$(CO)[C(=O)$CH_2CH_2CH(CH_3)NC_5H_5$]$^+BF_4^-$ (**17**). Methylamine and bis(oxacyclopentylidene) complex **12** give a nearly quantitative yield of the iridium hydride complex Ir(CR=CRCR=CR)$(PPh_3)_2(NH_2CH_3)$(H) (**19**), $CH_3NH_3^+BF_4^-$, and 2-(2(5*H*)-furanylidene)tetarhydrofuran (**20**; 92%). The mixed bis(carbene) complex **13** undergoes reaction with methylamine to give iridium hydride **19** and the carbene coupling products 2-(2(5*H*)-furanylidene)-5-methyltetrahydrofuran (**24**; 45%) and 2-(2(5-methyl)furanylidene)tetrahydrofuran (**25**; 55%). Iridium hydride **19** reacts with HCl to regenerate **1** and with HBF_4 in acetonitrile to regenerate the bis(carbene) precursor **5**. The mechanism of this novel carbene ligand coupling chemistry is discussed.

Introduction

Interest in the properties and reactivity of metal-carbene complexes has continued unabated since E. O. Fischer reported the first examples of this compound class over 20 years ago.[2] Current interest in this area stems from the role of metal carbenes in alkene metathesis,[3] alkene and alkyne polymerization,[4] and cyclopropanation chemistry,[5] and as intermediates in an impressive array of synthetic methodology.[6,7] In an effort to develop new

(1) (a) University of California, San Diego. (b) University of Delaware. (c) PRC Doering Fellow.

(2) Fischer, E. O.; Maasböl, A. *Angew. Chem.* **1964**, *76*, 645; *Angew. Chem., Int. Ed. Engl.* **1964**, *3*, 580.

(3) (a) Ivin, K. J. *Olefin Metathesis*; Academic: London, 1983. (b) Grubbs, R. H. In *Comprehensive Organometallic Chemistry*; Wilkinson, G., Stone, F. G. A., Abel, E. W., Eds.; Pergamon: New York, 1982; Vol. 8, p 499. (c) Dragutan, V.; Balaban, A. T.; Dimonie, M. *Olefin Metathesis and Ring-Opening Polymerization of Cyclo-Olefins*, 2nd ed.; Wiley-Interscience: New York, 1985.

(4) (a) Grubbs, R. H.; Tumas, W. *Science* **1989**, *243*, 907, and references therein. (b) Katz, T. J.; Lee, S. J.; Shippel, M. A. *J. Mol. Cata.* **1980**, *8*, 219. (c) Schrock, R. R.; Freudenberger, J. H.; Listemann, M. L.; McCullough, L. G. *J. Mol. Catal.* **1985**, *28*, 1. (d) Schrock, R. R. *Acc. Chem. Res.* **1986**, *19*, 342.

0002-7863/90/1512-6232$02.50/0

Probing Hydrogen Bonding and the Local Environment of Silanols on Silica Surfaces via Nuclear Spin Cross Polarization Dynamics

I-Ssuer Chuang and Gary E. Maciel*

Contribution from the Department of Chemistry, Colorado State University, Fort Collins, Colorado 80523-0002

Received May 12, 1995[⊗]

Abstract: By studying $^{1}H \rightarrow ^{29}Si$ cross-polarization dynamics of two untreated and two "dry" silica gel samples (one evacuated at 25 °C and one evacuated at 200 °C), we find that all the surface silanols on the two untreated silicas are hydrogen bonded, either to the hydroxyl groups of adjacent silanol(s) or to water molecule(s). About 46% and 47% of the geminal silanols and 53% and 58% of the single silanols that were hydrogen bonded only to water in the two untreated silicas become non-hydrogen bonded on the two "dry" silica surfaces, but the remainder of the silanols of the untreated silicas (i.e., those hydrogen bonded to other silanols) remain hydrogen bonded to other silanols upon drying. The ratio of the number of hydrogen-bonding single silanols to the number of hydrogen-bonding geminal silanols is 17-to-1 for a Fisher silica surface evacuated at 25 °C and 16-to-1 for a Baker silica surface evacuated at 200 °C. These results can be explained in terms of a generalized silica surface model based on the β-cristobalite crystal structure.

Introduction

Silicas and modified silicas are highly versatile materials with numerous applications, such as catalysis, separation science, microelectronics, consumer products, and composite materials. Many applications of silicas rely on their unique surface properties, which in turn are largely determined by the concentration, distribution, and nature of hydroxyls (silanols) on the surface.[1,2] Various NMR techniques,[3−18] infrared[3−6,15,19−24] and Raman[21,24,25] spectroscopies, chemical probes,[3,4,11,12,19−21] and various other analytical tools[1−3,19,26] have been utilized to investigate hydroxyls on silica surfaces.

The characterization of cross-polarization[27] (CP) spin dynamics[14,27−31] is not only a must for reliable quantitation in a CP-MAS NMR experiment,[32] but it also can provide a rough estimate for heteronuclear dipolar interaction strengths,[14,28−31] which are related to chemical structure (internuclear distances) and dynamics. In a previous article,[17] we indicated that for the ^{29}Si nuclei of isolated single silanols the cross-polarization time constant, T_{HSi} (*vide infra*), is at least five times larger than that for hydrogen-bonded single silanols. Therefore, by ^{29}Si CP-MAS NMR spectroscopy it is possible to distinguish hydrogen-bonded silanols from non-hydrogen-bonded silanols and at the same time to quantify the ratio of geminal silanols and single silanols on a silica surface under various conditions (e.g., untreated or evacuated at various temperatures). In that previous article, we also established that *both* geminal silanols and single silanols exist and are not hydrogen bonded on a silica surface that has been evacuated at 500 °C.

In this article, we show how the characterization of CP spin dynamics can be employed to probe hydrogen bonding and the local structural environments of various hydroxyl groups of silica surfaces in greater detail. We also show that a generalized

[⊗] Abstract published in *Advance ACS Abstracts,* December 15, 1995.

(1) Iler, R. K. *The Chemistry of Silica*; Wiley: New York, 1979.
(2) Brinker, C. J.; Scherer, G. W. *Sol-Gel Science: The Physics and Chemistry of Sol-Gel Processing*; Academic Press: New York, 1990.
(3) Köhler, J.; Chase, D. B.; Farlee, R. D.; Vega, A. J.; Kirkland, J. J. *J. Chromatogr.* **1986**, *352*, 275.
(4) Davydov, V. Y.; Kiselev, A. V.; Pfeifer, H.; Junger, I. *Russ. J. Phys. Chem.* **1983**, *57*, 1527.
(5) Haukka, S.; Lakomaa, E.-L.; Root, A. *J. Phys. Chem.* **1993**, *97*, 5085.
(6) Haukka, S.; Root, A. *J. Phys. Chem.* **1994**, *98*, 1695.
(7) Bronnimann, C. E.; Zeigler, R. C.; Maciel, G. E. *J. Am. Chem. Soc.* **1988**, *110*, 2023.
(8) Kinney, D. R.; Chuang, I-S.; Maciel, G. E. *J. Am. Chem. Soc.* **1993**, *115*, 6786.
(9) Maciel, G. E.; Sindorf, D. W. *J. Am. Chem. Soc.* **1980**, *102*, 7606.
(10) Sindorf, D. W.; Maciel, G. E. *J. Am. Chem. Soc.* **1983**, *105*, 1487.
(11) Sindorf, D. W.; Maciel, G. E. *J. Phys. Chem.* **1982**, *86*, 5208
(12) Maciel, G. E.; Bronnimann, C. E.; Zeigler, R. C.; Chuang, I-S.; Kinney, D. R.; Keiter, E. A. In *The Colloid Chemistry of Silica*; Bergna, H. E., Ed.; Advances in Chemistry Series 234, American Chemical Society: Washington, DC, 1994; p 269.
(13) Chuang, I-S.; Kinney, D. R.; Bronnimann, C. E.; Zeigler, R. C.; Maciel, G. E. *J. Phys. Chem.* **1992**, *96*, 4027.
(14) Walther, K. L.; Wokaun, A.; Baiker, A. *Mol. Phys.* **1990**, *71*, 769.
(15) Legrand, A. P.; Hommel, H.; Tuel, A.; Vidal, A.; Balard, H.; Papirer, E.; Levitz, P.; Czernichowski, M.; Erre, R.; Van Damme, H.; Gallas, J. P.; Hemidy, J. F.; Lavalley, J. C.; Barres, O.; Burneau, A.; Grillet, Y. *Adv. Colloid Interface Sci.* **1990**, *33*, 91.
(16) Tuel, A.; Hommel, H.; Legrand, A. P.; Chevallier, Y.; Morawski, J. C. *Colloids Surf.* **1990**, *45*, 413.
(17) Chuang, I-S.; Kinney, D. R.; Maciel, G. E. *J.. Am. Chem. Soc.* **1993**, *115*, 8695.
(18) Maciel, G. E.; Ellis, P. D. in *NMR Techniques In Catalysis*, Bell, A. T.; Pines, A., Eds.; Marcel Dekker: New York, 1994; p 231.
(19) Peri, J. B. *J. Phys. Chem.* **1966**, *70*, 2937.
(20) Hair, M. L. *Infrared Spectroscopy In Surface Chemistry*; Marcel Dekker: New York, 1967.
(21) Morrow, B. A.; McFarlan, A. J. *J. Non-Cryst. Solids* **1990**, *120*, 61.
(22) Hoffmann, P.; Knözinger, E. *Surf. Sci.*, **1987**, *188*, 181.
(23) Kiselev, A. V. *Discus. Faraday Soc.* **1971**, *52*, 14.
(24) Morrow, B. A.; McFarlane, R. A. *J. Phys. Chem.* **1986**, *90*, 3192.
(25) Brinker, C. J.; Tallant, D. R.; Roth, E. P.; Ashley, C. S. *J. Non-Cryst. Solids* **1986**, *82*, 117.
(26) Mikhail, R. S.; Robens, E. *Microstructure and Thermal Analysis of Solid Surfaces*; John Wiley & Sons: New York, 1983.
(27) Pines, A.; Gibby, M. G.; Waugh, J. S. *J. Chem. Phys.* **1973**, 59, 569.
(28) Mehring, M. *Principles of High Resolution NMR in Solids*, 2nd ed.; Springer-Verlag: New York, 1983.
(29) Klein Douwel, C. H.; Maas, W. E. J. R.; Veeman, W. S.; Buning, G. H. W.; Vankan, J. M. J. *Macromolecules* **1990**, *23*, 406.
(30) Eijkelenboom, A. P. A. M.; Maas, W. E. J. R.; Veeman, W. S.; Buning, G. H. W.; Vankan, J. M. J. *Macromolecules* **1992**, *25*, 4511.
(31) Slichter, C. P. *Principles of Magnetic Resonance*, 3rd ed.; Springer-Verlag: New York, 1989; p 79.
(32) Schaefer, J.; Stejskal, E. *J. Am. Chem. Soc.* **1976**, *98*, 1031.

0002-7863/96/1518-0401$12.00/0

model of silica surfaces based on β-cristobalite can account for our data.

Experimental Section

Fisher Scientific silica gel (S679−500; surface area: 456 m^2/g) was used directly without treatment (untreated Fisher) or with evacuation at 10^{-3} Torr at 25 °C for 24 h (Fisher evacuated at 25 °C). J. T. Baker silica gel (Analyzed Reagent, 34D5-01; surface area: 290 m^2/g) was used without treatment (untreated Baker) or with evacuation at 10^{-3} Torr and 200 °C (Baker evacuated at 200 °C). The untreated and 25 °C evacuated Fisher silica samples were loaded for ^{29}Si NMR measurements into 2.5 cm^3 "pencil"-type magic-angle spinning (MAS)[33,34] rotors (Chemagnetics) with zirconia sleeves. The untreated and 200 °C evacuated Baker silica samples were loaded for ^{29}Si NMR measurements into a Gay-type MAS rotor;[35] the Baker silica sample evacuated at 200 °C was sealed under reduced N_2 pressure in a glass tube to prevent moisture contamination.

^{29}Si NMR spectra were obtained at 39.75 MHz on a heavily-modified Nicolet NT-200 spectrometer under the conditions of $^1H-^{29}Si$ cross polarization, magic-angle spinning, and ^1H decoupling, using a 0.6 s repetition delay for the untreated Fisher and Baker silica samples, a 5 s repetition delay for the 25 °C evacuated Fisher sample, or a 6 s repetition delay for the 200 °C evacuated Baker sample. These repetition delays were chosen as apparently optimal for signal-to-noise ratio achieved within a specific time; these values are much too small to yield quantitative *absolute* intensities. However, since all the CP-MAS ^{29}Si signals of a specific sample yield the *same* proton spin−lattice relaxation time, T_1^H (see below), the choice of repetition delay does *not* impact on the quantitation of *relative* CP-MAS ^{29}Si signals *within* a given spectrum. The other conditions for CP-MAS experiments are described in the Results and Discussion section. The drive gas for MAS was air for the untreated Fisher and Baker samples and for the Baker sample evacuated at 200 °C and nitrogen for the Fisher silica evacuated at 25 °C. The radio frequency field strengths of both the ^1H and ^{29}Si channels were typically 30 kHz for the large-volume "pencil"-type MAS system and 40 kHz for the Gay-type system. ^{29}Si NMR chemical shifts are reported in ppm, referenced to liquid tetramethylsilane (by substitution), higher values corresponding to lower shieldings.

Measurements of T_1^H were made by a Freeman-Hill version of a CP-MAS T_1^H experiment, by detecting the ^{29}Si CP-MAS intensity that was cross polarized from protons.[36] The rotating-frame proton spin-lattice relaxation time ($T_{1\rho}^H$) was measured by varying the duration of a ^1H spin-lock period prior to a fixed $^1H \rightarrow ^{29}Si$ cross-polarization contact period (1 ms for Fisher samples and 5 ms for Baker samples). The cross-polarization time constants (T_{HSi}) were determined by analysis of variable contact-time experiments, using the independently-determined $T_{1\rho}^H$ values in a nonlinear least-squares fit of the variable-contact-time data.

Relaxation parameters were derived in two ways: on the basis of (a) peak heights and (b) areas derived from spectral deconvolutions. The T_{HSi} data presented in this paper were based on deconvolutions (*vide infra*), but data analysis based on peak heights yielded substantially similar results (not given here). Since ^{29}Si-detected T_1^H and $T_{1\rho}^H$ experiments produced sets of spectra for which peak shapes are invarient to variation in the relaxation period, peak heights were used to analyze these data.

Results and Discussion

With ^{29}Si in 4.7% natural abundance and the rather high proton density on the silica surface, the Hartmann-Hahn cross-polarized ^{29}Si NMR magnetization, $I(\tau)$, after a CP contact time τ can be described by[28]

$$I(\tau) = \frac{I^*}{1-\lambda}(1 - \exp\{-(1-\lambda)\tau/T_{HSi}\}) \exp\{-\tau/T_{1\rho}^H\} \quad (1)$$

where I^* is the ideal (full) cross-polarized ^{29}Si magnetization and $\lambda = T_{HSi}/T_{1\rho}^H$. In eq 1, which is valid for the case $T_{1\rho}^{Si} \gg T_{1\rho}^H$, T_{HSi}, the parameter T_{HSi}^{-1} is the $^1H-^{29}Si$ cross-polarization rate constant, which depends on the strength of the $^1H-^{29}Si$ and ^1H-^1H dipolar interactions and is roughly proportional to the inverse sixth power of $^1H-^{29}Si$ internuclear distance.[14,28-31] T_{HSi} and $T_{1\rho}^H$ values vary with different samples and they may have different values for different sets of ^{29}Si and ^1H within a given sample. Therefore, for a quantitative analysis, T_{HSi} and $T_{1\rho}^H$ must be determined for each peak.

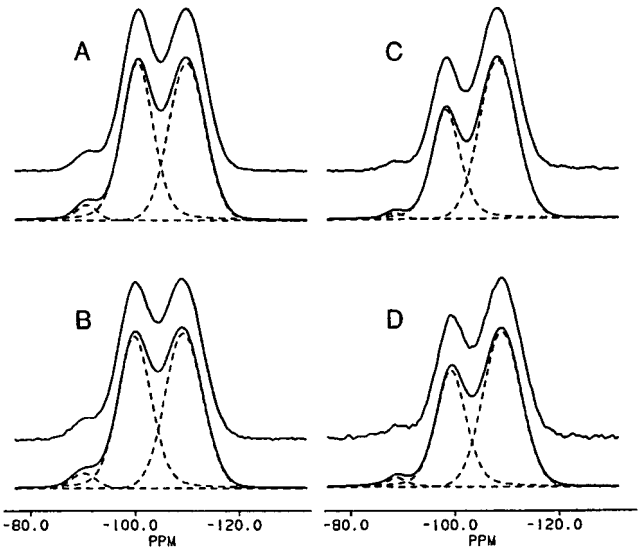

Figure 1. 39.75-MHz ^{29}Si CP-MAS spectra (upper) and their computer deconvolution simulations (lower) of the four samples of this study: A, untreated Fisher; B, Fisher evacuated; C, untreated Baker; D, Baker evacuated. CP contact time: 25 ms. MAS speed: 1.7 kHz (A, B), 2.2 kHz (C, D). Repetitions: 3000 (A), 1000 (B), 10000 (C), 2000 (D).

Figure 1 shows ^{29}Si CP-MAS spectra of the four samples of this study, together with the computer deconvolution/simulation plots that represent the quality of deconvolutions used in the analysis of relaxation data. One sees, especially for the untreated samples (Figures 1A and 1C), the characteristic pattern of three peaks: a small peak (or shoulder) at −89 ppm due to Q_2 silicons, i.e., $(\equiv SiO)_2\mathbf{Si}(OH)_2$; a peak at −99 ppm due to Q_3 silicons, i.e., $(\equiv SiO)_3\mathbf{Si}OH$; and a peak at −109 ppm due to Q_4 silicons, i.e., $(\equiv SiO)_4\mathbf{Si}$.

For a reliable and simplified fitting of eq 1, $T_{1\rho}^H$ values discussed in this article were measured independently, as described in the Experimental Section. For each of the silica samples of this study, essentially the same $T_{1\rho}^H$ value was obtained for single silanol, geminal silanol, and siloxane silicons. The results for the four silica samples studied are summarized in Table 1.

In order to obtain the parameters I^* and T_{HSi} in eq 1, variable-contact-time (VCT) experiments were performed. For each of the two untreated silica samples (Fisher and Baker silicas), a single T_{HSi} value is sufficient to fit each set of VCT data for geminal silanols or for single silanols. However, two T_{HSi} values are needed for a satisfactory fit of the VCT data of geminal silanols or of single silanols of the two dry silica samples, the 25 °C evacuated Fisher silica and the 200 °C evacuated Baker silica. Derived T_{HSi} values and the corresponding relative

(33) Andrew, E. R. *Prog. NMR Spectrosc.* **1971**, *8*, 1.
(34) Lowe, J. J. *Phys. Rev. Lett.* **1959**, *2*, 285.
(35) Gay, I. D. *J. Magn. Reson.* **1984**, *58*, 413.
(36) Frye, J. S. *Concepts in Magn. Reson.* **1989**, *1*, 27.

Table 1. Relaxation Time Constants and Relative Contributions for Various Silicas, As Determined by ^{29}Si CP-MAS NMR

	T_{HSi} (ms) and relative contribution[a]		$T_1^H\rho$ (ms)		T_1^H (s)	
	>Si(OH)$_2$ −89 ppm	≥SiOH −99 ppm	>Si(OH)$_2$ −89 ppm	≥SiOH −99 ppm	>Si(OH)$_2$ −89 ppm	≥SiOH −99 ppm
Fisher untreated	1.3 (0.056)	2.0 (0.94)	42.8	43.7	0.3	0.3
Fisher evac at 25 °C	0.50 (0.027)	1.2 (0.45)	189	179	5	5
	6.0 (0.023)	14 (0.50)				
Baker untreated	1.2 (0.041)	2.1 (0.96)	36	36	0.09	0.09
Baker evac at 200 °C	0.49 (0.026)	1.4 (0.40)	163	169	5.5	5.7
	5.9 (0.023)	14 (0.55)				

[a] Fraction of contribution in parentheses.

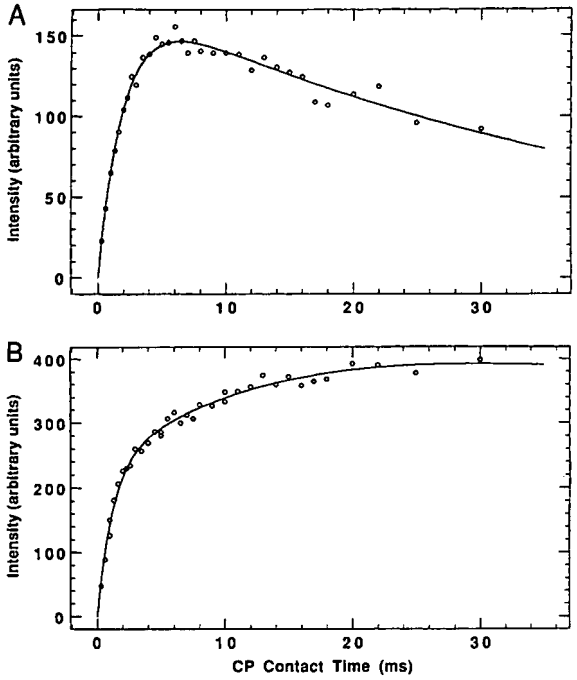

Figure 2. 39.75-MHz variable-contact-time ^{29}Si CP-MAS results and nonlinear least-square fits of the −99-ppm single-silanol peak for Fisher S-679 silica gel samples: (A) Untreated; (B) Evacuated at 10^{-3} Torr at 25 °C for 24 h. MAS speed 1.7 kHz. Repetitions: 3000 (A) or 1000 (B).

contribution of each T_{HSi} value for single silanols and for geminal silanols of the four silica samples are listed in Table 1, along with the corresponding $T_{1\rho}^H$ and T_1^H values. Figures 2A and 2B show the computer fitting of the VCT peak intensity data representing single-silanol silicons on the surfaces of the untreated and 25 °C evacuated Fisher silicas, respectively. Even better fits (not shown here), also requiring two T_{HSi} values for each of the data sets representing the two dry silica samples, were obtained from data analysis in terms of peak heights.

On the basis of measured T_{HSi} values and ^{1}H−^{1}H and ^{1}H−^{29}Si dipolar-dephasing characteristics (the former prior to ^{1}H→^{29}Si cross polarization), we previously indicated that internal (subsurface) single silanols have much smaller net ^{1}H−^{1}H and ^{1}H−^{29}Si dipolar interactions than those experienced by single silanols on the untreated silica surface.[17] We have shown that the T_{HSi} value for internal single silanols is roughly 4.5−5.0 times larger than T_{HSi} for external single silanols of untreated silica. This implies that the external single silanols of untreated

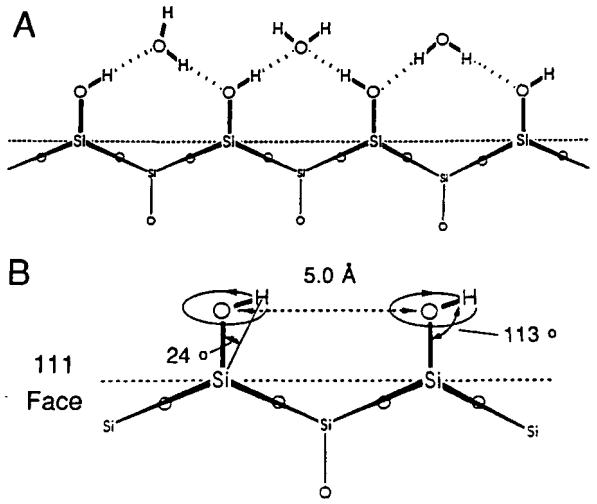

Figure 3. (A) Single-silanol surface structure with hydrogen bonding to water molecules. (B) Side view of the (111)-type plane (dotted line representing an edge of such a plane) of the β-cristobalite structure with a single silanol (drawn approximately to scale).

silica experience ^{1}H−^{29}Si dipolar interactions that are slightly more than twice as large as those experienced for internal single silanols. On the surfaces of untreated silica gels, hydroxyl rotation of single silanols may be hindered or held rigidly through strong hydrogen bonding with water,[8,17] as shown symbolically in Figure 3A; in addition, some of the silanols can also be rendered rigid through strong hydrogen bonding with neighboring silanols (*vide infra*). For non-hydrogen-bonded internal single silanols that freely rotate about the Si−O bond axis, the ^{1}H−^{29}Si dipolar interaction within a given SiOH moiety would be scaled down by the factor[37] (1/2)(3 cos^2 24° − 1) = 0.75 (cf. Figure 3B), in comparison to single silanols on the untreated silica surface.

If the external single silanols on an untreated silica surface are held together relatively rigidly via hydrogen bonding to bridging water molecule(s) or neighboring silanols, then the protons of these nearby molecules also contribute to the overall extent of ^{1}H−^{29}Si dipolar interactions of the silicons of single silanols on the surface. Hence, hydrogen bonding can be expected to increase the *net* efficiency of ^{1}H→^{29}Si cross polarization of single silanols relative to that of non-hydrogen-bonded single silanols by (1) increasing the number of protons that interact with each silanol silicon and (2) restraining motional averaging of the dipolar interactions. This overall differential

(37) Gutowsky, H. S.; Pake, G. E. *J. Chem. Phys.* **1950**, *18*, 162.

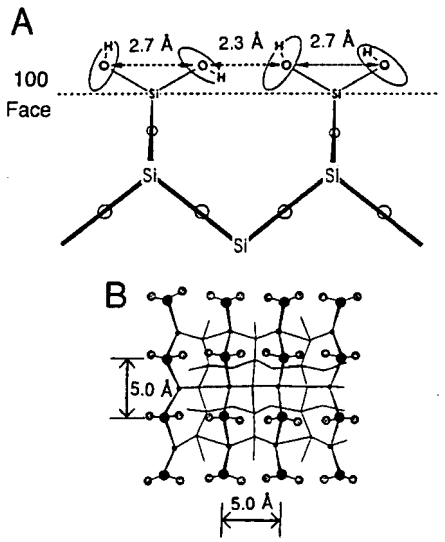

Figure 4. Representative (100)-type β-cristobalite face with geminal silanols (hydroxyl groups). (A) Side view of the (100)-type plane (dotted line representing an edge of such a plane) of the β-cristobalite structure with geminal silanols. (B) Top view of the (100)-type face (hydroxyl groups shaded; oxygen bridges not shown).

in CP efficiency makes it possible to distinguish between silanols with and without hydrogen bonds on the silica gel surface. The fact that just one T_{HSi} value is sufficient for fitting the VCT data for all single silanols and a different T_{HSi} value is sufficient for all geminal silanols on each of the untreated Fisher and Baker silicas indicates that the overall strengths of $^1H-^{29}Si$ dipolar interactions of each single silanol or geminal silanol are very similar to each other (within each silanol category), because all are involved in hydrogen bonding.

Previously, (111)-type and (100)-type faces of a β-cristobalite crystal structure, in which specific SiOSi moieties are replaced by SiOH moieties, have been discussed as models for surfaces containing single silanols and geminal silanols, respectively, of silicas.[1,2,10,11] According to this model and the discussion above, single silanols on a given (111)-type face of an undried silica sample are "bridged" via hydrogen bonding to water molecules. Adjacent geminal silanols on the same (100)-type face of an untreated silica surface are close enough together, with proper relative orientation, to form hydrogen bonds with each other (Figure 4A). Figure 4B is a top view of a (100)-type face; the hydroxyl groups on adjacent geminal silanols in the same row point toward each other, with a spatial relationship identical to that of the inner pair of hydroxyl groups in Figure 4A, and can hydrogen bond with each other. However, the hydroxyl groups on adjacent geminal silanols in the same column of Figure 4B have a similar spatial relationship to that of adjacent single silanols on the same (111)-type face (see Figure 3B) and cannot hydrogen bond with each other. On an untreated silica surface, the adjacent geminal silanols in the same column of Figure 4B are bridged via hydrogen bonding to water molecules, similar to the situation for single silanols on the same (111)-type face (cf. Figure 3A).

The fact that two T_{HSi} values are needed to fit the VCT results for peak intensities representing single silanols and two values are needed to fit the data for geminal silanols of both *dry* samples (Fisher and Baker silicas evacuated at 25 and 200 °C, respectively) implies that the $^1H-^{29}Si$ dipolar interactions of various single silanols have different magnitudes, and the same thing is true for the various geminal silanols. For single silanols of the dry (25 °C evacuated) Fisher sample, the large T_{HSi} value (14 ms) is almost identical to the T_{HSi} value reported for interior hydroxyl groups (non-hydrogen-bonding single silanols) in a previous article;[17] therefore, the T_{HSi} = 14 ms set of single silanols can be attributed to non-hydrogen-bonded single silanols. The single silanols with a 1.2 ms T_{HSi} value can be attributed to hydrogen-bonded single silanols. Similarly, those geminal silanols with a large T_{HSi} value (6 ms) are identified here as *not* hydrogen bonded; those geminal silanols with T_{HSi} = 0.5 ms are identified as involved in hydrogen bonding. It is presumably not coincidental that for each category of silanols, there is roughly a factor of 2 between the T_{HSi} values of single and geminal silanols.

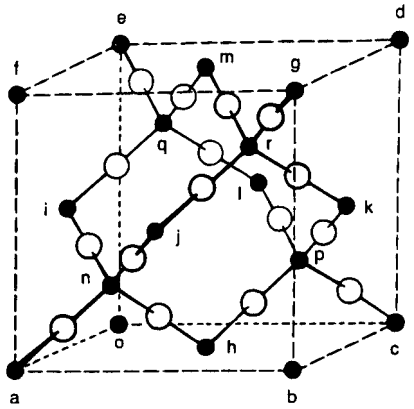

Figure 5. Unit cell of the β-cristobalite crystal structure, according to Wells.[39] Solid circles represent silicon sites and open circles oxygen sites. The Si−O−Si angle is 147° and each silicon is connected to four other silicons tetrahedrally through oxygen bridges.

The ratio of the number of hydrogen-bonding single silanols to the number of hydrogen-bonding geminal silanols on the surface of the Fisher silica evacuated at 25 °C is seen from the data shown in Table 1 to be about 17-to-1; and about 46% of the geminal silanols and 53% of the single silanols are not hydrogen bonded. The corresponding values for the surface of the Baker silica evacuated at 200 °C are 16-to-1, 47% and 58%, respectively. Any satisfactory model for the silica surface should be able to explain these results. The fact that single silanols on the same (111)-type face of a β-cristobalite structure are not hydrogen bonded to each other (*vide supra*) can easily account for 53−58% of the non-hydrogen-bonding single silanols on the surfaces of the Fisher and Baker silicas evauated at 25 and 200 °C, respectively; the remaining 47−42% hydrogen-bonded single silanols can be interpreted in terms of the β-cristobalite model, if one invokes the idea of intersections of individual (111)-type surface planes with other surface planes—(111)-type or (100)-type.[38]

Figure 5 represents the unit cell of β-cristobalite. If the cube represented in Figure 5 is *inside* the framework of a silica gel particle, and if position m in Figure 5 represents a missing silicon in an internal defect, then if each of the oxygen atoms that would have been bonded to silicon m in a perfect crystal is instead bonded to a hydrogen, there will be four single silanols with their **Si−OH** internuclear axes perpendicular to four different (111)-type planes (for simplicity in the discussion, we assume that the Si−O−Si angle is 180° instead of 147°),[2,40] and these four single silanols point toward each other tetrahedrally. The spatial relationship of each pair of such single silanols is similar to that of the inner pair of hydroxyl groups shown in Figures 4A and 4B (same row); they are expected to hydrogen bond with each other. In other words, when two

(38) Chuang, I-S., Maciel, G. E. *J. Non-Cryst. Solids* Submitted for publication.
(39) Wells, F. A. *Structural Inorganic Chemistry*, 5th ed.; Claredon Press: Oxford, U.K., 1984; p 1007.
(40) Reference 39, p 1006.

(111)-type planes intersect concavely, the single silanols situated at the intersection can hydrogen bond with each other across the intersection. Therefore, at such a defect position m inside the framework of silica gel, each single silanol will be involved in hydrogen bonding with the other three single silanols. If, in addition to a silicon missing at position m, silicon is also missing at position e or position g, then there will be six single silanols and one geminal silanol in this defect; the two hydroxyl groups of this geminal silanol can form hydrogen bonds with six single silanols, which corresponds to a 6:1 ratio of hydrogen-bonding single silanols to geminal silanols. Again, the spatial relationship of each pair of such a single silanol and its neighboring geminal silanols at the concave intersection of a (111)-type plane and a (100)-type plane is similar to that of the inner pair of hydroxyl groups shown in Figures 4A and 4B (same row); they can hydrogen bond with each other across the intersection. This kind of configuration could presumably be present on the outside surface and/or inside the bulk of silica gel.

One of our previous articles[17] indicated that all hydrogen-bonding single silanols and almost all geminal silanols (hydrogen-bonding or non-hydrogen-bonding) should be external, i.e., accessible to D_2O exchange. It was found that almost all hydroxyl groups inaccessible to D_2O exchange are non-hydrogen-bonding single silanols. Even though we do not rule out the possibility that one geminal silanol can be involved in hydrogen bonding with six single silanols and at the same time be accessible for D_2O exchange, we regard this defect configuration as only a minor population for hydrogen-bonding single silanols and geminal silanols. Other possible explanations for the experimentally determined relative numbers of hydrogen-bonding geminal silanols and single silanols are explored in the following paragraphs. We have already discussed the hydrogen-bonding possibilities between hydroxyl groups of geminal silanols on individual (100)-type silica surfaces (cf., Figure 4). If one considers the various kinds of intersections between (100)-type surface planes and (111)-type surface planes, then one finds various other possibilities for hydrogen bonding between hydroxyl groups of pairs of single silanols, and between hydroxyl groups of single silanols and geminal silanols on the silica surface.

According to the simple β-cristobalite model previously introduced for single silanols and geminal silanols on a silica surface,[38] based on (111)-type (Figures 3B and 6A) and (100)-type (Figures 4 and 6B) faces, respectively, the single silanols on the same (111)-type face should not be hydrogen bonded to each other. However, if a (111)-type face intersects concavely with a (100)-type face, those single silanols at the intersection can form hydrogen bonds with adjacent geminal silanols, as represented in shorthand fashion in Figures 6C and 6D. Similarly, Figure 6E represents in shorthand notation the situation in which two non-parallel (111)-type faces intersect concavely with each other. As discussed earlier,[38] two single silanols on the *same* (111)-type face of a β-cristobalite system cannot hydrogen bond with each other; however, hydrogen bonding between single silanols across the concave intersection of two (111)-type faces can occur in the kind of situation depicted in Figure 6E.

The kinds of detailed models of pore (or defect) structures that can be represented in terms of structures like that depicted in Figure 6H are consistent with the general idea that surface curvature can make hydrogen bonding possible in situations that would not be conducive to hydrogen bonding if the surface were "flat". A qualitatively similar view has been discussed by Legrand and co-workers.[16]

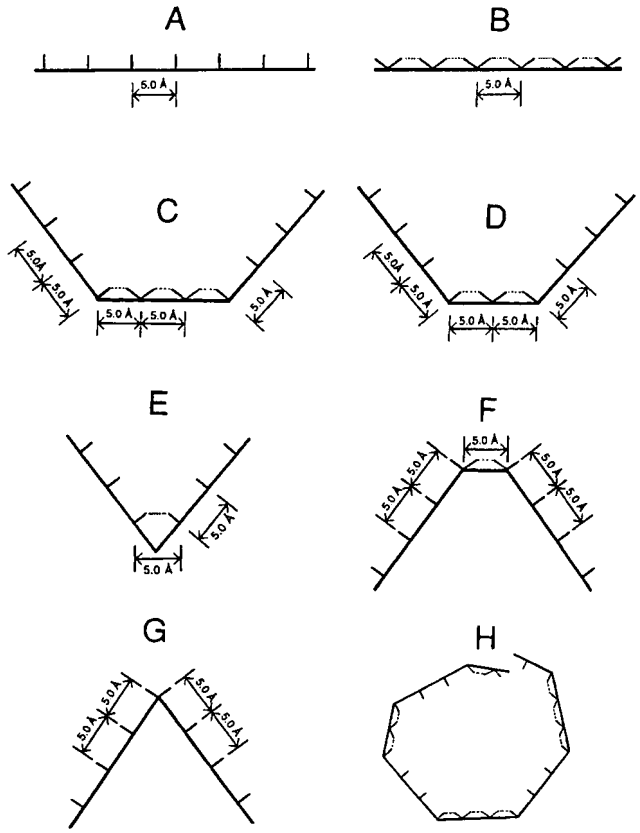

Figure 6. Parts A and B show shorthand notation for single (111)-type and (100)-type β-cristobalite faces, respectively, with short lines representing OH groups and long lines representing (111)-type and (100)-type faces of Figures 3B and 4A, respectively. Specific configurations are made possible by intersections of two (111)-type β-cristobalite faces with each other (E and G) or with a (100)-type face (C, D, and F), as represented by shorthand notation. (H) A hypothetical model of a defect structure or pore structure of silica, as represented by shorthand notation. Dotted lines represent hydrogen bonds.

If one represents the silica gel surface by a complex model of intersecting (100)-type and (111)-type β-cristobalite faces, as represented in Figure 6, then one can begin to interpret the NMR-based results on hydrogen-bonded and non-hydrogen-bonded silanols. Judging from the occurrence of 53−58% of non-hydrogen-bonding single silanols and 46−47% of non-hydrogen-bonding geminal silanols, and assuming *a priori* roughly the same probability for concave intersections (which provide hydrogen-bonding opportunities) and convex intersections (which do not) between different (111)-type faces or between a (111)-type face and a (100)-type face, the number of columns of geminal silanols corresponding to Figures 6C and 6D is probably very close to one for silica gel surfaces. Furthermore, the near 1-to-1 number ratio of hydrogen-bonding to non-hydrogen-bonding single silanols implies a large number of pores. This is consistent with the known characteristics of silica gel.

The β-cristobalite model of the silica surface can also account for the effects of 25 or 200 °C vacuum dehydration of silica gel on the ^{29}Si NMR data presented above. Figures 6F and 6G show the convex intersections of two non-parallel (111)-type faces with each other (Figure 6G) or with a (100)-type face (Figure 6F). According to our β-cristobalite silica surface model, for those single silanols on the same (111)-type face (Figure 6A) or at the convex intersection of (111)-type and (100)-type faces (Figure 6F), and for those columns of geminal silanols right at the convex intersection of two (111)-type faces (Figure 6G), hydrogen bonding with other silanols cannot occur.

However, on an untreated silica surface, these silanols form hydrogen bonds with bridging water, as depicted in Figure 3A. After a silica surface is evacuated at 25 or at 200 °C, all the physisorbed water has been eliminated from the surface and these silanols, which were initially hydrogen bonded to water, have become isolated silanols. On the other hand, for those single silanols at the concave intersection(s) of two (111)-type faces (Figure 6E), or of one (111)-type face and one (100)-type face (Figures 6C or 6D), hydrogen bonding can occur with other single silanols or with geminal silanols across the intersection(s). For those geminal silanols in the same row of a (100)-type plane, as shown in Figures 4 and 6B, or at the concave intersection(s) of one (100)-type plane and one (111)-type plane (Figures 6C and 6D), hydrogen bonding can occur with other geminal silanols or with single silanols across the intersection(s). The silanols which are hydrogen bonded to other silanol(s) can also form hydrogen bonds with bridging water on an untreated silica surface. After the elimination of physisorbed water from the silica surface, these initially hydrogen-bonded silanols are no longer hydrogen bonded to water; however, hydrogen bonding *between* silanols is not disturbed by the elimination of physisorbed water. Our model indicates that non-hydrogen-bonded silanols of an evacuated silica can be either single or geminal silanols, and hydrogen-bonded silanols (single or geminal) can participate in hydrogen bonding with single silanols and/or geminal silanols. Thus, our model is consistent with the experimental results presented above for untreated silicas or silicas evacuated at temperatures of 200 °C or lower.

The dehydration of silica under vacuum at temperatures between 200 and 500 °C involves additional kinds of issues, e.g., the splitting out of water as Si−O−Si bridges are formed, and has been studied by a variety of experiments.[2,7,8,17,19] As the temperature is raised within this range, hydrogen-bonded silanols (single or geminal) start to split out water to form low-strain Si−O−Si linkages—apparently, the stronger the hydrogen bonding between two silanols, the more facile the Si−O−Si formation. Single or geminal silanols that are not hydrogen bonded are essentially unaffected by evacuation in the 200 to 500 °C temperature range. When a silica is subjected to heating under vacuum at temperatures ≥600 °C, some of the non-hydrogen-bonded silanols begin to "readjust their positions" on the surface and are able to condense irreversibly to form highly-strained Si−O−Si linkages. The β-cristobalite model is also capable of accounting for this behavior. Such issues, and a more detailed examination of the primary issues considered in this paper, will be published elsewhere.[38]

Summary and Conclusions

From $^1H \rightarrow ^{29}Si$ cross-polarization spin dynamics, it is possible to distinguish hydrogen-bonded silanols from non-hydrogen-bonded silanols. All the silanols of two untreated silica gel samples are hydrogen bonded either to water molecules or to other silanols. After evacuation at 25 or at 200 °C, those silanols that were hydrogen bonded only to water molecules become isolated silanols (non-hydrogen-bonded silanols), which can be single silanols or geminal silanols. On a Fisher silica gel surface evacuated at 25 °C, 53% of the single silanols and 46% of the geminal silanols are not hydrogen bonded, and the ratio of the number of hydrogen-bonded single silanols to hydrogen-bonded geminal silanols is 17-to-1. On the surface of a Baker silica gel evacuated at 200 °C, 58% of the single silanols and 47% of geminal silanols are non-hydrogen-bonded; the ratio of the number of hydrogen-bonded single silanols to hydrogen-bonded geminal silanols is 16-to-1.

In the β-cristobalite model for the silica surface, single silanols are situated on (111)-type faces and geminal silanols are situated on (100)-type faces; and single silanols and geminal silanols can either be hydrogen-bonded or non-hydrogen-bonded, depending on their local structural environments. Single silanols on the same (111)-type face cannot be hydrogen bonded to each other, while neighboring geminal silanols on the same (100)-type face may or may not be hydrogen bonded to each other, depending on the relative orientation of their hydroxyl groups. The two hydroxyl groups on the same geminal silanol cannot form hydrogen bonds with each other due to an unfavorable geometrical arrangement. When one (111)-type face intersects concavely with a (100)-type face, the single silanols and geminal silanols at the intersection are in the same (100)-type face and can hydrogen bond with each other. When a (111)-type face intersects with a (100)-type face convexly, there are no hydrogen bonds between a single silanol and its neighboring geminal silanol. If two (111)-type planes intersect concavely, single silanols at the intersection will also be situated on the same (100)-type face and can hydrogen bond "across" the intersection. When two (111)-type faces intersect convexly, an array of geminal silanols are situated at the intersection, and no hydrogen bonds exist in this arrangement. All the hydrogen bonding silanols have a common feature; i.e., when any two silanols are hydrogen bonded to each other, the two silicon atoms containing them are also situated on a same (100)-type plane. The generalized β-cristobalite model can readily explain the reversible dehydration/rehydration behavior of silica heated below 500 °C, as well as the irreversible dehydration/rehydration behavior of silicas heated to temperatures above 600 °C.

Acknowledgment. The authors gratefully acknowledge partial support of this research by the National Science Foundation Grant No. CHE-9021003 and by Grant No. F49620-95-1-0192 from the Air Force Office of Scientific Research.

JA951550D

Reactions of Ethoxysilanes with Silica: A Solid-State NMR Study

Janet Blümel

Anorganisch-chemisches Institut der Technischen Universität München Lichtenbergstrasse 4, 85747 Garching, Germany

Received September 26, 1994

Alkoxysilane reagents find widespread application in the fields of immobilized catalysts[1-3] and reversed-phase chromatography,[1,4-8] because they provide strong bonding via up to three siloxane groups and high surface coverage without acidic reaction products. In spite of this, the nature of the coupling reaction of alkoxysilane reagents with the silica surface is still a matter of debate. In this paper it is demonstrated unequivocally by solid-state NMR spectroscopy that ethoxysilane reagents react directly with siloxane bonds of dehydrated silica.

^{29}Si and ^{13}C solid-state NMR spectroscopy nowadays provides the most detailed information about the nature and reactivity of inhomogeneous catalysts,[9] their support materials,[9,10] and especially modified silica.[4-7,11-18] ^{29}Si CP/MAS NMR spectroscopy,[10] e.g., showed that trialkoxysilane reagents do not exclusively form three siloxane bonds upon condensation reaction with silica surface silanol groups: there always exists a distribution of silane species bound by one, two, and three siloxane bonds.[5-7,14,19] Furthermore, the presence of polysiloxane, incompletely coating the surface, cannot be excluded.[6,14] Consequently, residual alkoxide signals can be found in the ^{13}C CP/MAS NMR spectra of the modified silica materials. However, the intensities of the ^{29}Si NMR signals do not match the intensities of the corresponding ^{13}C NMR signals.[6] According to ^{13}C NMR spectroscopy there are always more alkoxy groups present than would be anticipated from the silane region of the ^{29}Si CP/MAS NMR spectra, which shows all surface-bound silane species carrying residual alkoxy groups. This discrepancy was attributed to reaction of free alcohol, formed by condensation reaction, with surface silanol groups.[6] An IR study, however, suggested reaction of surface siloxane groups with the alkoxysilane reagents.[20] Both studies were unfortunately complicated by residual alkoxy groups bound to the silane reagents and cross-linking. Therefore, in order to find out the true mechanism, the reaction of the silica surface with alkoxysilanes was studied using the monoethoxy reagent trimethylethoxysilane (**1**).

When silica $SiO_2(600)$[21] is modified[22] with **1**, the silane region of the ^{29}Si CP/MAS NMR spectrum[23] shows a signal at 13.7 ppm, matching the data for silica modified with chlorotrimethylsilane[5,7,13] or hexamethyldisilazane.[11,15] The ^{13}C CP/MAS NMR spectrum[23] obtained after reaction of $SiO_2(600)$ with **1** at 25 °C is shown in Figure 1A. The signal at −0.4 ppm corresponds to the trimethylsilyl carbon atoms, and the signals at 59 and 16 ppm correspond to the methylene and methyl carbon atoms of a surface-bound ethoxy group. The relative signal intensities of about 1 to 3 of ethoxy and trimethylsilyl signals did not change when reaction temperatures up to 160 °C or simple high-power decoupling and long pulse delays (60 s) were applied, which can be anticipated from the high mobility of both methyl and ethoxy groups.[4,12,17] Therefore, the ethoxy groups are retained quantitatively. Since no residual ethoxy groups can be left at the surface-bound silane, there are, in principle, two possible explanations for this observation: The first possibility is that the ethanol from the condensation reaction of **1** with surface silanol groups (reaction 1) reacts quantitatively with further surface silanol groups (reaction 2).

$$(CH_3)_3SiOCH_2CH_3 + HO[SiO_2] \rightarrow (CH_3)_3SiO[SiO_2] + CH_3CH_2OH \quad (1)$$

$$CH_3CH_2OH + HO[SiO_2] \rightarrow CH_3CH_2O[SiO_2] + H_2O \quad (2)$$

The other possibility is an addition reaction of **1** with surface siloxane groups:

$$(CH_3)_3SiOCH_2CH_3 + [SiO_2]O[SiO_2] \rightarrow (CH_3)_3SiO[SiO_2] + CH_3CH_2O[SiO_2] \quad (3)$$

Reaction 3 explains the quantitative retainment of the ethoxy groups without further assumptions and has its analogs, for example, in the reactions of $Cp^*_2Th(CH_3)_2$,[24] BF_3,[25] NH_3, and H_2O[26] with surface siloxane groups. The sequence (1)/(2), however, requires reaction 2 to be faster than reaction 1 in order to allow quantitative retainment of the ethoxy groups. But under these reaction conditions, ethanol does not react with silica. This can be anticipated from the sluggish reaction of other alcohols with silica.[7,27,28] Even after silica $SiO_2(600)$ or $SiO_2(25)$[21] is boiled in ethanol for 24 h, there is only a small number of chemically bound ethoxy groups. The latter correspond to the

(1) Deschler, U.; Kleinschmit, P.; Panster, P. *Angew. Chem., Int. Ed. Engl.* **1986**, *25*, 236−252.
(2) Hartley, F. R. *Supported Metal Complexes*; D. Reidel Publishing Company: Dordrecht, 1985.
(3) Blümel, J. *Inorg. Chem.* **1994**, *33*, 5050−5056.
(4) Kelusky, E. C.; Fyfe, C. A. *J. Am. Chem. Soc.* **1986**, *108*, 1746−1749.
(5) Maciel, G. E.; Sindorf, D. W.; Bartuska, V. J. *J. Chromatogr.* **1981**, *205*, 438−443.
(6) Sindorf, D. W.; Maciel, G. E. *J. Am. Chem. Soc.* **1983**, *105*, 3767−3776.
(7) Bayer, E.; Albert, K.; Reiners, J.; Nieder, M.; Müller, D. *J. Chromatogr.* **1983**, *264*, 197−213.
(8) Scott, R. P. W. *Silica Gel and Bonded Phases*; John Wiley & Sons: Chichester, 1993; pp 142−147.
(9) Bell, A. T.; Pines, A., Eds. *NMR Techniques in Catalysis*; Marcel Dekker, Inc.: New York, 1994.
(10) Engelhardt, G.; Michel, D. *High-Resolution Solid-State NMR of Silicates and Zeolites*; John Wiley & Sons: Chichester, 1987.
(11) Sindorf, D. W.; Maciel, G. E. *J. Phys. Chem.* **1982**, *86*, 5208−5219.
(12) Zeigler, R. C.; Maciel, G. E. *J. Phys. Chem.* **1991**, *95*, 7345−7353.
(13) Köhler, J.; Chase, D. B.; Farlee, R. D.; Vega, A. J.; Kirkland, J. J. *J. Chromatogr.* **1986**, *352*, 275−305.
(14) Gilpin, R. K.; Gangoda, M. E. *J. Chromatogr. Sci.* **1990**, *28*, 277−281.
(15) Akapo, S. O.; Simpson, C. F. *J. Chromatogr. Sci.* **1990**, *28*, 186−193.
(16) Jinno, K. *J. Chromatogr. Sci.* **1989**, *27*, 729−734.
(17) Zeigler, R. C.; Maciel, G. E. *J. Am. Chem. Soc.* **1991**, *113*, 6349−6358.
(18) Albert, K.; Bayer, E. *J. Chromatogr.* **1991**, *544*, 345−370.
(19) Liu, D. K.; Wrighton, M. S.; McKay, D. R.; Maciel, G. E. *Inorg. Chem.* **1984**, *23*, 212−220.
(20) Dubois, L. H.; Zegarski, B. R. *J. Am. Chem. Soc.* **1993**, *115*, 1190−1191.

(21) The silica was obtained from Merck (silica 40) and dried in vacuo (10^{-2} Pa) at 25 °C ($SiO_2(25)$) or 600 °C ($SiO_2(600)$) for 24 h in order to remove adsorbed water or condensed surface silanol groups, respectively, and stored under dry nitrogen.

(22) In a typical experiment 1 g of silica was suspended in about 20 mL of dry toluene. After addition of 0.1 g of **1**, the slurry was stirred for 12 h at 25 °C. Then the liquid was decanted, the residue washed three times with toluene, and the silica dried in vacuo. Experiments without solvent gave the same results.

(23) All measurements were made with a Bruker MSL 300 NMR spectrometer using 7 mm ZrO_2 rotors: spinning speed, 4 kHz; external references, tetrakis(trimethylsilyl)silane (^{29}Si) and adamantane (^{13}C); proton 90° pulse, 6 μs.

(24) Toscano, P. J.; Marks, T. J. *Langmuir* **1986**, *2*, 820−823.
(25) Morrow, B. A.; Devi, A. *J. Chem. Soc., Faraday Trans. 1* **1972**, *68*, 403−422.
(26) Morrow, B. A.; Cody, I. A. *J. Phys. Chem.* **1976**, *80*, 1995−2004.
(27) Gay, I. D. *J. Phys. Chem.* **1974**, *78*, 38−42.
(28) Ballard, C. C.; Broge, E. C.; Iler, R. K.; St. John, D. S.; McWhorter, J. R. *J. Phys. Chem.* **1961**, *65*, 20−29.

0002-7863/95/1517-2112$09.00/0

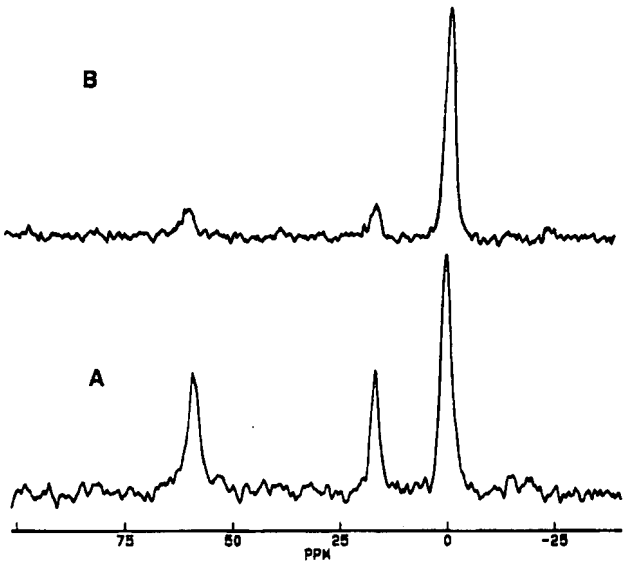

Figure 1. ^{13}C CP/MAS NMR spectra (75.5 MHz) of highly dehydrated silica $SiO_2(600)$[21] (A) and hydrophilic silica $SiO_2(25)$[21] (B) modified with $(CH_3)_3SiOCH_2CH_3$: contact time, 5 ms; pulse delay, 4 s; 1000 scans.

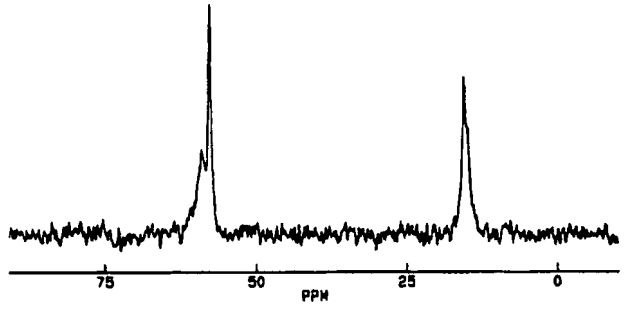

Figure 2. ^{13}C CP/MAS NMR spectrum (75.5 MHz) of silica $SiO_2(600)$[21] treated with ethanol (see text): contact time, 5 ms; pulse delay, 4 s; 4000 scans.

broad signals at 58.7 and 15.0 ppm in Figure 2. The partly overlapping narrow signals at 57.5 and 15.5 ppm with a line width of about 50 Hz can be attributed to physically adsorbed ethanol.[27,29]

Using CP, the optimal signal intensity for the adsorbed ethanol was obtained for contact times of 5 (Figure 2) to 6 ms. The signals decreased to half their original size with a contact time of 3 ms. When a 1 ms contact time was applied, the signals of the adsorbed species were reduced to little shoulders at the broad signals of the chemically bound ethoxy groups. However, the intensity of the narrow signals increased about 5-fold, when simple high-power decoupling was applied instead of CP. This behavior is typically observed with adsorbed in contrast to chemically bound species[30] and has its origin in their different mobilities.[30]

Further evidence against reaction 2 comes from the fact that the number of ethoxy groups is diminished when less rigorously dried silica $SiO_2(25)$[21] containing fewer siloxane groups is used, which can be seen in Figure 1B. However, their mere presence suggests that reaction 3 is even preferred to reaction 1. This is also supported by the observation that the surface coverage is greater under the applied reaction conditions for $SiO_2(600)$ (6.5% carbon content as determined by elemental analysis) than for $SiO_2(25)$ (4.5%). $SiO_2(600)$, modified with **1**, is remarkably stable toward hydrolysis,[31] probably due to its high hydrophobicity. This suggests its application as a reversed-phase stationary phase. The coverage of $SiO_2(600)$ with trimethylsilyl and adjacent ethoxy groups is even sufficiently dense to allow reversed-phase chromatography of highly sensitive organometallic compounds. For example, the material can be stirred with a solution of chromocene for more than 48 h without signs of decomposition of the latter. In contrast, $SiO_2(25)$, modified with **1**, leads to rapid decomposition of chromocene, as does commercial silylated silica prepared with chlorosilanes.

In conclusion, the use of **1** and ^{13}C solid-state NMR spectroscopy showed unequivocally that addition of alkoxysilane reagents to surface siloxane groups of silica does take place and might even be the preferred reaction pathway. Consequently, in contrast to common practice, highly dehydrated silica with a maximum number of siloxane groups should be applied both for the immobilization of catalysts with bifunctional ethoxysilane reagents[3] and for modifying silica with alkoxysilanes for chromatography.[4-8] Monoethoxysilanes have the additional advantage of providing a clean reaction without cross-linking and therefore well-defined surface bound species. Since each trimethylsilyl group inevitably has an adjacent ethoxy group, there is no more need for "end capping" in an additional step.

Acknowledgment. I am especially thankful for many fruitful discussions with Prof. R. K. Harris (University of Durham). Furthermore I thank the Fonds der Chemischen Industrie for a Liebig fellowship and financial support. I am also grateful for financial support by the Leonhard Lorenz Foundation and the Pinguin Foundation. Trimethylethoxysilane was generously provided by Wacker Chemie GmbH.

JA943171A

(29) Klinowski, J.; Anderson, M. W. *Magn. Reson. Chem.* **1990**, *28*, S68-81.

(30) Baltusis, L.; Frye, J. S.; Maciel, G. E. *J. Am. Chem. Soc.* **1986**, *108*, 7119-7120.

(31) The ^{13}C CP/MAS NMR spectrum of the material is not changed after boiling in H_2O for 8 h.

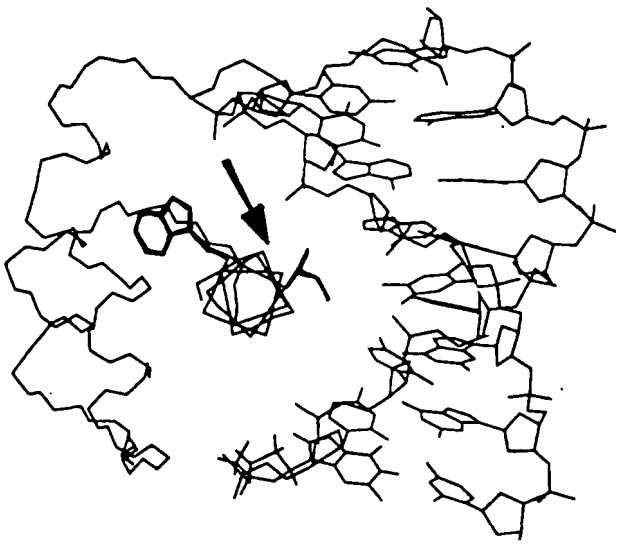

Figure 2. View along the axis of the recognition helix of one of the 16 NMR conformers representing the solution structure of the *Antp(C39S)* homeodomain-DNA complex (Billeter, M.; Qian, Y. Q.; Otting, G.; Müller, M.; Gehring, W. J.; Wüthrich, K., to be submitted). The presentation includes all heavy atoms of base pairs 5-12 of the 14-base-pair DNA, the polypeptide backbone of residues 8-56 of the *Antp(C39S)* homeodomain, and with bold lines, the side chains of Ile 47 and Trp 48 of the homeodomain. The arrow indicates the location of the hydration water molecules detected by NMR.

stringent requirements, it is likely that additional cross peaks representing intermolecular NOEs with hydration water were not identified as such. On the other hand, since several intermolecular NOEs were observed between the side chain of Ile 47 and the DNA (Billeter, M.; Qian, Y. Q.; Otting, G.; Müller, M.; Gehring, W. J.; Wüthrich, K., to be submitted), and since the amide proton of Trp 48 is next to Ile 47, we have well established that the few NOEs attributed to hydration waters are with hydrogen atoms in the interface between the protein and the DNA (Figure 2).

Only very few of the water molecules hydrating the homeodomain-DNA complex could be observed by NOEs. Apparently, most of the other solvent-solute NOEs are very weak, indicating that the residence times of water molecules in the surface hydration sites are shorter than about 0.5 ns, as was found in other peptides and proteins.[4] The negative sign and the higher intensities of the NOEs with the water molecules in the protein-DNA interface show that the lifetimes of these hydration water molecules are longer than 1 ns, and since these water molecules have the same chemical shift as the bulk water, we can also establish an upper limit for the lifetimes of about 20 ms.[12] This coincides with the behavior of hydration water in interior cavities of globular proteins, where the water molecules constitute integral parts of the molecular architecture.[4,6,12,13] The present studies thus indicate an important structural role of the hydration water in the protein-DNA interface. Since the lifetimes of these waters are much shorter than the lifetime of the complex,[14] they also show that the structure of the complex undergoes time fluctuations with similar frequencies and amplitudes as observed for globular proteins.[12]

Acknowledgment. We would like to thank Dr. W. Gehring and Dr. M. Müller, Biocenter of the University of Basel, for providing the homeodomain polypeptides used in this study, and Dr. M. Billeter for helpful discussions. Financial support was obtained from the Schweizerischer Nationalfonds (Project 31.32033.91).

(12) Otting, G.; Liepinsh, E.; Wüthrich, K. *J. Am. Chem. Soc.* **1991**, *113*, 4363-4364.
(13) Clore, G. M.; Bax, A.; Wingfield, P. T.; Gronenborn, A. M. *Biochemistry* **1990**, *29*, 5671-5676.
(14) Affolter, M.; Percival-Smith, A.; Müller, M.; Leupin, W.; Gehring, W. J. *Proc. Natl. Acad. Sci. U.S.A.* **1990**, *87*, 4093-4097.
(15) (a) Marion, D.; Ikura, M.; Tschudin, R.; Bax, A. *J. Magn. Reson.* **1989**, *85*, 393-399. (b) Bax, A.; Ikura, M.; Kay, L. E.; Zhu, G. *J. Magn. Reson.* **1991**, *91*, 174-178.

Reaction of Alkoxysilane Coupling Agents with Dehydroxylated Silica Surfaces

Lawrence H. Dubois* and Bernard R. Zegarski

AT&T Bell Laboratories
Murray Hill, New Jersey 07974

Received October 22, 1992

Alkoxysilane coupling agents are commonly used to bond polymers to glass surfaces by the following reaction:[1]

$$R'Si(OR)_3 + HOSi\equiv \rightarrow R'Si(OR)_2OSi\equiv + ROH \quad (1)$$

R is typically a methyl or ethyl group, and R' contains a functionality that can react readily with the polymer (e.g., mercaptan or epoxide). HOSi≡ can be either an isolated surface silanol or a hydrogen-bonded hydroxyl group. The rate of the coupling reaction can be further increased in the presence of water by first hydrolyzing the silane.[1] Until now, it was thought that reactive hydroxyl groups *must* be present on the surface in order for bonding to take place. Here we demonstrate that alkoxysilane coupling agents can react directly with highly strained siloxane bonds present on *dehydroxylated* silica, thus yielding a new mechanism for polymer-silica surface adhesion.

Strained siloxane bonds can be formed readily on high surface area silica samples by heating to temperatures in excess of 900 K.[2-4] The most reactive of these sites are edge-shared tetrahedra formed by the dehydroxylation of adjacent, isolated silanol groups.[2,3,5] The strain in these four-membered-ring structures

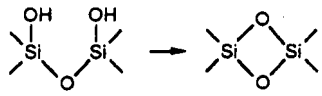

(2)

(estimated to be 23 kcal/mol of Si-O bonds[6]) is due to the large distortion of both the O-Si-O and Si-O-Si bond angles[4,7] and results in infrared active Si-O stretching modes at 888 and 908 cm^{-1}.[2-4]

The adsorption of methyltrimethoxysilane (MTMSi) on a dehydroxylated silica surface at 330 K is followed using infrared spectroscopy (Figure 1a).[8] From this data it is clear that the intensity of the CH_3 stretching vibrations from both the methyl (asym: 2978; sym: ~2920 cm^{-1}) and methoxy (asym: 2957; sym: 2851 cm^{-1}) groups increases as a function of time.[10] A corresponding decrease in the intensity of the bands due to the Si-O stretching modes of the strained siloxane rings is also observed.[10] These data, normalized to a constant peak height, are summarized in Figure 1b.

The intensity of the isolated (i.e., non-hydrogen-bonded) O-H stretching vibration (3750 cm^{-1}) remains constant at 0.104 ± 0.001

(1) Plueddemann, E. P. *Silane Coupling Agents*, 2nd ed.; Plenum: New York, 1991.
(2) Morrow, B. A.; Devi, A. *Trans. Faraday Soc.* **1972**, *68*, 403.
(3) Morrow, B. A.; Cody, I. A. *J. Phys. Chem.* **1976**, *80*, 1995, 1998.
(4) Bunker, B. C.; Haaland, D. M.; Ward, K. J.; Michalske, T. A.; Smith, W. L.; Binkley, J. S.; Melius, C. F.; Balfe, C. A. *Surface Sci.* **1989**, *210*, 406.
(5) Bunker, B. C.; Haaland, D. M.; Michalske, T. A.; Smith, W. L. *Surface Sci.* **1989**, *222*, 95.
(6) O'Keeffe, M.; Gibbs, G. V. *J. Chem. Phys.* **1984**, *81*, 876.
(7) Molecular analogs of these species are known and their structures well-characterized. See, for example: Fink, M. J.; Haller, K. J.; West, R.; Michl, J. *J. Am. Chem. Soc.* **1984**, *106*, 822.
(8) Silica substrates were prepared using the technique described in refs 9 and 10. Approximately 12 mg of Cab-O-Sil M5 was pressed into a fine tantalum screen to make a disk ~1.2 cm in diameter and ~0.3 mm thick. Samples were then mounted in a small, turbomolecular pumped vacuum cell (base pressure of $<1 \times 10^{-8}$ Torr) and dehydroxylated for 3-6 h at ≥1250 K by resistively heating the tantalum mesh. Spectra were collected in transmission mode using a Fourier transform infrared spectrometer (Mattson Instruments) and a liquid nitrogen cooled, wide band MCT detector. Typically 256 scans were averaged at 4 cm^{-1} resolution (~1 min acquisition time).
(9) Ballinger, T. H.; Wong, J. C. S.; Yates, J. T., Jr. *Langmuir* **1992**, *8*, 1676.
(10) Dubois, L. H.; Zegarski, B. R. *J. Phys. Chem.*, in press.

0002-7863/93/1515-1190$04.00/0